The Origins and Fate of Archaeal Intact Polar Lipids in Hydrothermally Altered Sediments of Cathedral Hill, Guaymas Basin, Gulf of California

By

Jeremy N. Bentley

A Thesis Submitted to
Saint Mary's University, Halifax, Nova Scotia
in Partial Fulfillment of the Requirements for
the Degree of Master of Science in Applied Science.

December 2019, Halifax, Nova Scotia

Approved: Dr. Todd Ventura
Supervisor

Approved: Dr. Andrew MacRae
Internal Committee Member

Approved: Dr. Clarissa Sit
External Committee Member

Approved: Dr. Penny Morrill
External examiner

Date: December 16, 2019

Man is a little germ that lives on an unimportant rock ball that revolves about a small star at the outskirts of an ordinary galaxy. ... I am absolutely amazed to discover myself on this rock ball rotating around a spherical fire. It's a very odd situation. And the more I look at things I cannot get rid of the feeling that existence is quite weird.

Alan Watts

Abstract

The Origins and Fate of Archaeal Intact Polar Lipids in Hydrothermally Altered Sediments of Cathedral Hill, Guaymas Basin, Gulf of California

By Jeremy N. Bentley

This study provides a survey of archaeal intact polar lipids (IPLs) and core lipids (CLs), focusing on archaeal lipids extracted from surface sediments within a push core transect that was collected at the Cathedral Hill hydrothermal vent complex in Guaymas Basin, Gulf of California. The main objectives of this study were to: 1) detect the subsurface microbial communities present, 2) determine the thermochemical stability of the lipids and, 3) evaluate if the thermochemical stability of these molecules influence lipid-based proxies used for the reconstruction of environmental change. In this study, a lipidome was detected providing evidence for the presence of archaeal communities that extend to sediment depths at ~145°C. These conditions are currently outside the known habitability of life. Evidence is provided that the archaeal communities adapt to the harsh conditions by modifying the core lipid structures of their cellular membranes. However, this adaptability appears to also impact the lipid-based proxies that are used to reconstruct present and past environmental conditions. These results suggest that an overprinting of original allochthonous signals is possible.

Date: December 16, 2019

Acknowledgments

I would like to thank Dr. Todd Ventura for all of the assistance and guidance over the course of this thesis as my primary supervisor. His generosity and support was greatly appreciated. Dr. Ventura has always challenged me to critically think about my data, this skill will forever be in my tool kit. I would also like to thank my committee members Dr. Clarissa Sit and Dr. Andrew MacRae for their continued support throughout this thesis, and for their edits and critical thoughts on this project. Thank you for being an integral part of my thesis. I would like to extend a special thanks to Dr. Carl Peters for being both, a guiding presence during my thesis and a friend. Our coffee breaks/science talks were both critical at helping me develop my understanding of lipidomics and were always a good laugh. I would like to thank my fellow graduate students in the office for entertaining my questions even if they seemed absurd and I never provided enough detail. Lastly I would like to thank my family for their support and care. I would not have had the opportunity to get to this point without you. I thank you will all my heart.

Table of Contents

List of Abbreviations

ANME	Anaerobic methanotrophic archaea
AOA	Anaerobic oxidation of ammonia
AOM	Anaerobic oxidation of methane
AR	Archaeol (sn-2,3-dibiphytanylglycerol)
brGDGT	Branched glycerol dialkyl glycerol tetraether
BIT	Branched isoprenoid tetraether (proxy)
BPC	Base peak chromatogram
CBT	Cyclization of branched tetraethers (proxy)
Cer	Ceramide
CL	Core lipid
cmbsf	cm below sea floor
cGDGT	Core GDGT
DAG	Diacylglycerol
DC	Degree of cyclization (proxy)
DCM	Dichloromethane
dw	Dry weight
EIC	Extracted ion chromatogram
ESI	Electrospray ionization
FA	Formic acid
GDD	Glycerol dibiphytanyl diether
GDGT or iGDGT	(isoprenoidal) Glycerol dialkyl glycerol tetraether
HCl	Hydrochloric acid
HPLC	High performance liquid chromatography
HOT_{86}	HydrOxy Tetraether index with 86 carbon atoms
IPA	Isopropanol
IPL	Intact polar lipid
LC	Liquid chromatography
MeOH	Methanol
MI	Methane index
MPa	Megapascal (unit of pressure)
MS	Mass spectrometer
MBD	Modified Bligh and Dryer extraction
MBT	Methylation of branched tetraethers (proxy)
m/z	Mass to charge ratio
qTOF	Quadrupole time of flight
RI	Ring index
SST	Sea surface temperature
TEX_{86}	TetraEther Index with 86 cacbon atoms
TLE	Total lipid extract
1G-	Monoglycosidic head group
2G-	Diglycosidic head group

List of Figures

List of Tables

Structure of Thesis

This study is comprised of four Chapters: Chapter 1 offers an outline to this thesis, providing background knowledge of the study area and key objectives. Chapter 2 describes the bulk of the organic geochemistry regarding the lipids that were found within the Cathedral Hill hydrothermal vent complex. This Chapter represents a stand alone manuscript that will likely be coupled with other data from a complementary study to produce a more robust paper. The submission of this manuscript to a publisher will be determined once the complementary study is complete. Chapter 3 describes the overprinting of molecular signatures that are frequently used in numerous molecular proxies. Since Chapters 2 and 3 are prepared as separate and independent manuscripts for journal submission, there is overlap between these two chapters. This is most noticeable with the introductions and methodology. Chapter 4 provides a brief summary of the key findings of this study and outlines future work.

Chapter 1: Introduction and background information

1.1. Introduction

1.1.1. General introduction

The deep ocean sediments are one of the most extensive microbial habitats on the planet, covering approximately 66% of the Earth's surface and extending downwards to approximately 4 km (Roussel et al., 2008). Single celled microorganisms from the domain of Archaea are thought to make-up a majority of the subsurface communities (representing ~ 87 %; Lipp et al., 2008). Along with the marine subsurface, Archaea are dominant components of the microbial biosphere in many other settings such as in soils, water columns of lakes and rivers, swamps, bogs and oceans, as well as in the sediments of these aquatic environments (Offre et al., 2013). The ubiquitous nature of Archaea may be related to the resiliency of these organisms based on their ability to survive in some of the most inhospitable settings, such as hot springs and hydrothermal vents (Erauso et al., 1993; Pearson et al., 2004). Archaea found in these extreme environments have been used as case studies to define the limits of life on Earth (Blöchl et al., 1997; Kashefi & Lovley, 2003; Takai et al., 2008). These studies are mostly based on culture experiments that often neglect, or cannot experimentally mirror, the complexity of natural environmental conditions.

To target microbial community dynamics within the natural environment, genomics-based techniques are frequently employed. These approaches amplify the extractable DNA of host sediment cells via polymerase chain reactions and match the resulting product DNA to gene libraries (Cann and Ishino, 1999). The result is a highly diverse phylogenetic tree that shows the genetic relationship between the detected

microbial taxa. These techniques can be scaled to reconstruct community compositions and metabolic or other biochemical activity by utilizing quantitative PCR and metagenomics strategies. These techniques are limited, however, in that they still represent an amplified signal that may not be representative of the actual natural habitat. Alternative approaches that focus on the cellular membrane constituents may be used to further define the upper limits of life. These approaches have less diagnostic information, but may provide key components (information) that are not possible with genomics.

The cellular membranes of Archaea can be found as both intact polar lipids (IPLs) and core lipids (CLs). Both of these compounds, either unmodified (in the case of IPLs). Alternatively and more commonly CLs, when found in sediments are the diagenetically modified components which can become fundamental molecular markers of sedimentary organic matter due to their relatively high preservation potential. IPLs are composed of a CL chemically bound to a polar head group (Figure 1.1). When IPLs are found in the geosphere, they are considered to be sourced from cells living within the porewaters and on the surfaces of sediment grains (Sturt et al., 2004). Upon cell lysis under ambient conditions, the polar head-groups quickly hydrolyze within days to weeks to yield more stable CLs (White et al., 1979; Harvey et al., 1986). Both IPLs and CLs are an attractive set of molecules to study, as they can be taxonomically distinct in the biological sense and useful in potentially reconstructing organic matter source inputs and environmental conditions. Along with taxonomic information that may be useful to establish environmental conditions, archaeal-based lipid proxies have been used to both make inferences about current and paleoenvironmental conditions. These proxies will be further

discussed in Chapter 3. Furthermore, these lipids may also be used to address the habitable range of life as direct products of cellular activity.

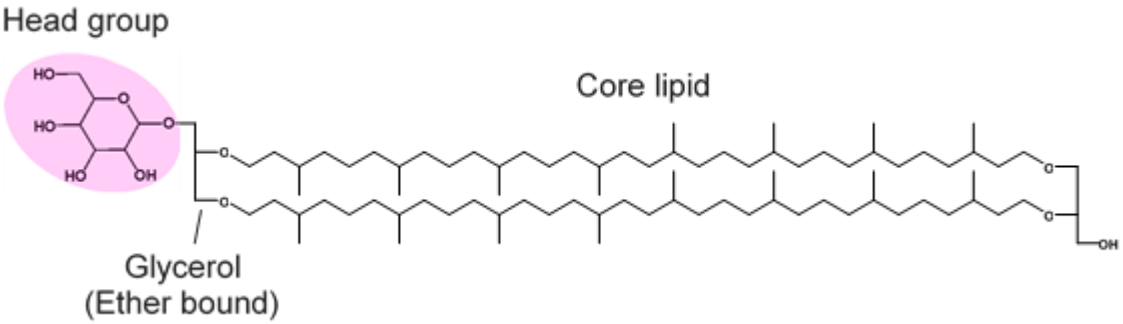

Figure 1.1 – Components of an IPL (1G-GDGT) showing a polar head group (1G or monoglycosidic headgroup) attached to a core lipid (GDGT) via an ether bond to the glycerol unit. This example contains two isoprenoidal hyrocarbon skeletons, ether bonded to the glycerol units.

This study primarily evaluates the diversity of archaeal lipids in a push core transect at a hydrothermal vent complex called Cathedral Hill within the Guaymas Basin, Gulf of California (Figure 1.2 A&B). We analyzed the sediments collected at depth and across the transect. This hydrothermal system provides a unique look into a highly productive subsurface that is a result of an influx of nutrients from vent fluids that produce elevated temperatures upwards of 155°C, which is currently out of the known habitability of Archaea.

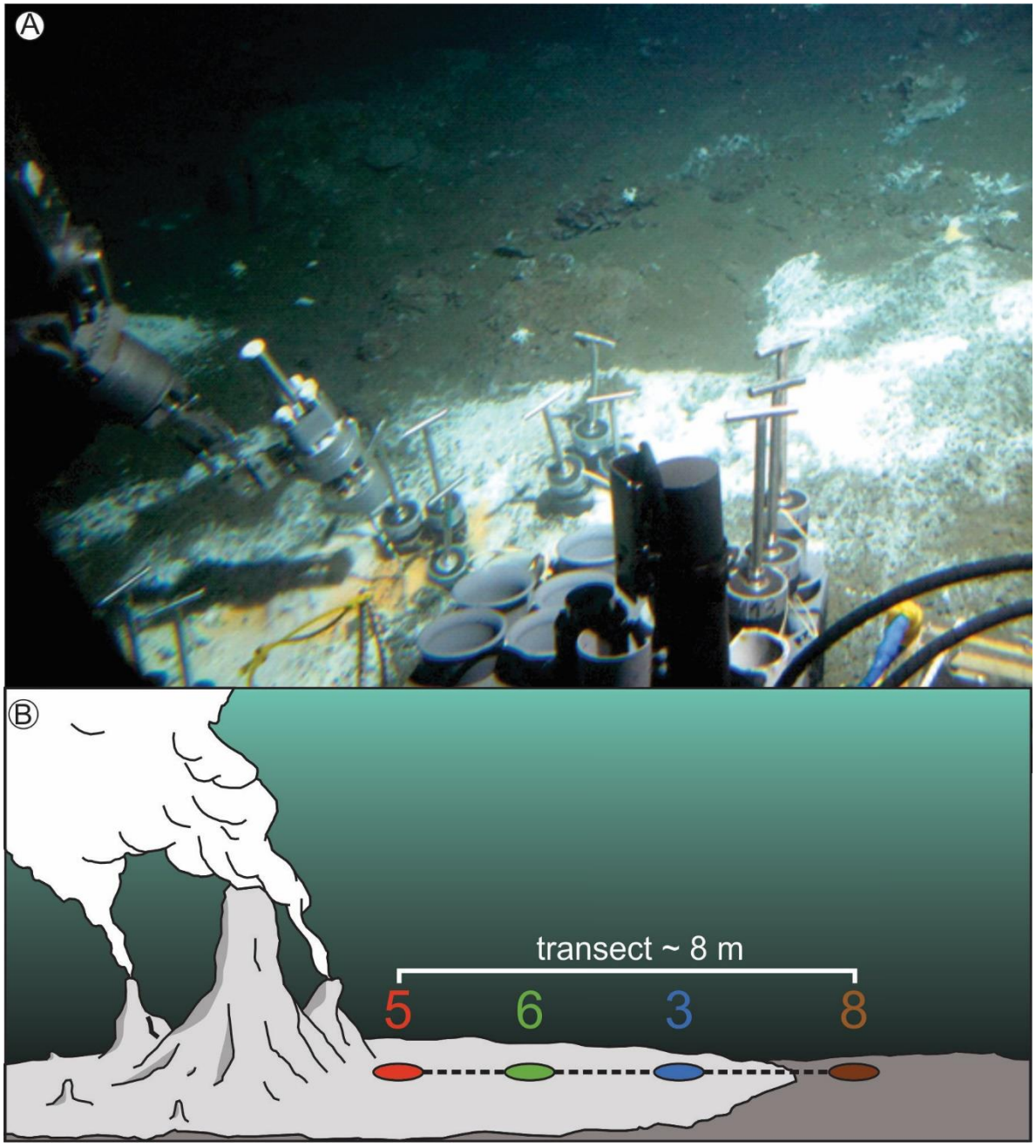

Figure 1.2 – A) View from the deep submergence vehicle (DSV) Alvin. Photo (A) taken from the submersible observation window showing the microbial mat present at Cathedral Hill with push cores pressed into the ocean floor sediments. B) - Schematic of the push core transect (the numbers are the ones assigned to the cores for reference).

1.1.2. Objectives

The main objectives for this thesis are to answer the following questions:

1) Can a subsurface microbial community at Cathedral Hill be detected using lipidomic techniques? If so, what can be learned about the community composition and the environmental controls that may limit its habitat?

2) What is the thermochemical stability of detectable polar lipids that are exposed to elevated vent pore water temperatures, and are the structures of those lipids preferentially selected by their surrounding environment?

3) Are lipid-based paleoclimate proxies influenced by hydrothermal subsurface sediment pore water temperatures? If so, to what degree does this occur and can constraints on the valid use of these proxies be defined?

1.2. Lipid signatures in sediments

Lipidomics is the comprehensive study of membrane lipid constituents. In this study, we focus on the archaeal membrane lipids extractable from ocean floor sediments. Lipids comprise the fundamental building blocks of cellular membranes that are responsible for providing structural rigidity and storage of energy to the cell. Environmental lipidomic studies are often used to characterize the *in situ* microbial communities in sediments to either identifying present-day environmental conditions, or

to generating paleo-environmental reconstructions (Schouten et al., 2013; Wörmer et al., 2017). Both the head group and the CL may be useful in describing the type of environment that may have ultimately played a role in the production of the molecule of interest. These molecules may be unique based on the conditions they are subjected to, and may often provide information on metabolism (Lipp & Hinrichs, 2009). Lipids provide valuable information, but when they are combined with other data sources, such as geochemical analyses or genomic analyses, the combined results tends to result in a more robust study.

The detection of lipids in environmental settings is a function of preservation and the analytical method chosen. The stability of an IPL is determined by the chemical structure of a lipid and its exposure to chemical and biological reactants from the external environment. In this regard, the lifespan of IPLs are often limited by the bond strength and potential chemical reactivity of the lipid's head group. In this regard, the head group linkage occurs either as an ester- or ether-bond to the glycerol of the core lipid. Studies have found that ester-bonded headgroups degrade more quickly than ether-bonded lipids (Schouten et al., 2010, Logemann et al., 2011). Nevertheless, when an IPL degrades there is still a high probability that the CL will survive. Therefore, the production of archaeal CLs often occurs after a cell's death, when the individual lipids that make up the cellular membrane separate from one another and the head groups are no longer attached (White et al., 1979). The resulting CLs that are incorporated into sediments are often referred to as "geo-lipids" or "fossil lipids".

The next three sections will briefly describe the differences between lipid membrane chemical signatures associated with archaeal, eukaryotic, and bacterial cells.

Their initial biological structures dictate the types of molecules that can be produced in an environment such as a hydrothermal vent system. Detailed descriptions of these molecules can be found in Chapter 2.

1.2.1. Archaeal signatures

Archaea are often composed of membrane-spanning (monolayer) lipids unlike bacterial or eukaryotic membranes that are often composed of lipid bi-layers. The signatures produced from Archaea are further distinct from that of a bacterial and eukaryotic signatures by being composed of hydrophobic chains of isoprene units rather than acyl (C_2) units. In this regard, archaeal IPLs often occur as tetraethers containing two biphytanes, but can also occur as diethers with two phytanyl chains. The polar head groups for archaeal lipids tend to be either glycosidic or phosphate based or potentially a mix of both (Rossel et al., 2008, Schouten et al., 2008, Strapoc et al., 2008). This limits the potential outcomes that may occur in our analysis as the diversity of head groups may be limited when investigating archaeal lipids. If an archaeal IPL containing a tetraether is hydrolyzed, the core lipids are liberated from the head groups forming glycerol-dialkyl-glycerol-tetraethers or GDGT's, one of the most common markers for Archaea (Figure 1.1; De Rosa & Gambacorta, 1988, Schouten et al., 2013). These molecules have been studied extensively as they tend to be the most abundant archaeal lipid present in marine sediments (Gliozzi et al., 1983; Kate 1993; Hanford & Peeples 2002; Pancost et al., 2009; Lipp et al., 2008; Schouten et al., 2013).

Due to the variable chemical complexities, their ubiquity, and ease of analytical detection, the different classes of GDGT biomolecules have been used to form a wide range of lipid-based indexes based on archaeal membrane adaptations that allow for better understanding of environmental conditions. These proxies have been used to reconstruct paleo-climate records (Schouten et al., 2002), anaerobic oxidation of methane (AOM; e.g., Zhang et al., 2011), or environmental stresses such as increased pH, redox, and salinity (Gliozzi et al., 1983; Quinn et al., 1986; Macalady et al., 2004; Pearson et al., 2004). The resilience of these proxies when applied to extreme sedimentary environments will be discussed in greater detail in Chapter 3.

1.2.2. Bacterial signatures

The Cathedral Hill hydrothermal vent site in Guaymas Basin is host to microbial mats that contribute bacterial IPLs to the sediments. These microbial mats are composed dominantly of *Beggiatoa*, which are sulfur oxidizing filamentous bacteria that are on the order of 25-35 µm in width, with some of the largest widths being around 120 µm (Nelson et al., 1989, MacGregor et al., 2013, Teske et al., 2016). These mats tend to range in thickness from 1-10 cm, extending into the subsurface with root like structures that provide stability; however, these mats can often form permeability barriers, which prevent the exchange of both fluids and gasses from the subsurface (Judd & Hovland, 2007). These mats migrate upwards to avoid burial from the rapid sedimentation rate and continually re-establish themselves at the surface of the seafloor (Mckay et al., 2012). The majority of bacterial lipids are ester bound, which is less stable and limits the thermal

stability of these molecules. This means that bacterial signatures should be excluded in areas that experience sufficiently elevated temperatures.

The mats at Cathedral Hill have been studied fairly extensively, because they show unique variations in color. This color sequence is due to a pigment within a filament in the mats (McKay et al., 2012, McGregor et al., 2013). However, there are some debates on the mechanism that creates this change in color. McKay et al. (2012) suggests that the color is related to a temperature process because the orange portion of the mats tend to be closer in proximity to the vent edifice. However, there is also speculation that it is related to a metabolic pathway, and that the color is due to the storage of elemental sulfur within vacuoles.

1.2.3. Eukaryotic signatures

Eukaryotes produce an array of lipids that serve various functions. Some examples of the biota responsible for eukaryotic lipid signatures include: terrestrial plants (e.g. waxes), heterokonts, Apicomplexa, diatoms, dinoflagellates, ciliates, Acantharea, other Radiolaria, and many others (Volkman & Johns, 1977; Edgcomb et al., 2002). However, the vast majority of marine organic matter is created by phytoplankton (Romankevich, 1984). A common marker for these organisms are chlorophylls, which become deposited and incorporated in the sediment. Chlorophyll likely comes from the upper water column, as deeper benthic organisms would not be capable of photosynthesis due to the water depth.

1.3. Geological setting

Guaymas Basin in the Gulf of California (Figure 1.3) is a large marginal rift between Baja California and Mexico formed by crustal extension between the Pacific and the North American plate boundaries (Lonsdale and Becker, 1985). This area has been actively spreading over the last 4 million years forming a series of smaller subbasins (Moore, 1973). Guaymas Basin is semi-enclosed, roughly in the middle of the Gulf of California, approximately 240 km in length and 60 km wide, and reaches depths between 1500-2000 m. The basin contains "Northern" and "Southern" troughs (Figure 1.4) that span approximately 40 and 20 km in length, respectively, and are a result of the extensive system of axial-parallel fault lines, which bound the troughs (Lonsdale and Becker, 1985). These troughs allow for the intrusion of basaltic sills into the sediments that perturb the heat-flow gradients of the larger surrounding area (Einsele et al., 1980; Teske et al., 2013). Studies have provided a range for the sediment thickness overlying the intrusive magmatic bodies of 300-500 m (Curray et al., 1979; Williams, 1979; Judd & Hovland, 2007).

The Cathedral Hill vent system is considered a sedimented hydrothermal system (Teske et al., 2014), resulting in the hydrothermal fluids propagating more diffusely through shelf sediment rather than faults that intersect the basaltic ocean floor as is observed with the Lucky Strike ridge segment near the Mid-Atlantic Ridge (Escartin, 2015) or the Lost City hydrothermal field (Kelley et al., 2005). For Guaymas Basin, most of the active hydrothermalism occurs within the Southern Trough (Lonsdale and Becker, 1985). Cathedral Hill represents one of many vent sites in the Southern Trough, that is

covered by a microbial mat (Teske et al., 2016). The push cores obtained for this study extend outward from the central vent complex into more distal sediments. Unfortunately, the descriptions for these cores are only basic description of their stratigraphy (Appendix A-2). However, there are no indications from these core descriptions that would indicate a large influx of sediments into the systems such as turbidites deposits. Thus the sedimentation is likely to be defined by normal sedimentation processes.

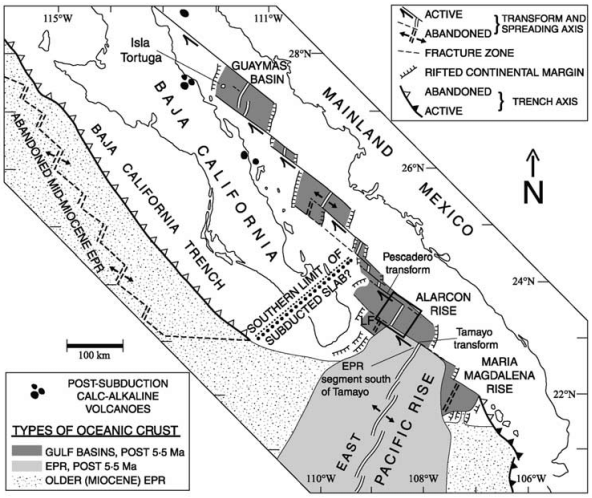

Figure 1.3 - Map of the Gulf of California, showing the tectonic regime (Castillo et al., 2002).

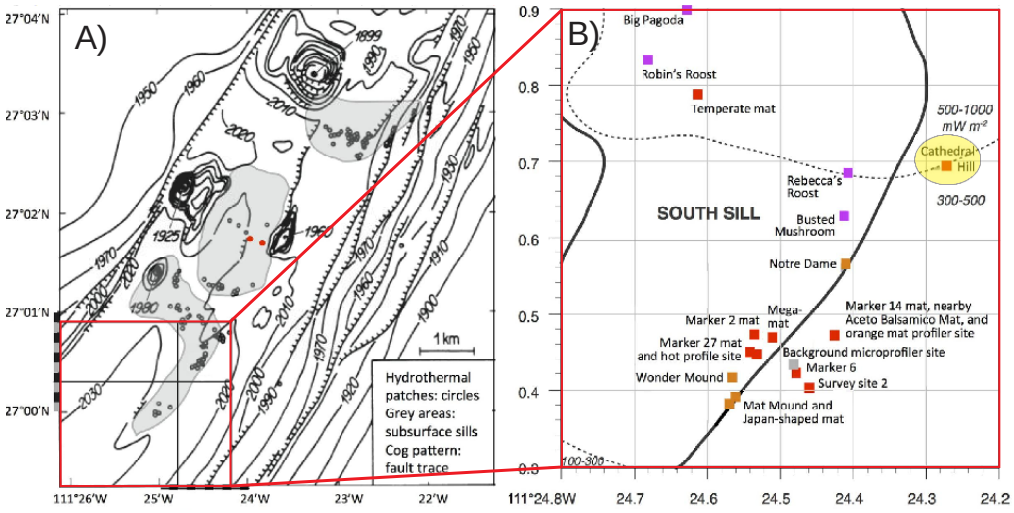

Figure 1.4 - Seafloor map of the Southern Trough in Guaymas Basin (A), Cathedral Hill is highlighted in yellow (B) (modified from Teske et al. 2016).

1.4. Sediment influx

The Guaymas Basin experiences high sedimentation rates (Curray et al., 1979; Gieskes et al., 1988) from the run-off of five major rivers that accounts for 50-90% of the total sedimentation along the eastern margin of the central and southern Gulf (Williams et al., 1979; Dean, 2006). Sediment is also produced by the deposition of organic matter in the highly productive water column mainly by diatoms and coccoliths (Figure 1.5; Williams et al., 1979). With all of this input, the organic carbon content in the Guaymas Basin is thought to be approximately 3-4% in surficial sediments (De la Lanza-Espino and Soto, 1999). Biological life on the seafloor or within the shallow sediment may also affect the organic matter content and volume through biodegradation and through the inevitable death and burial of the sediment macro and microfauna. The sedimentation rate within the Guaymas Basin is variable and not well constrained, with reported rates ranging from 0.4-2cm/yr (Calvert, 1966; Williams, 1979; Simoneit, 1985). Direct measurements of sedimentation rates at Cathedral Hill have not been made.

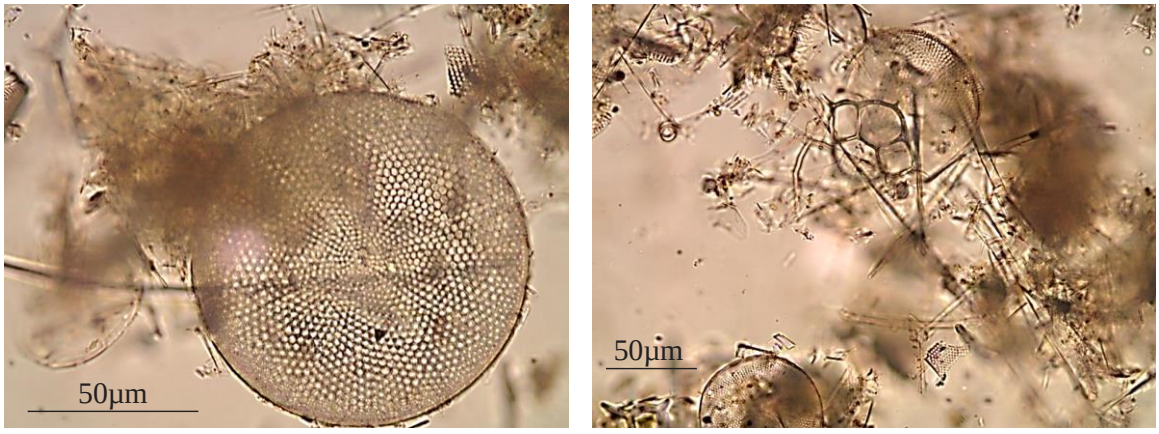

Figure 1.5 - Images of a smear slide produced for the surface of Core 3 (plane polarized light), showing a radial centric diatom (left) and a silicoflagellate and sponge spicules with diatoms (right).

1.5. Hydrothermal vent fluid chemistry

Hydrothermal vent fluids bring an array of dissolved ions and neutral molecules from depth to the surface where they may interact with the biological activity occurring at or near the seafloor. This chemical influx likely support the *in situ* biological systems in the subsurface sediments by supplying the right nutrients for chemotrophic life; it may also affect the surrounding rocks and sediments, altering them chemically (Gartman et al., 2014). These reactants can provide metabolic energy and fixed carbon for microbial communities to thrive (McCollom & Seewald, 2007). Dombrowski et al. (2017) suggests that there are biogeochemical interdependencies in organic matter utilization for systems within Guaymas Basin microbial communities, as determined by metagenomics assemblages. The presence of these assemblages suggests that there could be hydrocarbon degradation and sulfur cycling at Cathedral Hill.

There has been some documentation of hydrothermal fluid chemistry in Guaymas Basin. Studies such as Dick et al. (2009) and Dick & Tebo (2010) show that these fluids are enriched in NH_4^+, CH_4, Mn^{2+} and low molecular weight hydrocarbons C_nH_{2n+1}. They also indicate that sulfide forming metals such as copper and iron are often precipitated out and removed resulting in high Mn/Fe ratios within these fluids. Even so, little is known about how microbial communities respond to the influx of energy sources and nutrients such as H_2, NH_4^+, CH_4, H_2S, Fe^{2+}, Mn^{2+} and many others.

The temperature achieved by these fluids drastically impacts the life that is present at these types of systems. A study by Blöchl et al. (1997) extended the upper limit of life by finding Archaea that could persist at temperatures upwards of 113^{o}C at the Mid Atlantic Ridge. This is a noteworthy study, because previously it was thought that

biological life would be pasteurized at such high temperatures. More recent culture experiments by Kashefi & Lovley (2003) have extended the upper limit of life to 121°C demonstrating life's (archaea) surprising temperature resilience well into temperatures traditionally regarded as within the catagenic zone (60°C – 225°C; Tissot & Welte 1984) of hydrocarbon generation.

1.6. Methods

1.6.1. Push core sampling

A transect of push cores, of ~2 m spacing, was collected at the Cathedral Hill hydrothermal vent system in Guaymas Basin, Gulf of California (Figure 1.2 A&B). These push cores were collected by DSV-2 Alvin, a manned submersible from the Woods Hole Oceanographic Institution (WHOI) on Dive 4462 (10/22/08). The push cores are labeled Cores 5, 6, 3, and 8. The cores 5, 6, and 3 trend outboard from the vent complex, but are still within the region covered by the microbial mat, and Core 8 was collected furthest away from the vent within ambient temperatures and exterior to the mat. Accompanying these push cores are *in situ* pore water temperature measurements obtained by a thermal probe inserted into the sediments directly adjacent to each push core. Once the samples were collected they were subsampled into 2-3 cm intervals and immediately stored at −80°C. The subsamples were then freeze-dried, homogenized, and kept at −80°C until extraction.

1.6.2. Sediment extraction

Chemical extractions to isolate lipids have been done for decades, and initial protocols were first developed by Bligh & Dyer (1959). This liquid-liquid extraction method was first developed to isolate lipids from fish; however, with slight modification of the solvent mixes, as outlined by Sturt et al. (2004), lipids from sediments can be isolated. The principle idea of a chemical extraction is to isolate a molecule of interest, in this case IPLs and CLs of bacteria and archaea. This is done by using two immiscible liquid phases to distribute sample components of interest (Cantwell & Losier, 2002).

All samples were extracted using the modified Bligh and Dyer protocol after Sturt et al. (2004; Figure 1.6). Prior to extraction, the samples were spiked with a recovery standard (1-alkyl-2-acetoyl-*sn*-glycero-3-phosphocholine (PAF); Avanti Polar Lipids, Inc.). The samples were then extracted in six steps using 3 different solvent mixtures. For the first four steps, solvent mixtures of methanol/dichloromethane/buffer [2:1:0.8; v/v] were used. The first two steps used a phosphate buffer (5.5g/L Na_2HPO_4; Avantor Performance Materials, LLC.) adjusted to pH of 7.4 with HCl (Anachemia Co.), while the third and fourth steps employed a trichloroacetic acid buffer (50 g/L $C_2HCl_3O_2$; Avantor Performance Materials, LLC. (pH of 2)). The final two steps used a solvent mixture of methanol/dichloromethane [5:1; v/v]. Each extraction step used 6 ml of solvent mixture, which was sonicated for 5 minutes and centrifuged down for 5 minutes. After each extraction step, the solvent was decanted and combined in a separation funnel. Once all of the isolates from each step were combined, the extract was then purified with milliQ

water (Figure 1.6) and evaporated until dryness under a gentle steam of nitrogen while being heated at ca. 60°C. The resulting total lipid extract (TLE) was then spiked with 1, 2-diheneicosanoyl-*sn*-glycero-3-phosphocholine (C_{21}-PC; Avanti Polar Lipids, Inc.; for quantification) and subsequently stored at -20°C until time of mass spectral analysis.

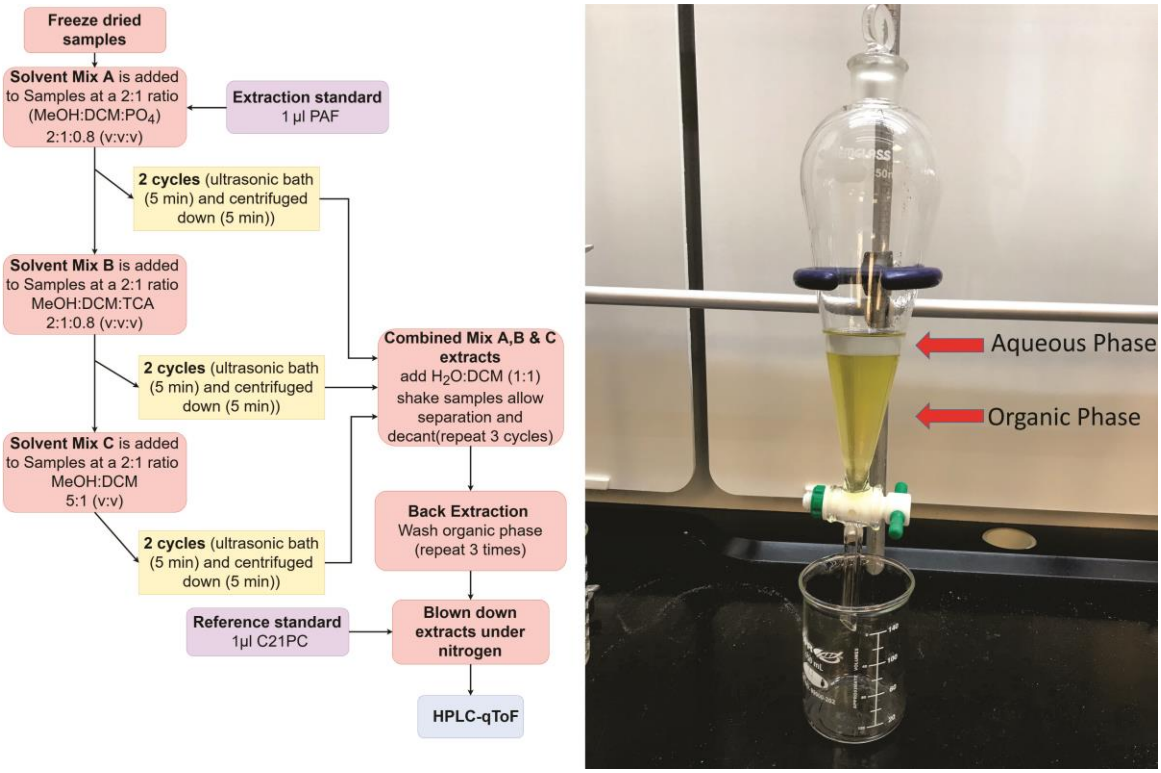

Figure 1.6 - The full protocol for the modified Bligh & Dyer extraction (left), An example of phase separation (right)

1.6.3. Liquid chromatography and mass spectrometry

High performance liquid chromatography (HPLC) is an analytical technique used to separate molecules, allowing them to be individually identified and quantified. The separation principle of an HPLC is based on the distribution of a sample between the mobile phase and the stationary phase or column. This allows for the sorting of molecules

as some molecules are slowed as they pass through a stationary phase before entering some form of detector, allowing for systematic change with retention time.

For our study, a reverse phase electrospray ionization (ESI) method with a scan range from 100-3000 *m/z* was chosen due to its ability to obtain simultaneous analysis of core lipids (CLs) and intact polar lipids (IPLs) of archaeal lipids. An aliquot of each sample representing 1% of the TLE was analyzed using an Agilent Technologies 1260 Infinity II HPLC coupled to an Agilent Technologies 6530 quadruple time-of-flight mass spectrometer (qToF-MS). Separation was achieved following the method described by Zhu et al. (2013) using an Agilent Technologies ZORBAX RRHD Eclipse Plus C18 (2.1 mm × 150 mm × 1.8 μm) reverse phase column, fitted with a guard column and maintained at 45°C. The flow rate was set to 0.25 mL/min. and the gradients were: mobile phase A (methanol/formic acid/ammonium hydroxide [100:0.04:0.10] v/v held at 100% for 10 min., followed by a linear gradient to 24% mixing with mobile phase B (propan-2-ol/formic acid/ammonium hydroxide [100:0.04:0.10] v/v extending for 5 min., a linear gradient to 65% B for 75 min., followed by 70% B for 15 min., that finished by re-equilibrating with 100% A for 15 min. The injection solvent was methanol. This reverse phase method produces chromatograms that start with molecules that are more polar and become less polar over the duration of the sample run.

1.6.4. Identification and quantification of lipid concentrations

Analyte identification was achieved by the interpretation of diagnostic ion and their fragmentation patterns (e.g., Knappy et al., 2009; Liu et al., 2010; Yoshinaga et al., 2011) using Agilent Technology's MassHunter software. Quantification was achieved by

summing the integration of peak areas of adducts $[M+H]^+$, $[M+NH^4]^+$, and $[M+Na]^+$ for the respective lipid class of interest. Once the integrated peak areas were determined for each lipid class of interest, concentration values were obtained relative to the internal C_{21}-PC standard and reported in µg/g dry weight sediment (concentration formula below).

$$\mathbf{C_{comp.}} = \mathbf{M_{std.}} \times \mathbf{A_{comp.}} / \mathbf{A_{std.}} \times \mathbf{M_{sed}}$$

Where the variables are:

$\mathbf{C_{comp.}}$ = concentration of compound [µg/g sed. dw.]

$\mathbf{M_{std.}}$ = mass of standard [µg]

$\mathbf{A_{comp.}}$ = area of compounds peak

$\mathbf{A_{std.}}$ = Area of standard peak

$\mathbf{M_{sed.}}$ = Dry weight (dw.) of sediment [g]

After concentrations were calculated a response factor was applied to the lipid class of interest as the ionization potential for lipid classes changes due to its chemical structure. Thus, these response factors were determined by a series of injections of standard solutions containing; 1,2-diacyl-3-O-(α-D-galactosyl1-6)-β-D-galactosyl-sn-glycerol (DGDG), 1,2-diacyl-3-O-β-D-galactosyl-sn-glycerol (MGDG), 1-alkyl-2-acetoyl-sn-glycero-3-phosphocholine (PAF), 1,2-di-O-phytanyl-sn-glycerol (Archaeol), 1',3'-bis[1,2-dimyristoyl-sn-glycero-3-phospho]-glycerol (14:0 Cardiolipin), 1,2-diheneicosanoyl-sn-glycero-3-phosphocholine (C_{21}-PC) from Avanti Polar Lipids, Inc., USA, and 2,2'-di-O-decyl-3,3'-di-O-(1'',ω''-eicosanyl)-1,1'-di-(rac-glycerol) (C_{46}-GTGT) from Pandion Laboratories, LLC) in amounts ranging from 100 pg to 30 ng. Concentrations of the standard mix were calculated from peak areas of molecular ions in

mass chromatograms. Response factors were calculated relative to C_{21}-PC, and the appropriate correction factor was applied to the particular lipid class of interest.

1.7.References

Akiya, N., & Savage, P.E., 2002. Roles of water for chemical reactions in high-temperature water. Chemical reviews, 102(8), 2725-2750.

Bligh, E.G., & Dyer, W.J., 1959. A rapid method of total lipid extraction and purification. Canadian journal of biochemistry and physiology, 37(8), 911-917.

Blöchl, E., Rachel, R., Burggraf, S., Hafenbradl, D., Jannasch, H.W., & Stetter, K.O., 1997. *Pyrolobus fumarii*, gen. and sp. nov., represents a novel group of archaea, extending the upper temperature limit for life to 113 C. Extremophiles, 1(1), 14-21.

Calvert, S.E., 1966. Accumulation of diatomaceous silica in the sediments of the Gulf of California. Geological Society of America Bulletin. 77: 569-596.

Cann, I.K. and Ishino, Y., 1999. Archaeal DNA replication: identifying the pieces to solve a puzzle. Genetics, 152(4), pp.1249-1267.

Cantwell, F.F., & Losier, M., 2002. Liquid—liquid extraction. In Comprehensive Analytical Chemistry (Vol. 37, pp. 297-340). Elsevier.

Castillo, P.R., Hawkins, J.W., Lonsdale, P.F., Hilton, D.R., Shaw, A. M., & Glascock, M.D., 2002. Petrology of Alarcon Rise lavas, Gulf of California: Nascent intracontinental ocean crust. Journal of Geophysical Research: Solid Earth, 107(B10).

Cruaud, P., Vigneron, A., Pignet, P., Caprais, J. C., Lesongeur, F., Toffin, L., Godfroy, A. & Cambon-Bonavita, M. A., 2015. Microbial communities associated with benthic faunal assemblages at cold seep sediments of the Sonora Margin, Guaymas Basin. Frontiers in Marine Science, 2, 53.

Curray, J. R., Moore, D.G., Lawver, L.A., Emmel, F.J., Raitt, R. W., Henry, M., & Kieckhefer, R., 1979. Tectonics of the Andaman Sea and Burma: convergent margins.

Dean, W.E., 2006. The geochemical record of the last 17,000 years in the Guaymas Basin, Gulf of California. Chemical Geology, 232(3), 87-98.

De la Lanza-Espino, G. and Soto, L.A., 1999. Sedimentary geochemistry of hydrothermal vents in Guaymas Basin, Gulf of California, Mexico. Applied Geochemistry, 14(4), pp.499-510.

De Rosa, M., & Gambacorta, A., 1988. The lipids of archaebacteria. Progress in lipid research, 27(3), 153-175.

Dhillon, A., Teske, A., Dillon, J., Stahl, D. A., & Sogin, M.L., 2003. Molecular characterization of sulfate-reducing bacteria in the Guaymas Basin. Applied and Environmental Microbiology, 69(5), 2765-2772.

Dick, G.J., Clement, B.G., Webb, S.M., Fodrie, F.J., Bargar, J.R., & Tebo, B.M., 2009. Enzymatic microbial Mn (II) oxidation and Mn biooxide production in the Guaymas Basin deep-sea hydrothermal plume. Geochimica et Cosmochimica Acta, 73(21), 6517-6530.

Dick, G. J., & Tebo, B. M., 2010. Microbial diversity and biogeochemistry of the Guaymas Basin deep-sea hydrothermal plume. Environmental microbiology, 12(5), 1334-1347.

Dombrowski, N., Seitz, K. W., Teske, A. P., & Baker, B. J., 2017. Genomic insights into potential interdependencies in microbial hydrocarbon and nutrient cycling in hydrothermal sediments. Microbiome, 5(1), 106.

Edgcomb, V.P., Kysela, D.T., Teske, A., de Vera Gomez, A., & Sogin, M.L., 2002. Benthic eukaryotic diversity in the Guaymas Basin hydrothermal vent environment. Proceedings of the National Academy of Sciences, 99(11), 7658-7662.

Einsele, G., Gieskes, J.M., Curray, J., Moore, D.M., Aguayo, E., Aubry, M.P., & Lyle, M., 1980. Intrusion of basaltic sills into highly porous sediments, and resulting hydrothermal activity. Nature, 283(5746), 441-445.

Erauso, G., Reysenbach, A.L., Godfroy, A., Meunier, J.R., Crump, B., Partensky, F., Baross, J.A., Marteinsson, V., Barbier, G., Pace, N.R. and Prieur, D., 1993. Pyrococcus abyssi sp. nov., a new hyperthermophilic archaeon isolated from a deep-sea hydrothermal vent. Archives of Microbiology, 160(5), 338-349.

Escartín, J., Barreyre, T., Cannat, M., Garcia, R., Gracias, N., Deschamps, A., & Ballu, V., 2015. Hydrothermal activity along the slow-spreading Lucky Strike ridge segment (Mid-Atlantic Ridge): Distribution, heatflux, and geological controls. Earth and Planetary Science Letters, 431, 173-185.

Galimov, E.M. and Kodina, L.A., 1983. Organic matter in oceanic sediments of high thermogradient (DSDP Leg 64, Gulf of California). Advances in Organic Geochemistry 1981, pp.431-437.

Gartman, A., Yücel, M., & Luther, G.W., 2014. An introduction to the major chemical components released from hydrothermal vents. Elsevier.

Gliozzi, A., Paoli, G., De Rosa, M. and Gambacorta, A., 1983. Effect of isoprenoid cyclization on the transition temperature of lipids in thermophilic archaebacteria. Biochimica et Biophysica Acta (BBA)-Biomembranes, 735(2), 234-242.

Hanford, M.J. and Peeples, T.L., 2002. Archaeal tetraether lipids. Applied biochemistry and biotechnology, 97(1), 45-62.

Harvey, H.R., Fallon, R.D. and Patton, J.S., 1986. The effect of organic matter and oxygen on the degradation of bacterial membrane lipids in marine sediments. Geochimica et Cosmochimica Acta, 50(5), pp.795-804.

Holden, J.F., Summit, M., & Baross, J.A., 1998. Thermophilic and hyperthermophilic microorganisms in 3–30 C hydrothermal fluids following a deep-sea volcanic eruption. FEMS Microbiology Ecology, 25(1), 33-41.

Hopmans, E.C., Weijers, J. W., Schefuß, E., Herfort, L., Damsté, J.S.S., & Schouten, S., 2004. A novel proxy for terrestrial organic matter in sediments based on branched and isoprenoid tetraether lipids. Earth and Planetary Science Letters, 224(1-2), 107-116.

Judd, A., & Hovland, M., 2009. Seabed fluid flow: the impact on geology, biology and the marine environment. Cambridge University Press.

Kashefi, K. and Lovley, D.R., 2003. Extending the upper temperature limit for life. Science, 301(5635), 934-934.
Kate, M., 1993. Membrane lipids of Archaea. In New Comprehensive Biochemistry (Vol. 26, pp. 261-295). Elsevier.
Kelley, D.S., Karson, J.A., Früh-Green, G.L., Yoerger, D.R., Shank, T.M., Butterfield, D.A., & Jakuba, M., 2005. A serpentinite-hosted ecosystem: the Lost City hydrothermal field. Science, 307(5714), 1428-1434.
Knappy, C.S., Chong, J.P. and Keely, B.J., 2009. Rapid discrimination of archaeal tetraether lipid cores by liquid chromatography-tandem mass spectrometry. Journal of the American Society for Mass Spectrometry, 20(1), 51-59.
Lindström, U.M., 2002. Stereoselective organic reactions in water. Chemical Reviews, 102(8), 2751-2772.
Lipp, J.S., & Hinrichs, K.U., 2009. Structural diversity and fate of intact polar lipids in marine sediments. Geochimica et Cosmochimica Acta, 73(22), 6816-6833.
Lipp, J.S., Morono, Y., Inagaki, F., & Hinrichs, K.U., 2008. Significant contribution of Archaea to extant biomass in marine subsurface sediments. Nature, 454(7207), 991-994.
Liu, X.L., Leider, A., Gillespie, A., Gröger, J., Versteegh, G.J. and Hinrichs, K.U., 2010. Identification of polar lipid precursors of the ubiquitous branched GDGT orphan lipids in a peat bog in Northern Germany. Organic Geochemistry, 41(7), 653-660.
Logemann, J., Graue, J., Köster, J., Engelen, B., Rullkötter, J., & Cypionka, H., 2011. A laboratory experiment of intact polar lipid degradation in sandy sediments. Biogeosciences, 8(9), 2547-2560.
Lonsdale, P., & Becker, K., 1985. Hydrothermal plumes, hot springs, and conductive heat flow in the Southern Trough of Guaymas Basin. Earth and Planetary Science Letters, 73(2-4), 211-225.
Macalady, J.L., Vestling, M.M., Baumler, D., Boekelheide, N., Kaspar, C.W. and Banfield, J.F., 2004. Tetraether-linked membrane monolayers in Ferroplasma spp: a key to survival in acid. Extremophiles, 8(5), 411-419.
MacGregor, B.J., Biddle, J.F., Siebert, J.R., Staunton, E., Hegg, E.L., Matthysse, A.G., & Teske, A., 2013. Why orange Guaymas Basin *Beggiatoa* spp. are orange: single-filament-genome-enabled identification of an abundant octaheme cytochrome with hydroxylamine oxidase, hydrazine oxidase, and nitrite reductase activities. Applied and environmental microbiology, 79(4), 1183-1190.
McCollom, T.M., & Seewald, J. S., 2007. Abiotic synthesis of organic compounds in deep-sea hydrothermal environments. Chemical Reviews, 107(2), 382-401.
McKay, L.J., MacGregor, B.J., Biddle, J.F., Albert, D.B., Mendlovitz, H.P., Hoer, D.R., Lipp, J.S., Lloyd, K.G. and Teske, A.P., 2012. Spatial heterogeneity and underlying geochemistry of phylogenetically diverse orange and white Beggiatoa mats in Guaymas Basin hydrothermal sediments. Deep Sea Research Part I: Oceanographic Research Papers, 67, pp.21-31.Moore, D. G. (1973). Plate-edge deformation and crustal growth, Gulf of California structural province. Geological Society of America Bulletin, 84(6), 1883-1906.
Nelson, D.C., Wirsen, C.O. and Jannasch, H.W., 1989. Characterization of large, autotrophic *Beggiatoa* spp. abundant at hydrothermal vents of the Guaymas Basin. Appl. Environ. Microbiol., 55(11), pp.2909-2917.

Offre, P., Spang, A. and Schleper, C., 2013. Archaea in biogeochemical cycles. Annual review of microbiology, 67, pp.437-457.

Pancost, R.D., Coleman, J.M., Love, G.D., Chatzi, A., Bouloubassi, I., & Snape, C.E., 2008. Kerogen-bound glycerol dialkyl tetraether lipids released by hydropyrolysis of marine sediments: A bias against incorporation of sedimentary organisms? Organic Geochemistry, 39(9), 1359-1371.

Pearson, A., Huang, Z., Ingalls, A.E., Romanek, C.S., Wiegel, J., Freeman, K.H., Smittenberg, R.H. and Zhang, C.L., 2004. Nonmarine crenarchaeol in Nevada hot springs. Applied Environmental Microbiology, 70(9), pp. 5229-5237.

Portail, M., Olu, K., Dubois, S.F., Escobar-Briones, E., Gelinas, Y., Menot, L., & Sarrazin, J., 2016. Food-web complexity in Guaymas Basin hydrothermal vents and cold seeps. PloS one, 11(9), e0162263.

Quinn, P.J., Brain, A.P.R., Stewart, L.C. and Kates, M., 1986. The structure of membrane lipids of the extreme halophile, *Halobacterium cutirubrum*, in aqueous systems studied by freeze-fracture. Biochimica et Biophysica Acta (BBA)-Biomembranes, 863(2), pp.213-223.

Radke, M., Welte, D.H. and Willsch, H., 1986. Maturity parameters based on aromatic hydrocarbons: Influence of the organic matter type. Organic geochemistry, 10(1-3), 51-63.

Romankevich, E.A., 2013. Geochemistry of organic matter in the ocean. Springer Science & Business Media.

Roussel, E. G., Bonavita, M. A. C., Querellou, J., Cragg, B. A., Webster, G., Prieur, D., & Parkes, R. J., 2008. Extending the sub-sea-floor biosphere. Science, 320(5879), 1046-1046.

Rossel, P.E., Lipp, J.S., Fredricks, H.F., Arnds, J., Boetius, A., Elvert, M. and Hinrichs, K.U., 2008b. Intact polar lipids of anaerobic methanotrophic archaea and associated bacteria. Organic Geochemistry, 39(8), 992-999.

Schouten, S., Baas, M., Hopmans, E.C. and Damste, J.S.S., 2008. An unusual isoprenoid tetraether lipid in marine and lacustrine sediments. Organic Geochemistry, 39(8), pp.1033-1038.

Schouten, S., Hopmans, E. C., & Damsté, J. S. S., 2013. The organic geochemistry of glycerol dialkyl glycerol tetraether lipids: a review. Organic geochemistry, 54, 19-61.

Schouten, S., Middelburg, J. J., Hopmans, E. C., & Damsté, J. S. S., 2010. Fossilization and degradation of intact polar lipids in deep subsurface sediments: a theoretical approach. Geochimica et Cosmochimica Acta, 74(13), 3806-3814.

Schubotz, F., Wakeham, S. G., Lipp, J. S., Fredricks, H. F., & Hinrichs, K. U., 2009. Detection of microbial biomass by intact polar membrane lipid analysis in the water column and surface sediments of the Black Sea. Environmental Microbiology, 11(10), 2720-2734.

Shioya, M. and Ishiwatari, R., 1983. Laboratory thermal conversion of sedimentary lipids to kerogen-like matter. Organic geochemistry, 5(1), pp.7-12.

Simoneit, B. R., 1993. Aqueous high-temperature and high-pressure organic geochemistry of hydrothermal vent systems. Geochimica et cosmochimica acta, 57(14), 3231-3243.

Simoneit, B., 1985. Hydrothermal petroleum: genesis, migration, and deposition in Guaymas Basin, Gulf of California. Canadian Journal of Earth Sciences, 22, 1919-1929

Simoneit, B.R. and Lonsdale, P.F., 1982. Hydrothermal petroleum in mineralized mounds at the seabed of Guaymas Basin. Nature, 295(5846), p.198-202.

Siskin, M., & Katritzky, A. R., 2001. Reactivity of organic compounds in superheated water: general background. Chemical Reviews, 101(4), 825-836.

Strąpoć, D., Picardal, F.W., Turich, C., Schaperdoth, I., Macalady, J.L., Lipp, J.S., Lin, Y.S., Ertefai, T.F., Schubotz, F., Hinrichs, K.U. and Mastalerz, M., 2008. Methane-producing microbial community in a coal bed of the Illinois Basin. Appl. Environ. Microbiol., 74(8), pp.2424-2432.

Sturt, H.F., Summons, R.E., Smith, K., Elvert, M. and Hinrichs, K.U., 2004. Intact polar membrane lipids in prokaryotes and sediments deciphered by high-performance liquid chromatography/electrospray ionization multistage mass spectrometry—new biomarkers for biogeochemistry and microbial ecology. Rapid Communications in Mass Spectrometry, 18(6), 617-628.

Teske, A., Callaghan, A. V., & LaRowe, D. E., 2014. Biosphere frontiers of subsurface life in the sedimented hydrothermal system of Guaymas Basin. Frontiers in Microbiology, 5, 362.

Teske, A., De Beer, D., McKay, L.J., Tivey, M.K., Biddle, J.F., Hoer, D., & Mendlovitz, H. P., 2016. The Guaymas Basin hiking guide to hydrothermal mounds, chimneys, and microbial mats: complex seafloor expressions of subsurface hydrothermal circulation. Frontiers in microbiology, 7.

Teske, A., Hinrichs, K.U., Edgcomb, V., de Vera Gomez, A., Kysela, D., Sylva, S.P. & Jannasch, H. W., 2002. Microbial diversity of hydrothermal sediments in the Guaymas Basin: evidence for anaerobic methanotrophic communities. Applied and Environmental Microbiology, 68(4), 1994-2007.

Teske, A., & Reysenbach, A. L., 2015. Hydrothermal microbial ecosystems. Frontiers in Microbiology, 6, 884.

Thunell, R.C., 1998. Seasonal and annual variability in particle fluxes in the Gulf of California: A response to climate forcing. Deep Sea Research Part I: Oceanographic Research Papers, 45(12), 2059-2083.

Tissot, B.P., 1984. Recent advances in petroleum geochemistry applied to hydrocarbon exploration. AAPG Bulletin, 68(5), 545-563.

Tissot, B.P. and Welte, D.H., 1984. From kerogen to petroleum. In Petroleum formation and occurrence. 160-198

Tsuzuki, N., Takeda, N., Suzuki, M., & Yokoi, K. (1999). The kinetic modeling of oil cracking by hydrothermal pyrolysis experiments. International Journal of Coal Geology, 39(1), 227-250.

Vigneron, A., Cruaud, P., Roussel, E. G., Pignet, P., Caprais, J.C., Callac, N., Ciobanu, M.C., Godfroy, A., Cragg, B.A., Parkes, J.R & Van Nostrand, J. D., 2014. Phylogenetic and functional diversity of microbial communities associated with subsurface sediments of the Sonora Margin, Guaymas Basin. PloS one, 9(8), e104427.

Wang, K., & Davis, E. E., 1992. Thermal effects of marine sedimentation in hydrothermally active areas. Geophysical Journal International, 110(1), 70-78.

White, D.C., Bobbie, R.J., King, J.D., Nickels, J., & Amoe, P., 1979. Lipid analysis of sediments for microbial biomass and community structure. In Methodology for biomass determinations and microbial activities in sediments. ASTM International, 87-103.

Williams, D.L., Becker, K., Lawver, L.A., & Von Herzen, R.P., 1979. Heat flow at the spreading centers of the Guaymas Basin, Gulf of California. Journal of Geophysical Research: Solid Earth, 84(B12), 6757-6769.

Wörmer, L., Lipp, J.S., & Hinrichs, K.U., 2017. Comprehensive analysis of microbial lipids in environmental samples through HPLC-MS protocols. Hydrocarbon and Lipid Microbiology Protocols: Petroleum, Hydrocarbon and Lipid Analysis, 289-317.

Xu, D., Li, R., Hu, C., Sun, P., Jiao, N., & Warren, A., 2017. Microbial Eukaryote Diversity and Activity in the Water Column of the South China Sea Based on DNA and RNA High Throughput Sequencing. Frontiers in microbiology, 8, 1121.

Yoshinaga, M.Y., Kellermann, M.Y., Rossel, P.E., Schubotz, F., Lipp, J.S. and Hinrichs, K.U., 2011. Systematic fragmentation patterns of archaeal intact polar lipids by high-performance liquid chromatography/electrospray ionization ion-trap mass spectrometry. Rapid Communications in Mass Spectrometry, 25(23), pp.3563-3574.

Zhang, Yi Ge; Zhang, Chuanlun L.; Liu, Xiao-Lei; Li, Li; Hinrichs, Kai-Uwe; Noakes, John E., 2011. Methane Index: A tetraether archaeal lipid biomarker indicator for detecting the instability of marine gas hydrates. Earth and Planetary Science Letters. 307 (3–4), 525–534.

Zhu, C., Lipp, J.S., Wörmer, L., Becker, K.W., Schröder, J., & Hinrichs, K.U., 2013. Comprehensive glycerol ether lipid fingerprints through a novel reversed phase liquid chromatography–mass spectrometry protocol. Organic Geochemistry, 65, 53-62.

Chapter 2: Archaeal polar lipid biosignatures of the Cathedral Hill hydrothermal vent complex in Guaymas Basin, Gulf of California.

Jeremy N. Bentley [a,*], Carl A. Peters [a], G. Todd Ventura [a]
[a] *Department of Geology, Saint Mary's University, Halifax, Nova Scotia B3H 3C3, Canada.*
* *Corresponding author: Jeremy.Bentley@smu.ca*

Number of pages: 52
Number of Figures: 13
Number of Tables: 3
For submission to: TBD

Abstract

A survey of intact polar lipids (IPLs) and core lipids (CLs) with a particular focus on archaeal lipids was conducted on a push core transect at the Cathedral Hill hydrothermal vent complex. This study was conducted by extracting sediments using a modified Bligh and Dyer extraction protocol and analyzing the resulting extract on an HPLC-QTOF-MS. Lipids were identified based on their elution patterns and mass spectral fragmentation as outlined in the literature. The IPLs from archaea, specifically monoglycosyl glycerol dialkyl glycerol tetraethers (1G-GDGTs), were identified indicating that archaeal communities extend into intervals that experience ~145°C, which is currently outside the known habitability range for life. This findings was supported by indications that these communities were adapting to the extreme conditions. For example, the ring index of 1G-GDGTs shows a preferential selection of core structures containing either GDGT-3, 4 or 5', which is likely as an adaptation strategy influence by lipid packing. Similar trends have been observed in the core lipid that are found in the sediments. Additionally this study suggests that GDGT recycling or assimilation occurs within the sediments of Cathedral Hill.

Highlights

1 – Archaeal intact polar lipids found at Cathedral Hill are limited to mono and diglycosidic head groups, ultimately showing a lack of diversity in IPLs within the system.

2 – The ring index for both IPLs (modified ring index) and core GDGTs show an adaptation to the environmental stresses, by increasing ring moieties.

3- 1G-GDGTs show a preference for GDGT-3, 4 and 5' in samples that experience elevated heat, which is likely related to lipid packing.

4 - 1G-GDGTs are found at ~145°C, potentially pushing the boundary for life.

1. Introduction

Signature lipids, such as phospho- and glycolipids are fundamental components of cellular membranes. These lipids are incorporated into soils and sediments from organisms living within the substrate or are components from senescenced cells that have been deposited as a component of immature sedimentary organic matter (Killops and Killops, 2005). Membrane lipid contributions in sediments are sourced from the three domains of life (Archaea, Bacteria and Eukarya). The membrane lipids of Archaea fundamentally differ from that of Eukarya and most bacteria in their structural configuration. For example, archaeal membrane lipids are composed of isoprenoidal phytanyl or biphytanyl hydrocarbon skeletons that are connected via ether bonds to a glycerol backbone (Koga et al., 2007). Alternatively, the membrane lipids of Eukarya and most bacteria are composed of acyl hydrophobic tails that are ester bound to a glycerol (White et al., 1992). Both ether and ester bonds help stabilize the lipid's hydrocarbon skeleton. However, ester bound lipids are less thermodynamically and kinetically stable. As such, the structural configuration of a cellular membrane plays an integral role in the stability of a membrane when exposed to environmental stress (Chang, 1994). Many Archaea also tend to form monolayers instead of lipid bilayers membranes, which are prominent in bacteria and Eukarya. The presence of a membrane-spanning lipid or monolayer allows for tighter packing of the cellular membrane, which increases the rigidity of the membrane itself (Vieille, & Zeikus, 2001; Gliozzi et al., 2002; Jeworrek et al., 2011).

Lipidomic studies tend to focus on both intact polar lipids (IPLs) and core lipids (CLs), which ultimately represent two different pools of life, the living (IPLs) and

the dead or fossil lipid (CL). This is due to the nature of the polar headgroups of IPLs, which are only stable for days to several weeks in the environment outside a living cell (Sturt et al., 2004; Lipp et al., 2008; Lipp and Hinrichs, 2009; Huguet et al., 2010). With such short longevity, these labile compounds represent diagnostic biomarkers of living microorganisms in sedimentary environments. IPLs are therefore commonly used to track the habitable range and thermal limits of the deep biosphere (Biddle et al., 2006; Lipp et al., 2008; Lipp and Hinrichs, 2009; Sollich et al., 2017). The archaeal communities appear to adapt their core lipids structures to the high temperature conditions of the surrounding environment (Gliozzi et al., 1983; De Rosa and Gambacorta, 1988) and these lipids may become preserved as fossil geolipids after cell death. Additionally, core lipids may be deposited from the water column and subsequently buried and preserved.

The thermochemical stability of a lipid ultimately determines its preservation potential. The potential for lipids to be preserved in sediments is much greater compared to the potential of carbohydrates, proteins, and simple to complex nucleic acids such as DNA, which are rather labile in nature. However, the amount of information that can be obtained out of an organism from its lipids is limited when compared to more detailed RNA and DNA signatures. This is mainly due to the biosynthesis of lipid classes overlapping across multiple phyla. Thus, it is not possible to fully constrain living subsurface communities with lipidomics alone.

Guaymas Basin has been an area of interest for a number of microbiological studies, as vent complexes that are dominated by microbial mats are present within the basin and at our study area of Cathedral Hill (Canganella et al., 1998; McKay et al., 2012; Meyers et al., 2013). However, for a comprehensive overview of the basin and the biota

present, specifically within the Southern Trough region, the reader is referred to Teske et al. (2016).

Archaeal core lipids in Guaymas Basin have been investigated by Schouten et al. (2003) who documented the distribution and isotopic compositions of GDGTs, finding that anaerobic oxidation of methane by methanotrophic Archaea occurs in the subsurface and hot sediment layer of active hydrothermal sites. This indicates that thermophilic Archaea in the area are capable of oxidizing methane at temperatures greater than 30°C. Another study is by McClymont et al. (2012), who used sediment traps to reconstruct sea surface temperatures (SST) which have demonstrated that seasonal variations occur within glycerol dialkyl glycerol tetraethers (GDGTs) based proxies. Additionally, degradation products of GDGTs in Guaymas Basin samples were determined by Liu et al. (2016), showing the plausible degradation pathways from glycerol ethers to isoprenoidal fatty acids.

This study investigates the stratigraphic trends of archaeal lipids, and to a much lesser extent, bacterial and eukaryotic lipid diversities observed within a push core transect collected at the Cathedral Hill hydrothermal vent system at Guaymas Basin, Gulf of California. This transect traverses a wide range of pore water temperatures that result from mixing of the hydrothermal vent fluids that have been reported to reach up to 350°C (Campbell et al., 1985; Haberstroh & Karl, 1989; Teske et al., 2014) with cold 2°C ocean bottom waters. High sedimentation rates coupled with high upper water column productivity have resulted in near uniform accumulations of organic-rich sediments (Calvert, 1966; Gieskes et al., 1988; Williams et al., 1979). The sediments of this transect enable assessment of organic matter preservation and microbial community structure through a system that experiences similar inputs from sedimentation. However, the

sediments experience vastly different subsurface geochemical conditions that are largely driven by exposure to hydrothermal vent fluids and the associated high temperatures. In addition to potentially identifying community differences, the thermal stability of these lipid classes are also evaluated in a natural setting. This study attempts to shed light on the upper limits on the thermostability of these lipids, which may be useful in better understanding the upper temperature limits of life.

2. Material and methods

2.1. Samples

A transect of four push cores sampled at ~ 2 m spacing was collected at Cathedral Hill (27°0.629' N, 111°24.265' W), within the Guaymas Basin, Gulf of California at a water depth of approximately 2000 m using the DSV-2 Alvin, a manned submersible from Woods Hole Oceanographic Institution (WHOI) on Dive 4462 (10/22/08). Accompanying these push cores was also the collection of *in situ* thermal-probe measurements collected every 5 cmbsf. These data points were then extrapolated linearly producing the thermal model for the system (figure 2.1). Once collected, the push cores were sectioned into 2-3 cm intervals. The sediments were transferred to combusted glass vials stored at −80°C until samples could be freeze-dried and again stored under the same refrigerated conditions.

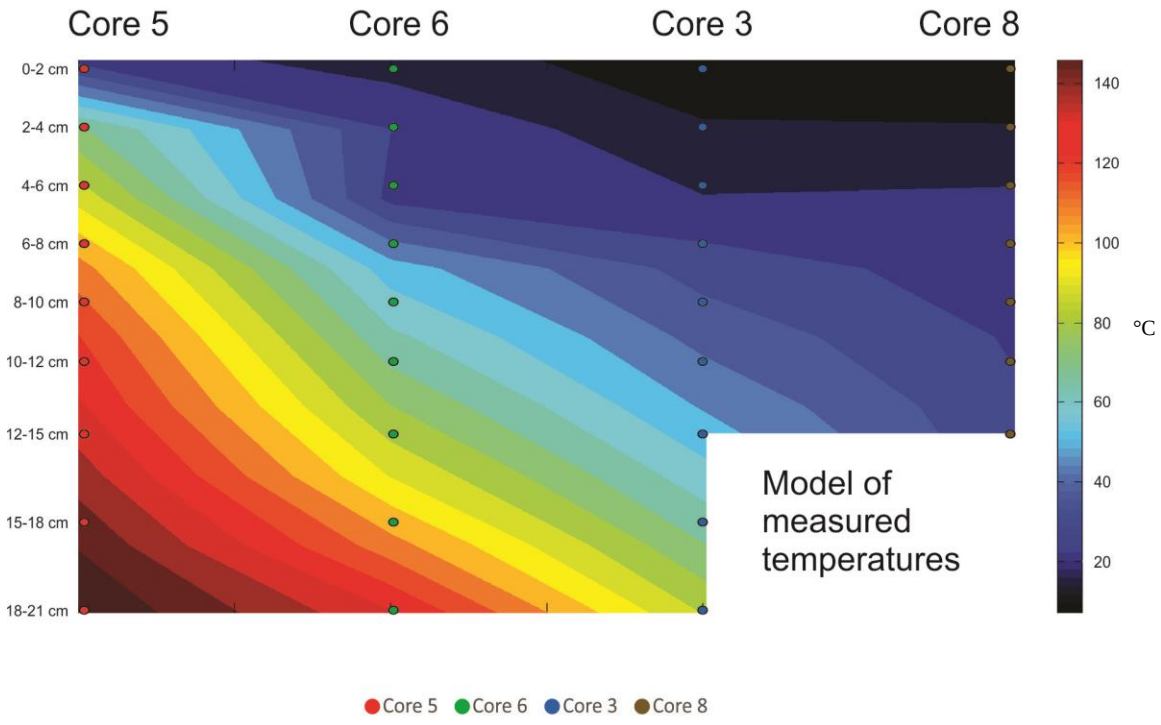

Figure 2.1- Reconstructed temperature model generated from in situ temperature measurements using a thermal probe. Horizontal position is approximately over an 8 m distance, but exact lateral position of the cores is not accurate. Dots represent the middle of the depth interval for each sample.

2.2. Sample extraction

Each dry-powdered, sediment sample was homogenized and spiked with an internal standard (1-alkyl-2-acetoyl-sn-glycero-3-phosphocholine (PAF)) prior to extraction by a modified Bligh and Dyer (MBD) protocol as outlined in Sturt et al. (2004). Lipids were extracted in six steps with varying solvent mixtures. The first four steps were performed with ~ 6 ml of methanol/dichloromethane/buffer [2:1:0.8; v/v] with steps one and two employing a phosphate buffer (5.5g/L Na_2HPO_4 adjusted to pH of 7.4) and steps three and four using a trichloroacetic acid buffer (50 g/L $C_2HCl_3O_2$ with a pH of 2). The final two steps used a ~ 6 ml methanol/dichloromethane [5:1; v/v]. Each

extraction step was sonicated for 5 minutes followed by 5 minutes of centrifugation at 1250 rpm. The solvent was then decanted and combined in a separation funnel. The resulting total lipid extract (TLE) was purified with milli-Q water and evaporated to dryness under a continuous stream of dry nitrogen at 60 °C. The TLE was then spiked with 1,2-diheneicosanoyl-sn-glycero-3-phosphocholine (C_{21}-PC) and stored at -20°C until analysis. For each extraction, approximately 2-3 grams of freeze-dried sediment was used.

2.3. Analysis of lipids

An aliquot of each sample representing 1% of the TLE was injected into an Agilent 1260 infinity high performance liquid chromatography-quadrupole time of flight mass spectrometer (HPLC-qToF-MS). The HPLC was fitted with a ZORBAX RRHD Eclipse Plus C18 column (2.1 mm × 150 mm × 1.8 μm) with an Agilent Guard Column maintained at 45 °C using a flow rate of 0.25 mL/min. The reverse phase electrospray ionization (ESI) method for this study was modified from Zhu et al. (2013). Each analysis started with mobile phase A (methanol/formic acid/ammonium hydroxide [100:0.04:0.10] v/v) held at 100% for 10 min., which was then progressively mixed with a second mobile phase B (propan-2-ol/formic acid/ammonium hydroxide [100:0.04:0.10] v/v) following a linear gradient that transitioned from: 100% A to 76% A and 24% B over 15 min., 35% A and 65% B to 90 min., that finished by reverting back to 100% A for column cleaning to complete a 120 minute run.

2.4. Quantification of lipids

Quantification was achieved by summing the integration peak areas of $[M+H]^+$, $[M+NH_4]^+$, and $[M+Na]^+$ for the respective lipids of interest. Once the values for the integrated sample peak were measured, analyte concentrations were calculated relative to the internal C_{21}-PC standard and reported in μg/g sediment. For simplicity, identification of lipids in section 3 are reported only as $[M+H]^+$; however, concentration values are based on the sum of all three adducts.

Response factors from the instrument were determined by a series of injections of standard solutions containing: (1,2-diacyl-3-O-(α-D-galactosyl1-6)-β-D-galactosyl-sn-glycerol (DGDG), 1,2-diacyl-3-O-β-D-galactosyl-sn-glycerol (MGDG), 1-alkyl-2-acetoyl-sn-glycero-3-phosphocholine (PAF), 1,2-di-O-phytanyl-sn-glycerol (Archaeol), 1',3'-bis[1,2-dimyristoyl-sn-glycero-3-phospho]-glycerol (14:0 Cardiolipin), 1,2-diheneicosanoyl-sn-glycero-3-phosphocholine (C_{21}-PC) from Matreya, USA; Avanti Polar Lipids, USA and 2,2'-di-O-decyl-3,3'-di-O-(1'',ω''-eicosanyl)-1,1'-di-(rac-glycerol) (C_{46}-GTGT) Pandion Laboratories, LLC) in amounts ranging from 100 pg to 30 ng. Concentrations of the standard mix were calculated from peak areas of molecular ions in mass chromatograms. Response factors were calculated relative to C_{21}-PC, and the appropriate correction factor was applied to the particular lipid class of interest.

3. Results

3.1. Total lipid extract

The TLEs obtained from the MBD are reported in µg/g sediment (Table 1). These values were also plotted with depth (Figure 2.2). Cores 5, 6, and 3 show similar trends of decreasing TLE with depth. Core 5 has the highest TLE concentration observed at the surface interval (~11550 µg/g sediment). The TLE concentrations in Core 5 decreases with depth to concentrations of ~ 1700 µg/g sediment. Furthermore, within all of the cores within the microbial mat (5, 6 and 3) the TLE concentration levels off with depth, to yield a uniform recovery of ~1800 µg/g of sediment. These trends are not observed in Core 8 in which the TLE progressively increases with depth.

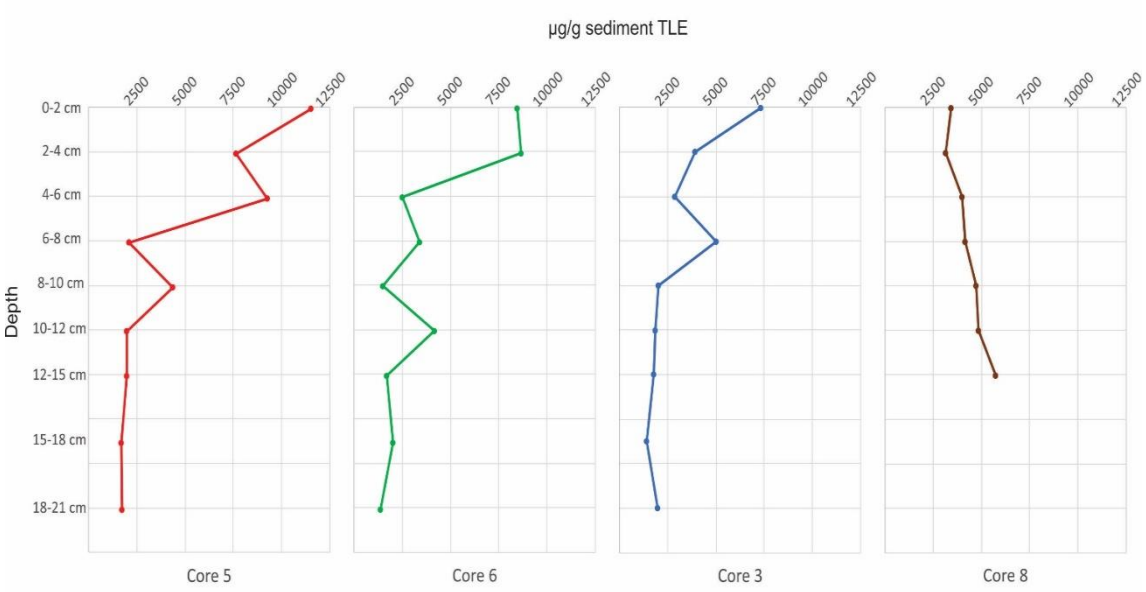

Figure 2.2 – Down core profiles of TLE concentrations for each core showing systematic decreases in Core 5, 6 and 3 with depth, and a gradual increase in TLE with depth for core 8.

Table 1 - overview of sample set

Core ID	Depth Interval (cmbsf)	Pore water temperature (°C)	Dry sediment weight (g)	Total lipid extract (TLE) weight (µg/g)
GB4462-5	0-2	19	2.40	11552.30
GB4462-5	2-4	67	2.10	7648.24
GB4462-5	4-6	85	2.04	9266.01
GB4462-5	6-8	105	2.83	2088.34
GB4462-5	8-10	117	2.48	4378.05
GB4462-5	10-12	125	2.52	1972.22
GB4462-5	12-15	135	2.62	1992.37
GB4462-5	15-18	145	3.01	1691.03
GB4462-5	18-21	153	2.94	1722.03
GB4462-6	0-2	11	2.12	8476.19
GB4462-6	2-4	22	2.30	8653.51
GB4462-6	4-6	20	3.30	2509.15
GB4462-6	6-8	47	2.84	3383.80
GB4462-6	8-10	60	3.34	1480.48
GB4462-6	10-12	73	2.39	4185.87
GB4462-6	12-15	87	3.50	1694.29
GB4462-6	15-18	105	3.50	2011.56
GB4462-6	18-21	125	3.48	1382.18
GB4462-3	0-2	3	2.81	7313.17
GB4462-3	2-4	8	2.88	3909.72
GB4462-3	4-6	15	2.45	2864.75
GB4462-3	6-8	26	2.80	5003.58
GB4462-3	8-10	34	2.80	2017.99
GB4462-3	10-12	43	3.15	1863.49
GB4462-3	12-15	54	3.15	1777.78
GB4462-3	15-18	66	2.45	1428.57
GB4462-3	18-21	80	2.80	1981.95
GB4462-8	0-2	0	2.80	3440.43
GB4462-8	2-4	8	2.80	3166.06
GB4462-8	4-6	16	2.55	4000.00
GB4462-8	6-8	18	2.80	4185.45
GB4462-8	8-10	21	3.33	4755.29
GB4462-8	10-12	23	2.44	4843.62
GB4462-8	12-15	25	0.32	5741.94

Table 2 - Summary of lipids present within the transect

Peak #	Domain	Chemical name	Abbreviated name	Rt (Min)	Molecular ion $[M+H]^+$	Diagnostic fragment ion	References
1	A	Diglycosidic Archaeol	2G-AR	20	977.7862	653, 373	Lipp and Hinrichs, 2009; Yoshinaga et al., 2011
2	A	Monoglycosidic Archaeol	1G-AR	22	815.7334	653, 373	Lipp and Hinrichs, 2009; Yoshinaga et al., 2011
3	E	Hydroxychlorophyll *a*	OH-Chlo	22	909.5502	593.3, 533.5	Chen et al., 2015
4	E	Hydroxypheophytin *a*	OH-Pheo	23	887.5782	591, 609	Chen et al., 2015; Milenkovic et al., 2012
5	E	Chlorophyll *a*	Chlo	26	893.5422	593.3, 533.5	Chen et al., 2015; Milenkovic et al., 2012
6	E	Pheophytin *a*	Pheo	28	871.5721	591, 609	Chen et al., 2015
7	A	Archaeol	AR	30	653.6806	373.3	Lipp and Hinrichs, 2009; Yoshinaga et al., 2011
8	E	Unknown ceramide - 1	U-Cer-1	38.9	*946.9543	510.5, 492.5	Yurkova et al., 2005; Burla et al., 2018
9	E	Unknown ceramide - 2	U-Cer-2	40	*948.9718	512.5, 494.5	Yurkova et al., 2005; Burla et al., 2018
10	A	Methoxy-Archaeol	1MeO-AR	41	667.6963	373.3, 355.4	Elling et al., 2014
11	B?	Unknown diglyceride - 1	U-DAG-1	48	*829.7251	551.5	-
12	B?	Unknown diglyceride - 2	U-DAG-2	55	*855.7200	579.5, 551.5, 441.4	-

13a-c	A	Hydroxylated glycerol dialkanol diether	OH-GDD (0-2)	57	1262.2913, 1260.2757, 1258.2601,	686.6	Liu et al., 2012
14a-c	A	Hydroxyl diglycosidic glycerol dialkyl glycerol tetraether	2G-OH-GDGT-0; 2G-OH-GDGT-2	59	1642.4283, 1640.4075, 1638.3919	1318.3, 760.7, 668.7	Lipp and Hinrichs, 2009; Liu et al., 2012c
15	B & A?	Branched glycerol dialkyl glycerol tetraether	brGDGT	63	1022.01, 1019.99, 1017.98, 1036.03, 1034.01, 1031.99, 1050.04, 1048.03, 1046.01	Ia) 525.5, 489.6	Schouten et al., 2000; Hopmans et al., 2004, De Jonge et al., 2013
16	A	Hydroxyl monoglycosidic glycerol dialkyl glycerol tetraether	1G-OH-GDGT (0-2)	65	1480.3704, 1478.3548, 1476.3391	1318.3, 760.7, 668.7	Lipp and Hinrichs, 2009; Liu et al., 2012c
17	A	Diglycosidic glycerol dialkyl glycerol tetraether	2G-GDGT-0; 2G-GDGT-2	71	1626.4283, 1624.4127, 1622.3970,	1302.3, 743.7, 651.7	Stuart et al., 2004; Meador et al., 2014
18a-f	A	Glycerol dialkanol diether	GDD	72	1246.2965, 1244.2808, 1242.2652, 1240.2495, 1238.2339, 1236.2182	669.6	Liu et al., 2012a
19a-c	A	Hydroxyl Glycerol dialkyl glycerol tetraether	OH-GDGT-0; OH-GDGT-2	79	1318.3176, 1316.3019. 1314.2863	1302.3, 743.7, 651.7	Liu et al., 2012a
20a-f	A	Monoglycosidic glycerol dialkyl glycerol tetraether	1G-GDGT-0; 1G-GDGT-5+5’	82	1464.3755, 1462.3598, 1460.3442, 1458.3285 1456.3129, 1454.2972	1302.3, 743.7, 651.7	Stuart et al., 2004
21a-f	A	Glycerol dialkyl glycerol tetraether	GDGT-0; GDGT-5+5’	95-100	1302.3226, 1300.3070, 1298.2914, 1296.2757, 1294.2601, 1292.2444	1302.3, 743.7, 651.7	Hopmans et al., 2000; Schouten et al., 2013; Lengger et al., 2018

*all reported mass fragment ions are of structures containing no cyclization.
5’ indicates the regioisomer of the lipid of interest.
Domains are reported as letters where A represents Archaea, B represents Bacteria and E represents Eukarya. The “?’ is used to define current uncertainty in the literature.

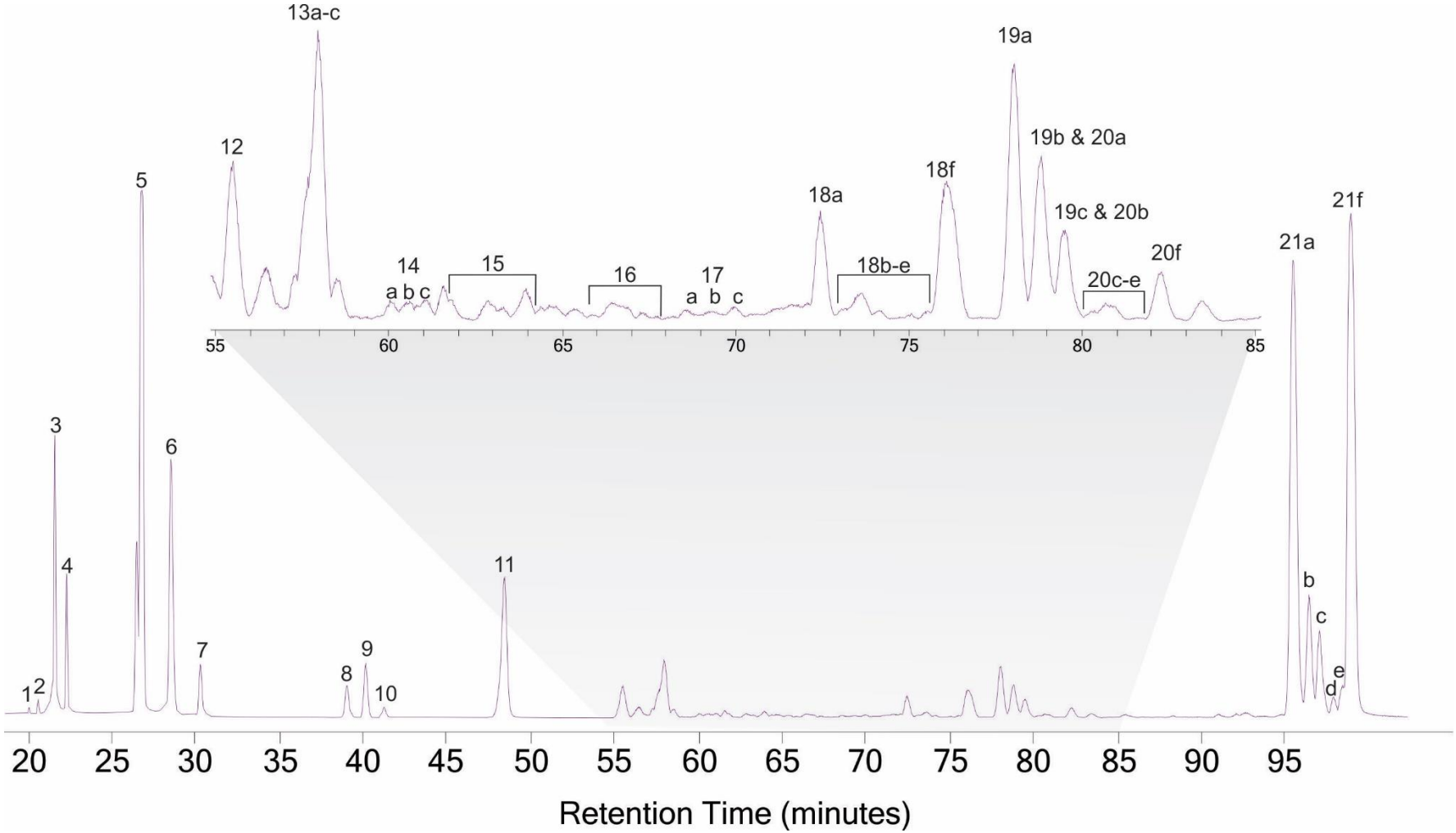

Figure 2.3 - Reconstructed base peak chromatogram (BPC) indicating the detectable lipids extracted from the Cathedral Hill sediments (corresponding identification from the numbered peaks is provided in Table 2).

Table 3 - Lipid concentrations by core (μg/g sediment)

Sample ID	cGDGTs	brGDGTs	OH-GDGTs	1G-GDGTs	1G-OH-GDGTs	2G-GDGTs	2G-OH-GDGTs	GDDs	OH-GDDs	C-AR	1G-AR	1MeO-AR	2G-AR	OH-Pheo	Pheo	OH-Chlorophyll *a*	Chlorophyll *a*
GB4462-5 0-2 cm	506.01	5.19	25.76	14.86	1.41	2.46	4.28	31.37	2.59	13.68	0.77	1.60	0.73	4.09	0.28	6.21	1.09
GB4462-5 2-4 cm	459.21	5.75	24.07	13.37	1.86	1.74	2.97	35.39	3.16	31.52	1.37	1.49	0.75	1.21	0.06	1.74	0.28
GB4462-5 4-6 cm	204.18	2.37	10.38	6.00	0.82	0.00	1.10	17.71	1.18	6.81	0.80	0.57	0.41	0.04	0.00	0.06	0.00
GB4462-5 6-8 cm	153.66	1.98	6.69	4.31	0.97	0.00	0.66	14.84	0.87	4.89	0.94	0.40	0.30	0.00	0.00	0.00	0.00
GB4462-5 8-10 cm	60.10	1.07	2.41	3.19	0.78	0.00	0.07	8.59	0.17	2.49	0.67	0.07	0.03	0.00	0.00	0.00	0.00
GB4462-5 10-12 cm	49.73	1.52	1.63	1.66	0.28	0.00	0.00	8.62	0.18	2.14	0.32	0.05	0.00	0.00	0.00	0.00	0.00
GB4462-5 12-15 cm	84.29	3.29	1.39	1.39	0.06	0.00	0.00	10.29	0.00	3.75	0.12	0.10	0.00	0.00	0.00	0.00	0.00
GB4462-5 15-18 cm	44.91	1.12	0.43	0.11	0.00	0.00	0.00	9.89	0.00	2.11	0.00	0.06	0.00	0.00	0.00	0.00	0.00
GB4462-5 18-21 cm	39.84	0.86	0.26	0.00	0.00	0.00	0.00	9.75	0.00	2.17	0.00	0.05	0.00	0.00	0.00	0.00	0.00

Sample ID	cGDGTs	brGDGTs	OH-GDGTs	1G-GDGTs	1G-OH-GDGTs	2G-GDGTs	2G-OH-GDGTs	GDDs	OH-GDDs	C-AR	1G-AR	1MeO-AR	2G-AR	OH-Pheo	Pheo	OH-Chlorophyll *a*	Chlorophyll *a*
GB4462-6 0-2 cm	595.98	7.05	28.84	16.20	1.53	2.32	3.62	37.37	3.60	11.19	0.94	1.97	1.08	9.75	0.56	12.53	1.99
GB4462-6 2-4 cm	267.74	4.00	14.81	6.69	0.78	1.03	1.77	22.93	1.97	4.84	0.53	0.88	0.25	1.64	0.10	2.25	0.28
GB4462-6 4-6 cm	88.12	1.68	4.67	2.27	0.49	0.31	0.47	13.93	0.69	3.18	0.47	0.17	0.23	0.02	0.00	0.03	0.00
GB4462-6 6-8 cm	71.46	2.80	3.08	3.33	0.93	0.08	0.24	10.55	0.37	4.28	1.04	0.10	0.23	0.00	0.00	0.00	0.00
GB4462-6 8-10 cm	49.63	1.29	1.81	1.98	0.59	0.00	0.03	10.25	0.18	2.46	0.58	0.07	0.04	0.00	0.00	0.00	0.00
GB4462-6 10-12 cm	53.18	1.51	2.07	1.97	0.35	0.00	0.00	8.26	0.21	3.43	0.60	0.08	0.02	0.00	0.00	0.00	0.00
GB4462-6 12-15 cm	45.19	1.12	1.37	1.00	0.16	0.00	0.00	10.40	0.14	2.80	0.31	0.07	0.00	0.00	0.00	0.00	0.00
GB4462-6 15-18 cm	22.95	0.66	0.12	0.00	0.00	0.00	0.00	9.66	0.00	1.74	0.00	0.03	0.00	0.00	0.00	0.00	0.00
GB4462-6 18-21cm	31.82	1.00	0.35	0.00	0.00	0.00	0.00	9.95	0.00	2.63	0.00	0.04	0.00	0.00	0.00	0.00	0.00

Sample ID	cGDGTs	brGDGTs	OH-GDGTs	1G-GDGTs	1G-OH-GDGTs	2G-GDGTs	2G-OH-GDGTs	GDDs	OH-GDDs	C-AR	1G-AR	1MeO-AR	2G-AR	OH-Pheo	Pheo	OH-Chlorophyll *a*	Chlorophyll *a*
GB4462-3 0-2 cm	513.50	7.73	30.60	14.17	1.22	1.72	3.28	42.46	4.07	4.21	0.43	2.00	0.26	17.28	0.62	20.51	2.07
GB4462-3 2-4 cm	309.79	4.07	15.89	7.56	0.84	0.98	1.63	20.98	1.97	3.64	0.65	0.98	0.21	10.42	0.39	11.32	1.15
GB4462-3 4-6 cm	284.17	3.82	14.77	6.38	0.63	0.74	1.23	21.76	1.84	3.46	0.43	0.83	0.19	4.16	0.34	5.32	1.17
GB4462-3 6-8 cm	276.48	4.18	15.24	6.79	0.79	0.94	1.43	24.89	1.76	5.02	0.52	0.72	0.17	2.05	0.20	2.79	0.69
GB4462-3 8-10 cm	252.32	5.19	13.69	5.18	1.00	0.73	1.25	24.48	2.11	5.03	0.91	0.66	0.11	0.37	0.00	0.63	0.08
GB4462-3 10-12 cm	229.71	5.20	13.21	5.33	1.70	0.66	1.12	21.74	1.84	7.88	1.32	0.28	0.15	0.12	0.00	0.28	0.00
GB4462-3 12-15 cm	180.75	5.11	10.08	6.53	1.85	0.00	0.28	16.93	1.00	8.58	1.47	0.19	0.13	0.01	0.00	0.03	0.00
GB4462-3 15-18 cm	254.38	10.99	12.38	6.45	1.92	0.00	0.41	14.47	1.18	11.47	2.59	0.21	0.16	0.00	0.00	0.00	0.00
GB4462-3 18-21 cm	186.72	4.88	9.31	5.22	1.29	0.00	0.18	15.08	0.80	11.02	1.80	0.18	0.00	0.00	0.00	0.00	0.00

Sample ID	cGDGTs	brGDGTs	OH-GDGTs	1G-GDGTs	1G-OH-GDGTs	2G-GDGTs	2G-OH-GDGTs	GDDs	OH-GDDs	C-AR	1G-AR	1MeO-AR	2G-AR	OH-Pheo	Pheo	OH-Chlorophyll *a*	Chlorophyll *a*
GB4462-8 0-2 cm	486.08	6.36	27.77	11.12	0.95	1.14	1.67	36.92	3.37	3.22	0.42	1.46	0.08	14.65	0.41	18.73	1.60
GB4462-8 2-4 cm	419.45	5.43	21.35	8.83	0.85	0.87	1.28	30.56	2.57	3.11	0.45	1.05	0.08	7.83	0.41	10.32	1.74
GB4462-8 4-6 cm	482.69	6.64	26.81	11.03	1.17	1.18	1.86	35.20	3.41	4.19	0.53	1.35	0.16	8.96	0.47	11.50	1.64
GB4462-8 6-8 cm	361.13	4.68	18.60	8.82	0.94	0.84	1.26	26.61	2.23	3.16	0.42	0.79	0.11	6.40	0.29	8.27	0.98
GB4462-8 8-10 cm	154.65	2.22	9.66	2.42	0.42	0.37	1.52	16.27	0.80	2.41	0.32	0.15	0.00	1.04	0.06	1.27	0.16
GB4462-8 10-12 cm	462.82	6.77	23.28	6.47	1.15	2.01	3.43	34.16	3.43	6.23	0.79	0.68	0.00	7.64	0.19	9.20	0.47
GB4462-8 12-15 cm	517.35	6.27	22.57	6.05	0.75	0.00	0.00	29.61	3.67	5.61	1.01	0.60	0.00	4.72	0.00	8.11	0.00

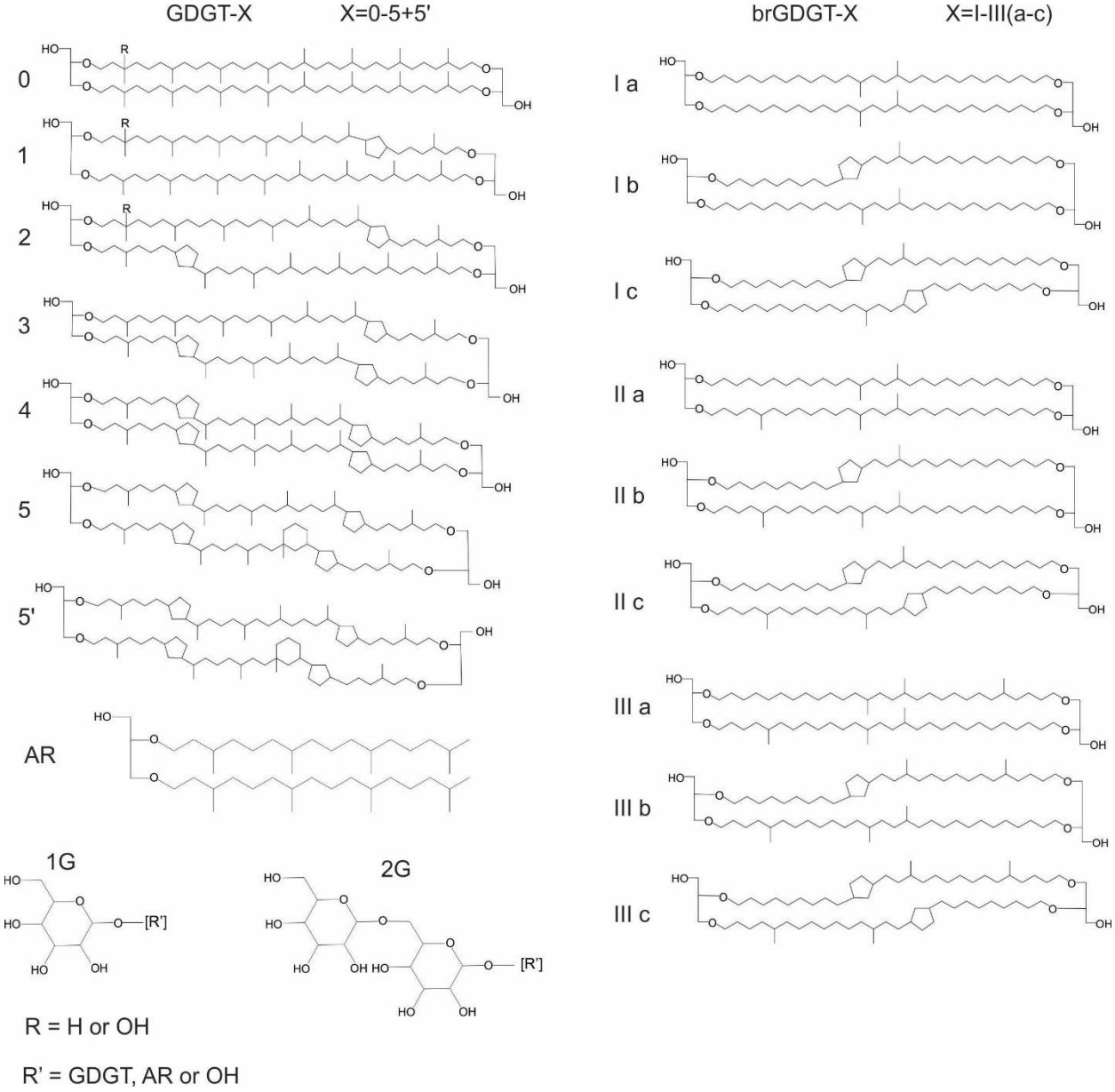

Figure 2.4 - Chemical structures of lipids of various archaeal and bacterial lipids identified at the Cathedral Hill vent site.

3.2. Archaeal lipids

3.2.1. Intact archaeal lipids

All archaeal IPLs within the push core sample set are tentatively identified by their mass spectral characteristics and elution pattern as previously presented from the literature (Table 2). The identified archaeal IPLs are exclusively glycolipids containing either monoglycosyl (1G) or diglycosyl (2G) head groups linked to either a C_{40} glycerol dialkyl glycerol tetraether (GDGT) or a C_{20} diphytanyl diether (archaeol). Monoglycosyl IPLs include 1G-GDGT, which is represented by peak 20 in Figure 2.3 and adjacent peaks 20 a-f structures with isoprenoid core lipid having 0-4 cyclopentyl moieties. The last GDGT structure (peak 20f) contains four cyclopentyl and one cyclohexyl moiety (Figure 2.3). The signals for these compounds were monitored as $[M+H]^+$ on the *m/z* 1464.38, 1462.36, 1460.34, 1458.33 1456.31, 1454.30 mass chromatograms. Additionally, mass fragments consistent with the loss of a biphytane (*m/z* 743.7) were observed. Mass spectral identification and quantification of 1G-GDGTs was potentially impacted by co-elution of core OH-GDGTs, however, stratigraphic trends do not appear to be affected, indicating that these values are likely not impacted. 1G-GDGTs in Core 8 have an average concentration of ~ 8 µg/g sediment (Table 3) with slightly elevated concentrations of 11 µg/g sediment at the surface and slightly depleted concentrations of 6 µg/g sediment at the bottom of the core. The surface concentrations for Cores 5, 6 and 3 (within the microbial mat) have concentrations of ~ 15 µg/g sediment, however, the subsurface concentrations of 1G-GDGT varies slightly from core to core. In Core 5 the signature for 1G-GDGTs extends to 15-18 cm below seafloor (cmbsf) having a concentration of 0.11 µg/g sediment at 145°C. In Core 6 the

signature for 1G-GDGTs extends to 12-15 cmbsf having a concentration of 1.00 µg/g sediment at 87°C. In Core 3, the signature of 1G-GDGT persists all the way down core (18-21 cmbsf) having a concentration of 5.22 µg/g sediment at 80°C.

Tentatively identified 2G-GDGTs represented by peak 17 (Table 2) (with 17 a-c being associated with increasing number of cyclopentyl moieties (0-2) (Figure 2.3) within the core structure) were also identified based on their molecular ions $[M+H]^+$ monitored by *m/z* 1626.43, 1624.41, 1622.39 ion chromatograms, having similar fragments as previously discussed. 2G-GDGTs appear to be one of the more stratigraphically zoned and less thermodynamically stable archaeal lipids as it is only found in the top 4 cm of Core 5 having 2.46 µg/g sediment at 0-2 cm and 1.74 µg/g sediment at 2-4 cmbsf (Table 3), before falling below the level of detection in the next interval. In Core 6, 2G-GDGTs extend deeper to 6-8 cmbsf (0.08 µg/g sediment) and, lastly in Core 3, 2G-GDGT extends to 10-12 cmbsf (0.66 µg/g sediment).

The hydroxylated counterparts of 1G and 2G-GDGT elute approximately 20 minutes earlier (peaks 14 and 16; Table 2). However, 1G- and 2G-OH-GDGTs are limited to 0-2 cyclopentyl moieties represented by a-c in Figure 2.3. Both IPLs were tentatively identified based on their molecular ions $[M+H]^+$ monitored by *m/z* 1480.3704 and 1642.4283 mass chromatograms, respectively. Both of these IPLs have characteristic fragments of *m/z* 1318.37 (characterized by the loss of head groups or head group).

Intact polar lipids 1G- and 2G-archaeol (AR; identified as peaks 1 and 2; Table 2) were tentatively identified based on their molecular ions $[M+H]^+$ monitored by *m/z* 977.78 and 815.73 mass chromatograms, respectively. Both of these IPLs have characteristic fragments of *m/z* 653 (characterized by the loss of head groups or head group) and *m/z* 373 (loss of a phytane

chain). Both of these IPLs respond similarly to 1G- and 2G-GDGTs in regards to their occurrence with depth and laterally across the transect. In Cores 5 and 6 the surface concentrations are ~1 µg/g sediment for both 1G and 2G-AR. However, in both cores 1G extends to 12-15 cmbsf (~0.2 µg/g sediment), whereas 2G-AR only extends to 8-10 cmbsf in Core 5 and 10-12 cmbsf in Core 6. 1G-AR persists all the way down both Core 3 and 8, going from ~0.42 µg/g sediment at the surface for both cores to 2.59 µg/g sediment at 15-18 cmbsf (Core 3) and 1.01 µg/g sediment at 12-15 cmbsf (Core 8).

3.3.2. Archaeal core lipids

The most common CLs of the Cathedral Hill transect are isoprenoidal GDGTs (iGDGTs) with 0-4 cyclopentyl moieties and crenarchaeol, GDGT-5, and the regioisomer of crenarchaeol GDGT-5' containing four cyclopentyl moieties and one cyclohexyl moiety. These iGDGTs are one of the most dominant lipid classes within Figure 2.3 represented by peak 21a-f with signals at *m/z* 1302.32, 1300.31, 1298.29, 1296.28, 1294.26, 1292.24 $[M+H]^+$. In addition to the iGDGTs, hydroxylated versions of this compound class are also present. Similar to their IPL precursors, the OH-GDGTs exclusively contain 0, 1, and 2 cyclopentyl moieties. The OH-GDGTs are represented by peak 19a-c at a *m/z* signal of 1318.32, 1316.30, and 1314.28 $[M+H]^+$ (Figure 2.3; Table 2). Both iGDGTs and OH-GDGTs follow similar stratigraphic trends with Core 8 having consistent concentrations of ~ 400 (iGDGTs) and ~ 20 (OH-GDGTs) µg/g sediment all the way down the core. However, in Core 5, 6 and 3 there is a systematic decrease in both iGDGT and OH-GDGT with depth, though these compounds exist all the way down core.

Archaeol (AR), a core lipid comprised of two phytanyl chains ether bonded to a single glycerol, has been found in all three groups of archaea, (methanogens, halophiles and thermophiles Kate, 1993) and is commonly found in marine settings (Gambacorta et al., 1995). Archaeol, tentatively identified as peak 7 (Figure 2.3), was monitored with a *m/z* signal of 653.68 and further constrained by the presence of a dominant fragment of *m/z* 373.37, which corresponds to the cleavage of one phytanyl chain. AR is another lipid that starts with high surface concentrations in both Cores 5 and 6, of 13.68 and 11.19 μg/g sediment respectively, which decreases to ~ 2 μg/g at the bottom of both cores. However, in Core 3 there is a systematic increase from 4.21 μg/g sediment at the surface to ~11 μg/g near the bottom of the core. Core 8 is different as it has an average value of ~ 4 μg/g sediment all the way down core.

Lastly, a methoxy derivative of archaeol (1MeO-AR) that was reported by Elling et al. (2014) to be methylated at the sn-1 position of the headgroup attachment site, was likewise observed. Methoxy-archaeol is thought to be produced in the water column via a currently unknown biosynthetic pathway by planktonic Archaea and its biological function is also currently unknown (Elling et al., 2014). We have tentatively identified 1MeO-AR as peak 10 with a *m/z* signal of 667.68 $[M+H]^+$, with dominant fragments of *m/z* 385.3, 355.4. 1MeO-AR occurs rather uniformly across the whole transect surface at ~ 2 μg/g sediment at the surface. In each core the concentration of 1MeO-AR decreases with depth, never being completely eliminated. The decrease for this molecule is much more drastic in cores that experience elevated temperatures.

3.3.3. Archaeal core lipids degradation products

Another common core lipid class found within sediments are glycerol dibiphytanol diethers (GDDs), which are composed of two biphytanyl chains bonded to a glycerol via two ether linkages. The terminal carbon atoms on the biphytanyl chains are bonded by hydroxyl groups. GDDs lack a direct biological IPL precursor. As the structure of GDD is similar to that of a GDGT minus a second glycerol backbone, it has been suggested that these compounds are partial GDGT degradation products (Liu et al., 2012a; Meador et al., 2014). GDDs have been tentatively identified and are represented by peaks 18a-f (Figure 2.3), which once again are associated with an increasing number of cyclopentyl moieties (0-5). The suite of GDDs were identified by monitoring the *m/z* signals of 1246.29, 1244.28, 1242.27, 1240.25, 1238.23, 1236.2 $[M+H]^+$ (Table 2). These peaks show the characteristic *m/z* 669.67 fragment ion associated with the loss of a phytane from the original GDD structure (Liu et al., 2012a). GDDs concentration patterns follow similar trends to the concentration patterns of GDGTs. Both have increased surface values, with the highest concentration being found at the surface of Core 3, having 42.46 µg/g. Both Core 5 and Core 6 have surface concentrations of ~ 35 µg/g sediment that decrease to ~ 9 µg/g sediment at the bottom of the cores. Once again, Core 8 has a rather consistent GDD concentration of ~ 30 µg/g sediment all the way down the core with a minor decrease in concentration with depth (Table 3).

In addition, a variety of GDD structures hydroxylated at the sn-3 position were also tentatively identified as peak 11a-c (Figure 2.3) containing 0, 1, and 2 cyclopentyl moieties exclusively. OH-GDDs were monitored by *m/z* signals of 1262.29, 1260.28, and 1258.26 $[M+H]^+$

(Table 2). OH-GDDs are observed to have the highest concentration at the surface of Core 3, having 4.07 µg/g sediment. Both Cores 5 and 6 show slightly lower surface OH-GDD concentrations of 2.59 and 3.60 µg/g sediment, respectively. The signal at depth in Core 5 dissipates after 10-12 cm where the concentration is 0.18 µg/g sediment, whereas the signal in Core 6 extends slightly deeper to the 12-15 cm interval having 0.14 µg/g sediment. In Core 8 OH-GDDs concentrations remain fairly consistent down core having concentrations of ~ 3 µg/g sediment.

3.4. Bacterial and eukaryotic lipids

Bacterial and eukaryotic lipids do not achieve ideal separations with the selected method. However, a number of bacterial and eukaryotic lipids which may act as a marker for the microbial mat, have been identified (see Table 2).

3.4.1. Bacterial lipids

Two bacterial IPLs with unknown head groups have been tentatively identified (peak 11 & 12) (Table 2; Figure 2.3) as having a signal *m/z* of 829.73 (UDAG-1) and 855.72 (UDAG-2) $[M+H]^+$ (Figure 2.5). Fragments from these extracted ion chromatograms show dominant fragments of *m/z* 551.5, which are consistent with core structures of C32:0 diacylglycerol. Both UDAG-1 and UDAG-2 are found in Core 5. At the surface of Core 5 UDAG-1 has a

concentration of 1.82 µg/g sediment where UDAG-2 has a concentration of 5.77 µg/g sediment (Supplementary Table A3-6). Both of these unknown lipids extend to 4-6 cm in Core 5 having concentrations of 0.43 (UDAG-1) and 0.29 (UDAG-2) µg/g sediment. However, UDAG-1 does extend slightly deeper into the subsurface (8-10 cm) the concentrations of the two deeper intervals are 0.07 and 0.02 µg/g sediment. Similar concentrations are found in Core 6 and extend to the same interval as Core 5. Furthermore, similar to the above observations, the surface sediment of Core 3 has the highest concentrations of both unknown lipids 4.25 µg/g sediment of UDAG-1 and 7.18 µg/g sediment of UDAG-2. In this core both unknown lipids extend further into the subsurface reaching 10-12 cm with ~ 0.70 µg/g sediment concentrations. For Core 8 these unknown compounds remain consistent down core with concentrations of ~ 3 (UDAG-1) and ~ 4.5 (UDAG-2) µg/g sediment.

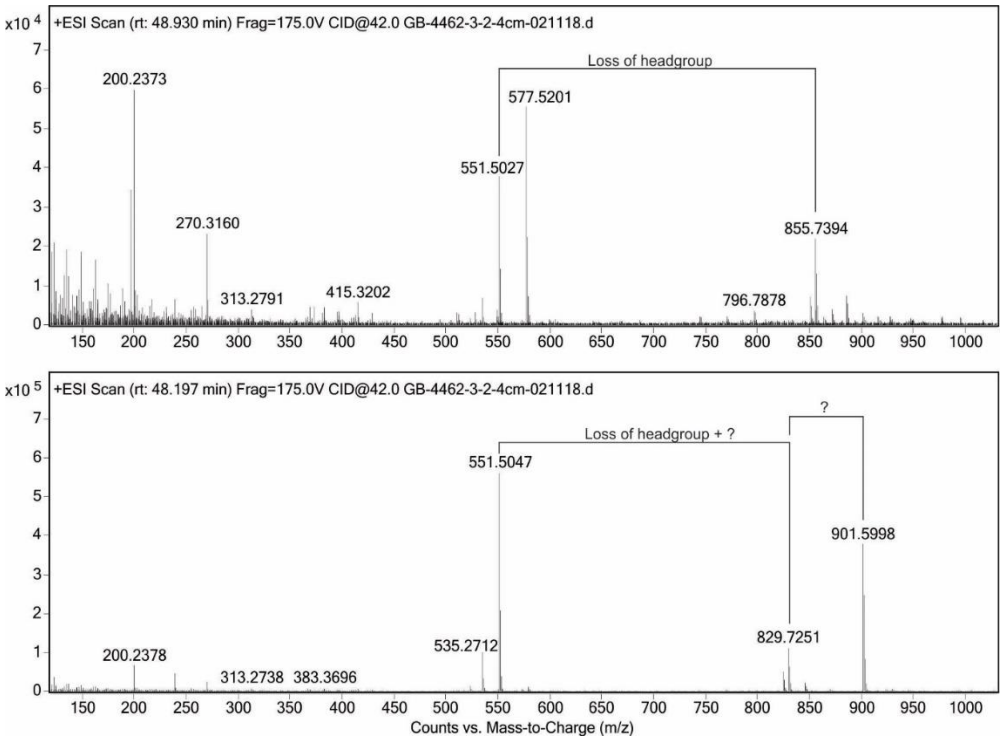

Figure 2.5 - Mass spectra for UDAG-1 and UDAG-2.

Additionally, bacterial core lipids in the form of branched GDGTs (brGDGTs) were identified in all transect samples. These non-isoprenoidal compounds were first discovered with new LC-MS techniques and unambiguously identified with NMR by Damsté et al. (2000). Membrane-spanning lipids have been used as taxonomic indicators of Archaea (Weijers et al., 2006). However, these membrane spanning lipids are thought to be a result of a biosynthetic pathway produced from anaerobic bacteria. Currently, the exact source and biological function is unknown, but thought to be related to acidic conditions in peat bogs and soils (Weijer et al., 2006). More recent studies have demonstrated that brGDGTs can be found in the water columns of both oxic and anoxic lakes (Sinninghe Damsté et al., 2009; Bechtel et al., 2010) adding complexity to their sourcing. These lipids and their associated proxies are further discussed in section 2.4. and 3.4. in Chapter 3.

Within the Cathedral Hill transect samples brGDGT Ia (*m/z* 1022.01), Ib (*m/z* 1019.99), Ic (*m/z* 1017.98), IIa (*m/z* 1036.03), IIb (*m/z* 1034.01), IIc (*m/z* 1031.99), IIIa (*m/z* 1050.04) and IIIb (*m/z* 1048.03) $[M+H]^+$ were tentatively identified. These lipids are represented as peak 15 (Table 2; Figure 2.3) and the associated lipid structures are provided in Figure 2.4. Concentrations of brGDGTs follows similar stratigraphic trends to other reported compounds with higher lipid concentrations at the surface of Cores 5, 6 and 3 of 5.19, 7.05 and 7.73 µg/g sediment respectively (Table 3). In both Cores 5 and 6 the concentrations at the bottom of the core systematically decrease until reaching 0.86 and 1.00 µg/g sediment. The bottom of Core 3 has a concentration of 4.88 µg/g, still showing a decrease down core but are not as drastic as Cores 5 and 6. In Core 8, the consistency down core continues with an average concentration of ~ 6 µg/g sediment.

3.4.2. Eukaryotic Lipids

Two tentatively identified ceramide lipids with unknown structural configurations were identified (peak 8 & 9; Supplementary Table A2-6; Figure 2.3) based on signal *m/z* 946.96 (U-Cer-1) and *m/z* 948.97 (U-Cer-2) $[M+H]^+$ (Figure 2.6), respectively. The target masses are consistent with core structures comprising of 18:0/14:0 (*m/z* 512.5, 494.5 mass fragments), and 18:1/14:0 (*m/z* 510.5, 492.5 mass fragments) as seen in Fig 3.3-1 & Fig 3.3-2. The observed spectra likewise match those of Yurkova et al. (2005) and Burla et al. (2018), suggesting that these peaks are ceramide lipids. Ceramide lipids have the potential to be human contamination within the samples. However, if this was the case the concentrations would be uniformly distributed in all samples or found in deeper intervals that were sterilized by nature. Both U-Cer-1 and U-Cer-2 are found in Core 5, at the ocean bottom surface layer. U-Cer-1 has a concentration of 5.77 µg/g sediment, where U-Cer-2 has a concentration of 11.00 µg/g sediment (Supplementary table A2-6). In Core 5, U-Cer-1 extends to 4-6 cm having concentrations of 0.29 µg/g sediment, whereas U-Cer-2 extends slightly deeper to 10-12 cm having a limited concentration of 0.03 µg/g sediment. Similar concentrations are found in Core 6 and extend to the same interval as Core 5. In Core 3 the concentrations at the surface for both unknown lipids remain the same, but extend deeper in the subsurface. U-Cer-1 extends to 10-12 cm having a concentration of ~ 0.77 µg/g sediment, where U-Cer-2 extends to the bottom of the core having a concentration of 0.83 µg/g sediment. Lastly, in Core 8 these unknowns remain consistent down core having concentrations of ~ 5 (U-Cer-1) and ~ 9 (U-Cer-2) µg/g sediment. These trends indicate the ceramide lipids represent primary sourced lipid signatures and not contamination.

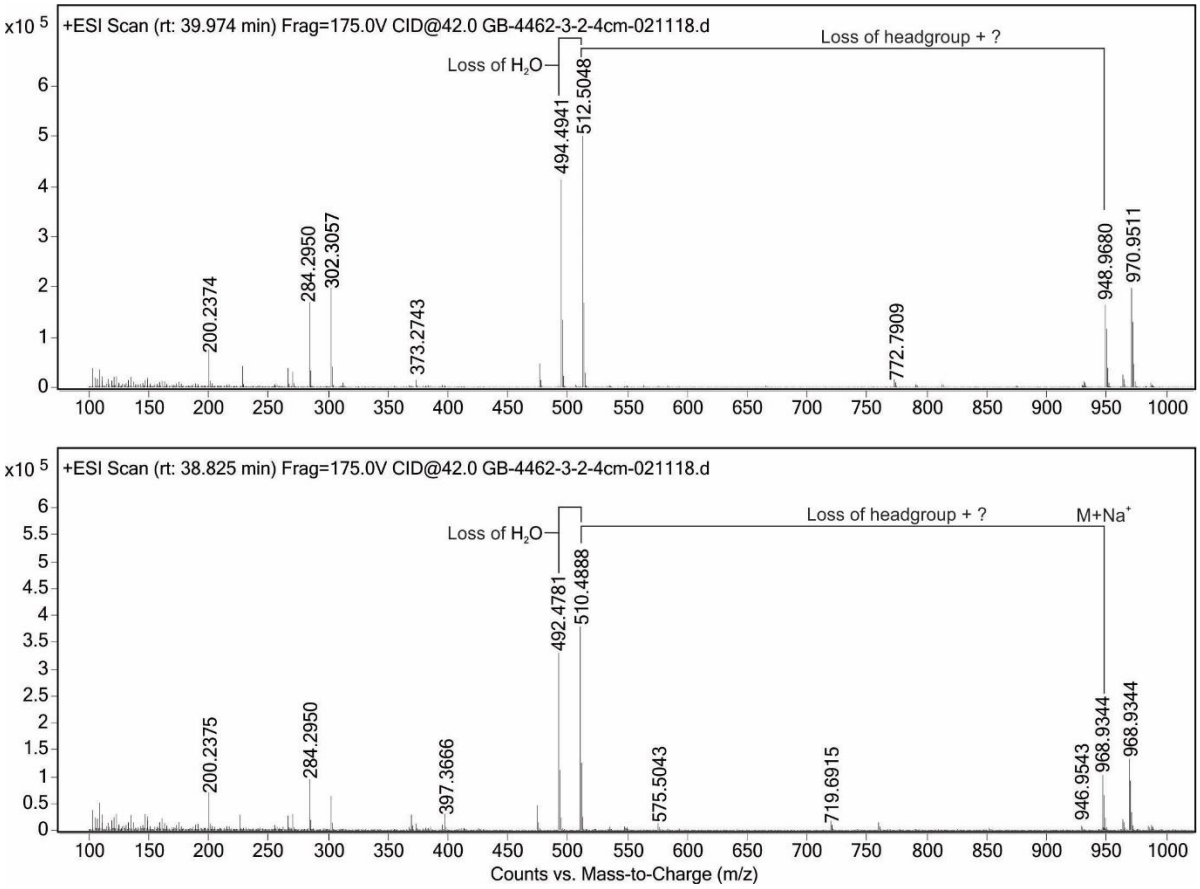

Figure 2.6 - Mass spectra of U-Cer-1 and U-Cer-2.

3.5. Chlorophyll & Pheophytin

An integral pigment within photosynthetic organisms such as plants and algae is chlorophyll *a*. Pheophytin *a,* is a breakdown product of chlorophyll *a,* and is formed when the central magnesium atom of the tetrapyrrole ring is replaced by two hydrogen atoms via a catabolic reaction (Schelbert et al., 2009). In addition to this breakdown product, both chlorophyll *a* and pheophytin *a* can have a hydroxyl group substituted for a hydrogen atom at the C-13[2] position. This carotenoid derivative is thought to be an oxidation product of the precursor

molecule, which may be associated with declines in algal populations (Steele et al., 2015). Other varieties of chlorophyll were not identified within the transect sediments. Observed peaks 3-6 (Table 2; Figure 2.3) respectively at *m/z* of 909.54, 887.57, 893.54 and 871.57 $[M+H]^+$ have been tentatively identified as hydroxy-chlorophyll *a*, hydroxy-pheophytin *a*, chlorophyll *a* and pheophytin *a*. Fragmentation patterns from Chen et al. (2015) and Milenkovic et al. (2012) are consistent with the observed mass spectra, showing the characteristic *m/z* fragments of 593.3 and 533.5. The concentrations for all of the chlorophyll derivatives follow similar trends to that of the unknown bacterial and eukaryotic lipids, with the exception that the surface concentrations vary more drastically with Core 5 surface concentrations being half that of Core 6, and of Core 6 having approximately half of Core 3 and Core 8 (Table 3). For example, OH-chlorophyll *a* in the surface sediments of Core 5 is 6.21 µg/g sediment, and in Core 6 the concentration is 12.63 µg/g sediment, whereas in Cores 3 and 8 the concentrations are 20.51 and 18.73 µg/g sediment respectively. In Core 5 these pigments are limited to the upper 4 cm, with the exception of the hydroxylated derivatives extending slightly deeper to 6 cm, being found in trace concentrations of ~ 0.05 µg/g sediment. This same trend is observed in Core 6, extending to the same intervals, having minor traces in hydroxylated derivatives one interval deeper. In Core 3 the hydroxylated derivatives extend to 12-15 cm, once again having minuscule concentrations of ~0.02 µg/g sediment. Their non-hydroxylated counterparts only extend to 6-8 cm. In Core 8 these compounds react rather uniquely. The concentrations of the bottom of this core essentially represents a halving of the surface concentration (excluding the last interval due to limited sample). For example, OH-chlorophyll *a* has a concentration of 18.73 µg/g sediment at the surface and 9.20 µg/g sediment at 10-12 cm.

3.6. Transect trends

3.6.1. Across transect trends

Trends across the push core transect for both IPLs and CLs can primarily be observed at the ocean bottom surface (0-2 cmbsf), having similar values for most lipids. However, this pattern is quickly lost as deeper intervals experience varying temperatures with proximity to the vent. Since the surface concentrations for all cores show similar concentration values regardless of being on or off the microbial mat (Table 3), this likely represents the relative input of terrestrial and water column input. Core 8, representing the ambient sedimentation and also the background benthic community, has similar lipid concentrations (Figure 2.7). However, across transect concentration trends quickly fade with depth likely due to the exposure to higher thermal gradients.

3.6.2. Stratigraphic trends

The IPLs and CLs display well defined stratigraphic trends across the transect. The IPL and CL abundances in Core 8 are fairly consistent down core with the exception of the interval of 8-10 cm. This sample is thought to be heavily affected by oil staining, which in turn has resulted in ion suppression during analysis. The bottom of that core, interval 12-15 cm is also problematic as the sample only contained 0.31 g of sediment, which makes the integrity of this sample questionable. Compound specific concentrations were addressed in sections 3.2-3.5, but

this section will highlight the more important trends and investigate variations within the structures of IPL and CL GDGTs.

As previously described, down core trends follow a general pattern of decreasing IPL and CL diversity and concentration with depth that is tightly coupled to the sediment pore water geothermal gradient. This is demonstrated in Figure 2.7, a summary plot of each lipid of interest. With respect to IPLs, lipids with 2G head groups are observed to be less abundant and are potentially less stable with respect to changes to the thermal gradient. In Core 5, for example, they are not observed past the upper 4 cm, which reaches upwards of ~ 70°C. In addition to this, 2G-IPLs progressively extend deeper extending outward from the hydrothermal vent edifice reaching depths that experience similar temperature. The hydroxylated counterpart of 2G-IPLs extend slightly deeper into the subsurface, often one interval (2 or 3 cm) deeper.

Comparatively, 1G-IPLs extend further into the subsurface than 2G-IPLs. The 1G-GDGTs extends down into the 15-18 cm interval in Core 5, with corresponding pore water temperatures of up to ~ 145°C. The mass spectral signal at this interval is low and close to the instrument's limit of detection (less than 100 pg/µl; likely close to 10 pg/µl). The measured lipids are also limited to only 1G-GDGT-0. However, all 1G-GDGT structures were detected at the 12-15 cm interval (~ 135 °C) with confidence. In addition, 1G-OH-GDGTs extend into the subsurface to the same intervals as its non-hydroxylated counterpart, unlike the 2G-OH-GDGT, which are found deeper than 2G-GDGT.

The archaeal core lipids such as iGDGTs, OH-GDGTs, GDDs, AR, MeO-AR along with bacterial brGDGTs, persist all the way down core in all cores, similar to iGDGTs. However the most dominant lipid present are iGDGTs, which represent ~ 70% of all observed lipids (Figure 2.7)

the large percentage of iGDGT leads to scaling issues when displaying core lipid data; thus, core lipids are depicted as relative abundance.

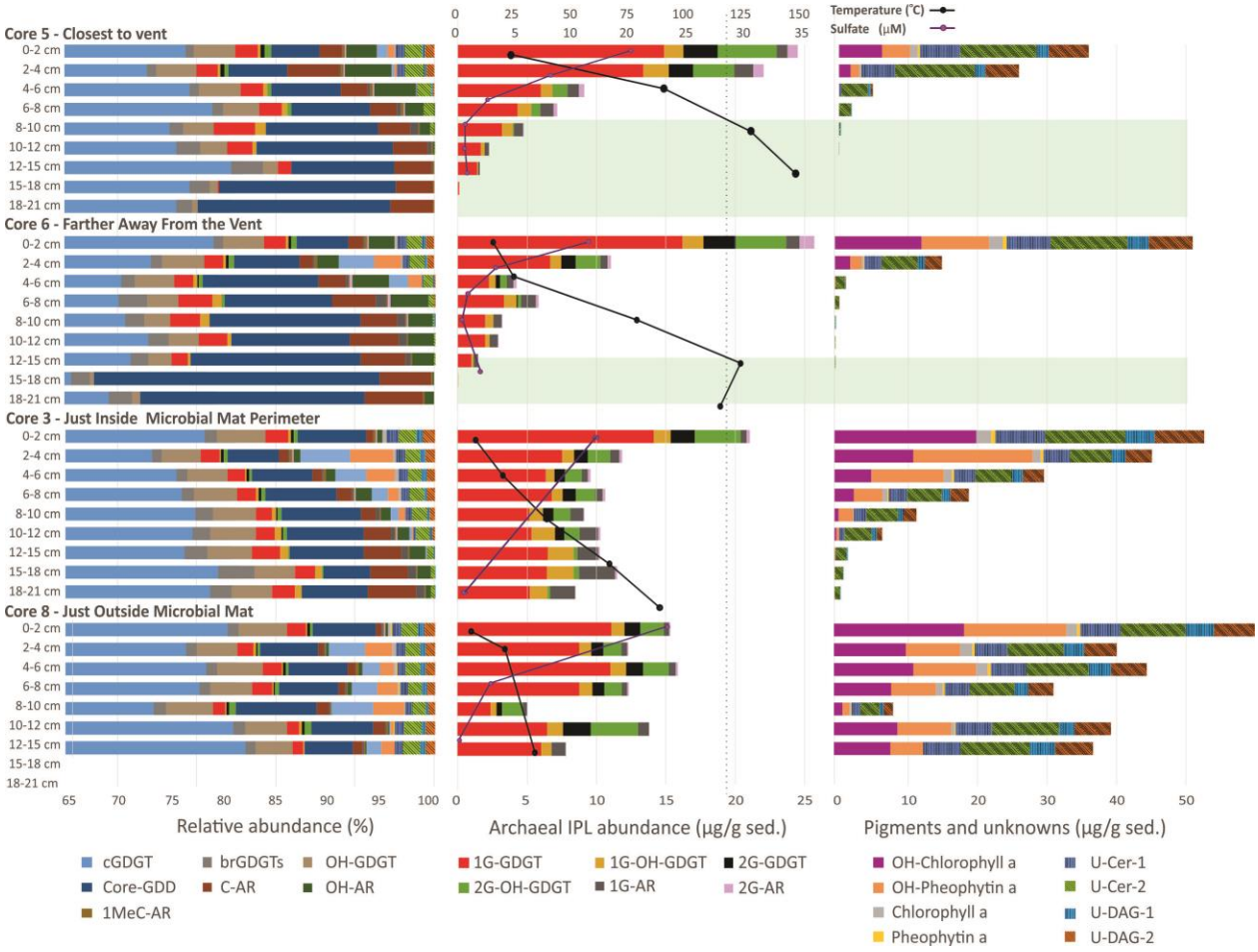

Figure 2.7 - Summary of all compounds of interest within the Cathedral Hill vent site. Relative abundance of all lipids (Left), abundance of IPLs, temperature (black line), and pore fluid sulphate concentration (purple line) (middle), abundance of pigments and unknowns (right). The horizontal green bars in the background represent the thermal zones that are currently outside the known habitibility for Archaea (121°C).

The total and relative abundances of individual 1G-GDGTs and core GDGTs systematically change with depth (Figure 2.7 and 2.8). The most notable variations are a systemic

decrease in lipid abundance with elevated pore water temperatures, and the increase in 1G-GDGT-3, 4 and the 5' structures with depth (a trend most pronounced in core 5 that decreases outwards from the vent center). Concomitant with this is a systematic decrease of the 1G-GDGT-5 isomer in samples that experience elevated temperatures (Figure 2.8). This change does not appear in ambient sediments of Core 8.

The GDGT core lipids have a similar trend of increasing, GDGT-3 and 4 in Cores 5 and 6, however, GDGT-5' does not significantly increase as observed with the 1G-GDGT. Unlike the 1G-GDGT structures that are absent in Core 8, all GDGT structures are observed in Core 8.

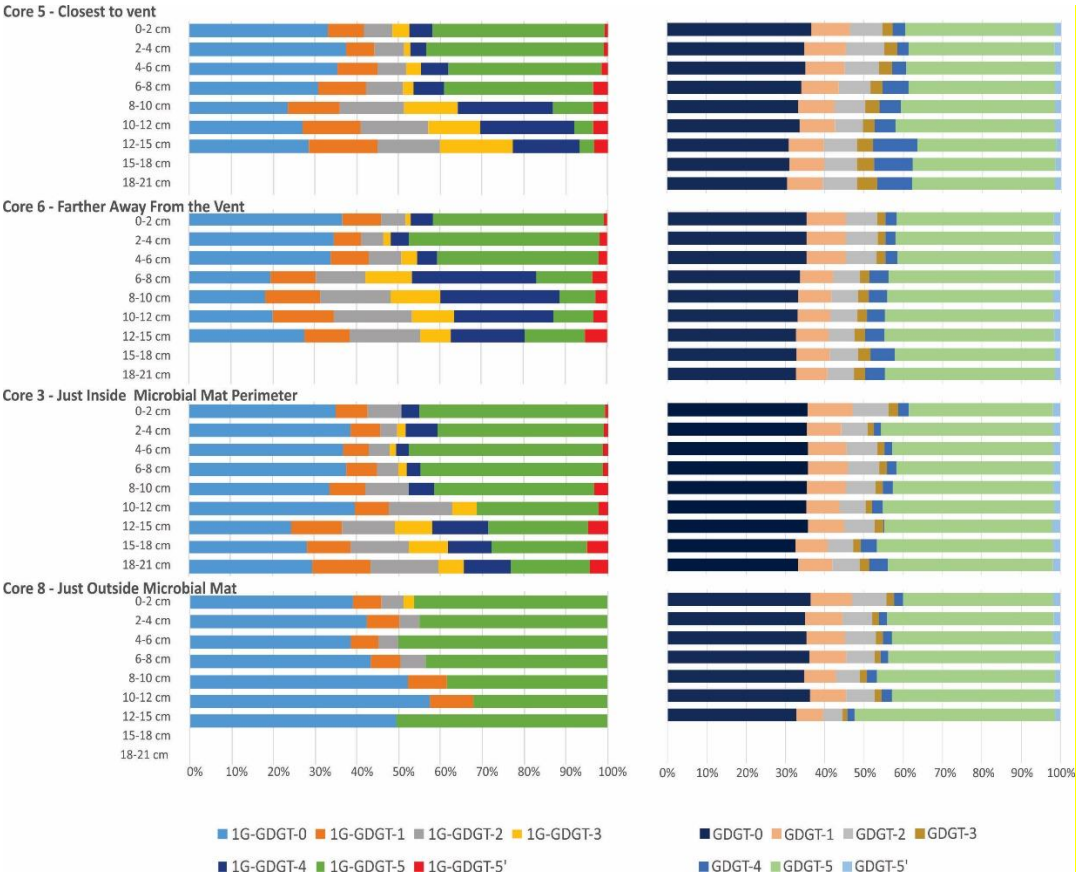

Figure 2.8 - Relative abundance of 1G-GDGT structures (left) and core GDGT structures (right).

4. Discussion

4.1. Intact polar lipid diversity

The polar head groups for archaeal lipids tend to be either glycosidic or phosphate based, or potentially a mix of both (Rossel et al., 2008; Schouten et al., 2008; Strapoc et al., 2008). However, the diversity of the IPLs in this study appears to be limited to 1G and 2G derivatives and contains no phosphate head groups. However, the purpose of a glycosidic head-group is to some degree enigmatic. Sollich et al. (2017) suggested that sugar head groups may represent a microbial strategy to conserve energy at the cellular membrane level in environments that include high temperature, low pH, phosphate limitations, and potentially, substrate limitations. Furthermore, glycolipid-rich membranes may also be more resilient in high temperature environments because the hydrogen bonds between the head groups are tighter than that of phospholipids (Kleinschmidt & McMahon, 1970; Murga et al. 1999; Kanduč et al. 2017).

Various hyperthermophiles ferment sugars via unique pathways that do not include phosphorylated intermediates (Lewalter & Müller 2006). Such strategies may explain the lack of phosphate headgroups with the Cathedral Hill sediments. Additionally, other forms of anaerobic respiration with nitrate or forms of acetogenesis (He et al., 2016) may be present, further negating the need for phosphate head groups to obtain energy, as it appears that there are rather unique metabolic pathways that exist in Archaea as outlined in studies such as Sakuraba et al. (2004) and Siebers et al. (2002).

4.2. Lipid sourcing

The detected Cathedral Hill lipids from mass spectral analysis are likely sourced from the shallow sediment microfauna or as a detrital, marine snow from the overlying water column. In aquatic environments, CLs are often sourced from the water column (Wuchter et al., 2005). However, CLs can also be produced within terrestrial soils and marine sediments (Hopmans et al., 2004; Schouten et al., 2013).

To untangle these various CL pools, the sum of terrestrially-derived brGDGTs (biomarkers for terrestrial soil input; Hopmans et al. 2004) were compared to the mixed sourced core iGDGTs with sediment depth (Figure 2.9). For Core 8, a near equal offset between these two lipid classes is observed, suggesting their source inputs are fundamentally related and mostly allochthonous. Additionally, the concentrations of brGDGTs are also similar in the 0-2cm layer of surface sediments across the transect, indicating there is little spatial heterogeneity to the upper-water column input across the transect and that the expulsion of vent fluids does not disrupt sedimentation patterns. Down-core covariations of Core 8 brGDGTs and iGDGTs requires that these lipids be predominantly sourced from the upper water column. In this regard, an average water column GDGT input can be calculated from the average brGDGT and iGDGT concentration differences of Core 8. This iGDGT weighting parameter was then applied to the down core brGDGTs yields of the other transect sediments to estimate the detrital input of iGDGTs (grey line on Figure 2.9). The predicted iGDGTs values closely match the actual iGDGT recoveries of the surface sediments along the transect (Figure 2.9). However, the predicted iGDGTs values progressively overestimate the actual iGDGT recoveries with depth (grey shaded area of Figure 2.9). These trends suggest the system is preferentially losing

iGDGTs over brGDGTs. The addition of archaeal lipids from the sediment microfauna should yield an overproduction (not underproduction) of these lipids. Furthermore, thermogenic decay, diagenetic alteration, or biodegradation would not be expected to preferentially affect isoprenoid over branched GDGTs. Alternatively, GDGTs are thought to potentially recycle core structures as described in Takano et al. (2010). This recycling and or assimilation of core GDGTs may be a common adaptive strategy for these organisms, allowing them to survive in harsh conditions such as those at Cathedral Hill. This appears to be the case, as thermogenic decay should be reflective in the RI for core GDGTs, ultimately producing lower RI values as pyrolysis experiments from Schouten et al. (2004) have demonstrated a preferential destruction of GDGTs 3-5+5'. Likewise, it has been stated that thermal maturation of GDGTs is only thought to occur in temperatures above 240˚C (Schouten et al., 2004), well above the temperatures at Cathedral Hill.

Furthermore, if the majority of GDGTs were produced in the water column then the degree of GDGT ring cyclization of core GDGTs in the vent interior should match that of the Core 8 sediments of the vent exterior. The RI values for Core 8 cluster rather closely with values of ~2.55 (Figure 2.10) with the exception of the two problem intervals 8-10 cm (oil impregnation?) and 12-15 cm (0.32 g of material). However, Cores 5, 6, and 3 all show systematic increases in RI with increased temperature. This change in RI appears to be tracking the subsurface archaeal communities and thus the majority of GDGTs must be produced *in situ*. This once again suggests the potential for recycling or assimilation of the GDGTs as the ring index would not adjust if the signal was predominately detrital. Alternatively, these GDGTs could potentially be broken down into intermediates, which were not detected with the current methodology, but will be a point of interest for a follow up study.

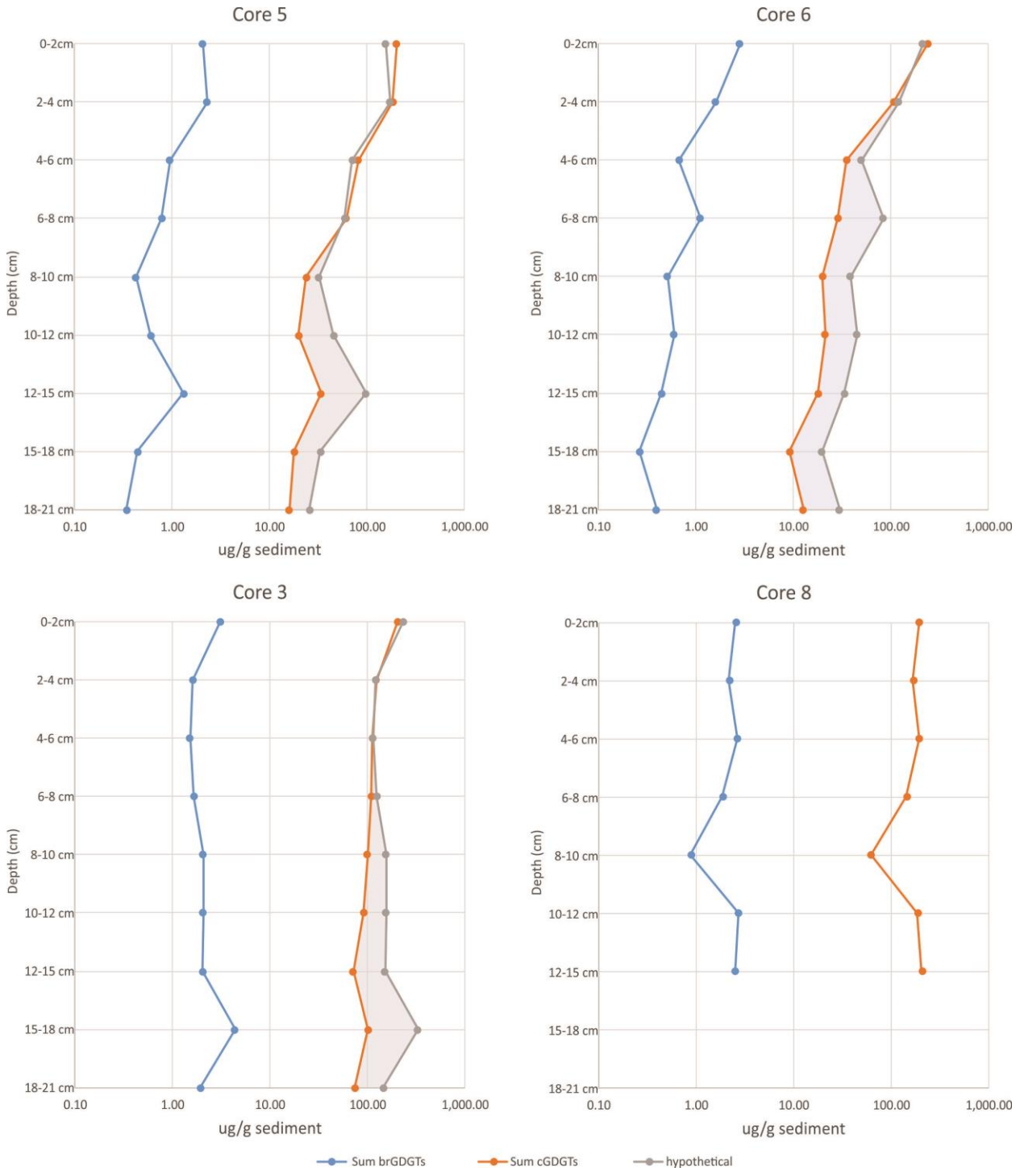

Figure 2.9 - Comparison of the sum of cGDGTs and brGDGTs. Predicted values of iGDGTs (grey line) were calculated based on the ratio of the offset in Core 8 as described in the text. The grey area represents the potential loss of GDGTs with increased depth.

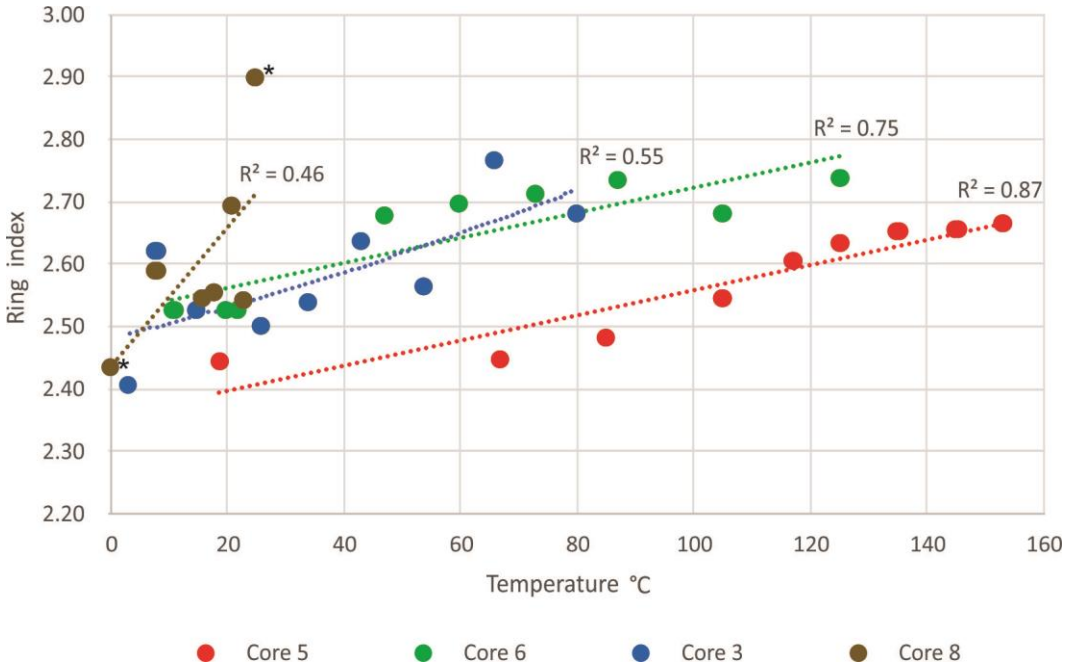

*Figure 2.10 - Ring index versus temperature of core GDGTs. The plot shows systematic increases in RI values in cores exposed to elevated temperatures. Note that in Core 8 the highest ring index value (outliers indicated with *) is likely related to the extraction of a small amount of material from this sample. Where the lowest ring index value is likely due to ion suppression. The lines of best fits were obtained using a linear fit (color coded) where equations are the following; Core 5(y = 0.002x + 2.36), Core 6(.y = 0.002x + 2.52), Core 3 (y = 0.003x + 2.47) and Core 8 (y = 0.0113x + 2.43).*

4.3. Lipid indicators of physiological adaptations to temperatures stress

A comparative ring number metric to assess cellular membrane compositions in relation to environmental conditions was first employed by de Rosa et al. (1980) to demonstrate that the degree of lipid cyclization was an organismal response to growth temperature. The ring index is a weighted average of the number of rings spanning 0-5 found within GDGTs core lipids structure (Eq. (1)). The index calculated after Pearson et al. (2004) is linked to an adaptive strategy that regulates the flow in and out of a cellular membrane by decreasing fluidity, but increasing rigidity (Gliozzi et al., 1983). The GDGTs of Core 5 and 6 compositionally change to

higher ring numbers in conjunction with elevated temperature of the pore waters (Figure 2.10). The RI values obtained are supportive of adaptation to environmental stress in both Core 5 and Core 6 where calculated R^2 values of 0.87 and 0.75 were respectively obtained (Figure 2.10) (where an R^2 value greater than 0.6 is considered to be well correlated). However, this finding is not new as increasing ring index values with *in situ* temperature has been previously investigated in studies such as Pearson et al. (2004) and Boyd et al. (2010).

$$RI = \frac{0\,x\,(GDGT\ 0) + 1\,x\,(GDGT\ 1) + 2\,x\,(GDGT\ 2) + 3\,x\,(GDGT\ 3) + 4\,x\,(GDGT\ 4) + 5\,x\,(GDGT\ 5 + GDGT\ 5')}{(GDGT\ 0)+(GDGT\ 1)+(GDGT\ 2)+(GDGT\ 3)+(GDGT\ 4)+(GDGT\ 5+5')} \quad (1)$$

Both of these cores appear to show an adapting microbial community as it was previously suggested, but the values are slightly lower for Core 5 than Core 6. The difference between core 5 and 6 can potentially arise by specific archaeal communities inhabiting different biozones outbound from the vent center. Alternatively, the more central core could be exposed to higher ammonia concentrations. Evans et al. (2018) demonstrated RI suppression when archaeal cultures were exposed to high levels of ammonia. Various localities within Guaymas Basin, such as Balsamico Mat, have well-documented high ammonia porewaters (Von Damm et al., 1985; Jeffery Seawald, personal communication).

When the RI is applied to the 1G-GDGTs as an attempt to evaluate only lipids that are considered to be living, the trends observed do not support the theory of adaptation with temperature (Figure 2.11). This outcome is counter to the observed trend of a systematic increase in 1G-GDGT-3, 4 and 5' along with a decrease in 1G-GDGT-5 (Figure 2.8). However, the RI is a weighted average; therefore, the function is negatively impacted by the decrease in concentrations of 1G-GDGT-5 with depth. This observed trend of decreasing 1G-GDGT-5 is

potentially due to lipid packing, and, or, limited to mesophilic Archaea, thus it would not be present in elevated temperature, which is the ability to tightly pack lipids together in a cellular membrane. The reason for a systematic decrease in 1G-GDGT-5 is unknown. However, a possible cause could be that the organism that biosynthesizes 1G-GDGT-5 are mesophilic. Alternatively, the presence of a fifth ring might not be advantageous to survival at elevated temperatures. Cellular packing is also another explanation, which has been previously investigated by Damsté et al. (2002). The specific molecule that impacts the packing is an archaeal lipid containing the core structure of GDGT-5. This structure contains a cyclohexane ring, which decreases its ability to densely pack the cellular membrane, due to the "bulge" that is produced with the cyclohexyl ring. The packing of these membranes is another form of adaptation to increased environmental stress, decreasing fluidity and permeability while increasing rigidity and making these membranes more thermally stable. Thus with the relative increase in 1G-GDGT-3, 4 and 5' and the notion that the relative decrease in 1G-GDGT-5 is likely due to lipid packing there is sufficient evidence to support the idea of adaptation to environmental stress from these archaeal membrane lipids.

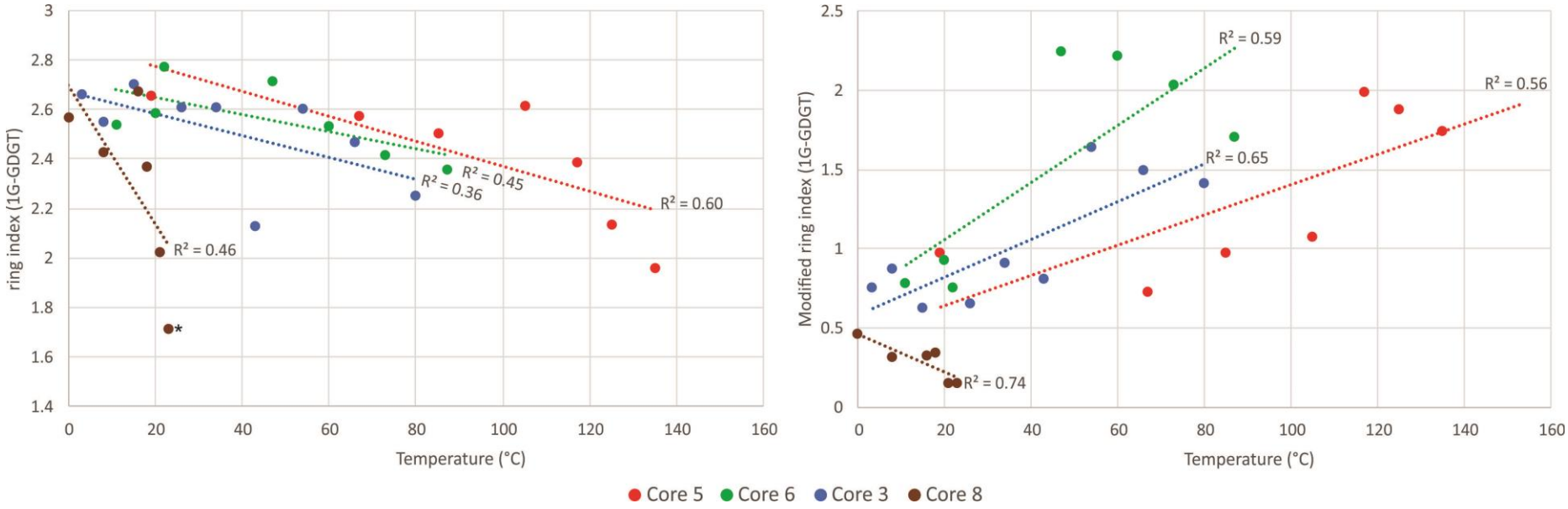

*Figure 2.11 - Ring index (1G-GDGT) vs temperature showing decreasing values with increased temperature (left). Lowest ring index value in Core 8 of 1.71 is outlined with an * to indicate that it is an outlier due to ion suppression. The negative slopes are likely due to a decrease in 1G-GDGT-5. Equations of these lines are the following; Core 5 (y = -0.0051x + 2.88), Core 6 (y = -0.0034x + 2.72), Core 3 (y = -0.0044x + 2.67) and Core 8 (y = -0.0281x + 2.70) A modified ring index (excluding 1G-GDGT-5 and 5') vs. Temperature (right), shows that there is first an increase, then a peak RI value, with slightly decreased values with increased temperature. This plot shows lower values that increase, followed by a jump followed by a decrease in high temperatures. Equations of these lines are the following; Core 5 (y = 0.0095x + 0.45), Core 6 (y = 0.018x + 0.70), Core 3 (y = 0.0118x + 0.59) and Core 8 (y = -0.012x + 0.46).*

4.3. Lipid indicators to metabolic responses in the subsurface

All correlation coefficients obtained from the linear relationships between methane index (MI; Equation 2, Zhang et al. 2011) and temperature are between 0.20 and 0.38 (Figure 2.12), which is not supportive of significant anaerobic oxidation of methane (AOM) at this site. However, Zhang et al. (2011) has suggested that MI values of 0.30-0.50 mark a boundary between normal marine and high AOM conditions. The Cathedral Hill values could ultimately represent methanotrophs present in some intervals where higher MI values were obtained. Schouten et al. (2003) has indicated that there is AOM in hot sediments in the Guaymas Basin. Even though our data indicates that it is plausible based on the MI values (>0.3), it is inconclusive without additional information.

$$MI = \frac{(GDGT\ 1) + (GDGT\ 2) + (GDGT\ 3)}{(GDGT\ 1) + (GDGT\ 2) + (GDGT\ 3) + (GDGT\ 5) + (GDGT\ 5')} \quad (2)$$

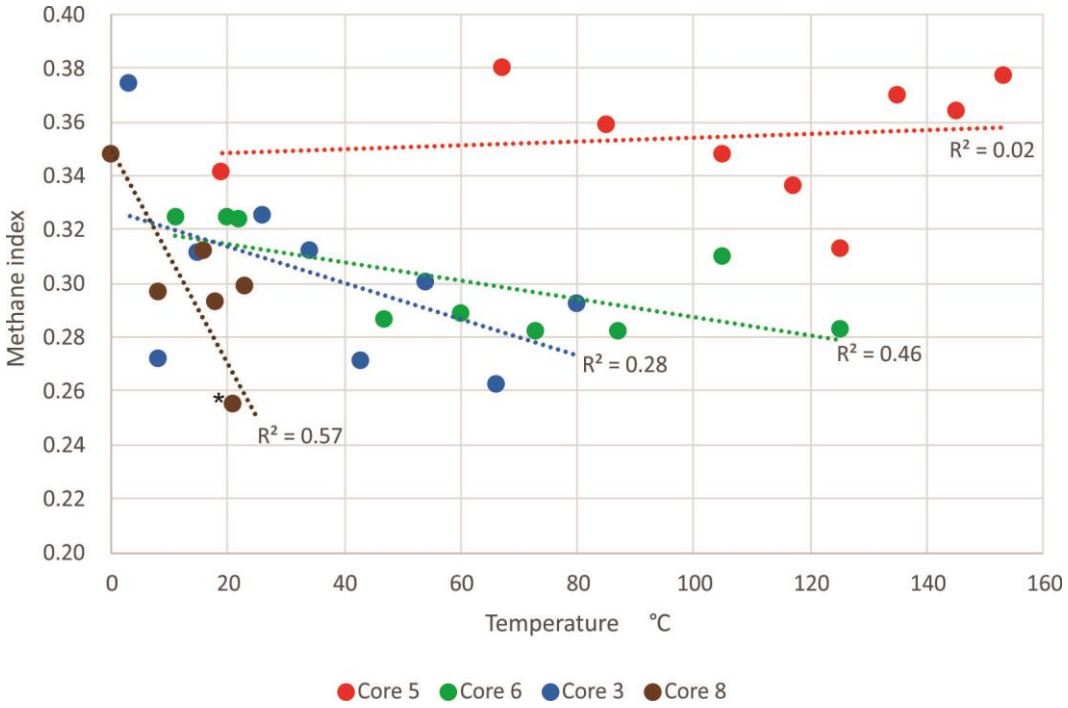

*Figure 2.12 - Methane Index (Zhang et al., 2011) vs. Temperature. Values above 0.30 indicate a transition between normal marine and areas with high AOM (>0.50). Equations of these lines are the following; Core 5 (y = 7E-05x + 0.35), Core 6 (y = -0.0003x + 0.32), Core 3 (y = -0.0007x + 0.33) and Core 8 (y = -0.004x + 0.35). The lowest methane index value from Core 8 is denote with an * which indicates low sample material.*

We further suggest that there is the potential for ammonia oxidizing archaea (AOA) as they are some of the most abundant microbes in the world's oceans (Karner et al., 2001; Schattenhofer et al., 2009) and that the vent fluids in Guaymas Basin tend to be rich in ammonia (Von Damm et al., 1985). However, genetic studies would be needed to confirm this claim.

4.4. MeO-AR/MeO-AR+cAR

Methoxy archaeol (MeO-AR) is a potential biomarker of planktonic marine thaumarchaea (Elling et al., 2014). The biosynthesis and biological function of MeO-AR

is still currently unknown (Evans et al., 2018), but its presence in ocean floor sediments likely indicates upper-water column inputs of organic matter. Figure 2.13 depicts elevated MeO-AR/MeO-AR+cAR (Calculated after Evans et al. (2018) (Eq. (3)) in less hydrothermally impacted, surficial sediments. The warmer intervals in Cores 5 and 6 show lower values that appear to taper out towards zero. However, the most prominent depositional signature is observed in Core 3, where there is a systematic decrease in the ratio with temperature and depth. This curve could indicate that MeO-AR is likely being deposited, buried and then either biodegraded or there is some other unknown zonation that is forcing this function to approach zero above 40°C. These findings are consistent with Elling et al. (2014) who suggested that MeO-AR is limited to the upper water column. However, more knowledge of MeO-AR is needed to draw inferences on the origin of this potential marker, and ultimately what the application for this equation could be.

$$MeO - AR/D = \frac{MeO - AR}{MeO - AR + AR} \quad (3)$$

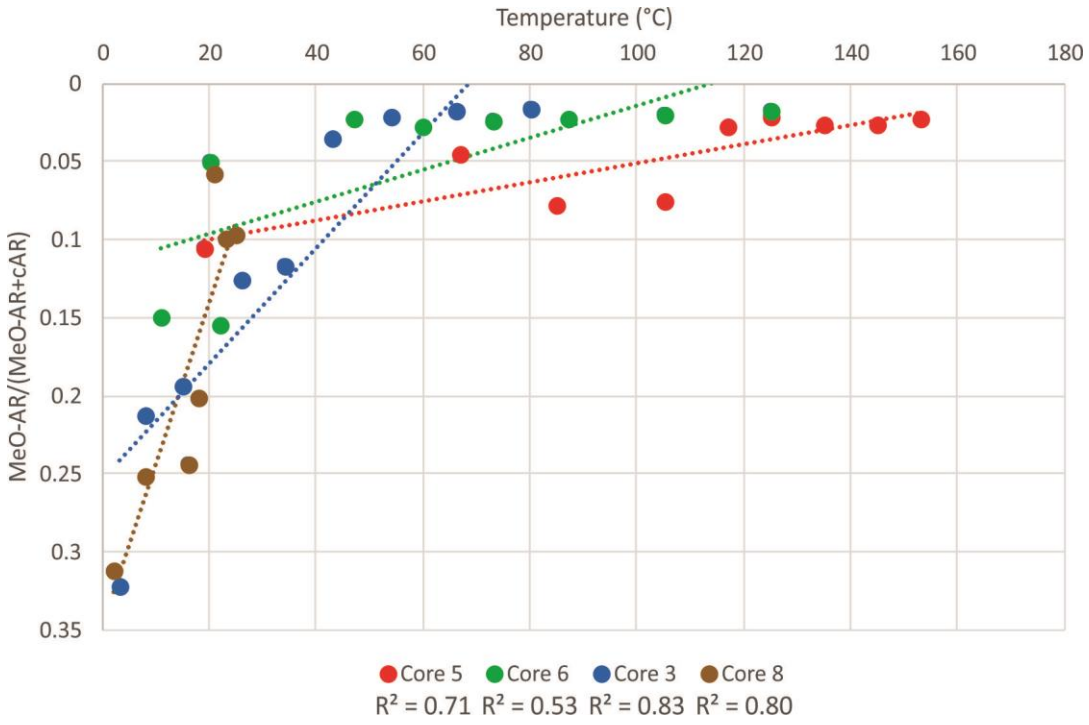

Figure 2.13 - MeO-AR/MeO-AR+cAR vs. Temperature, showing the ratio approaching zero with elevated temperature. Equations of these lines are the following; Core 5 (y = -0.0006x + 0.11), Core 6 (y = -0.001x + 0.12), Core 3 (y = -0.0037x + 0.25) and Core 8 (y = -0.0103x + 0.35), where R^2 values are found below the corresponding core in the legend.

4.6. Thermal limit of life

The ultimate thermal limit of life on Earth is of interest for identifying new target locations to look for microbial life on extra-terrestrial planets, learn more about the potential origins of life, and to more accurately constrain how deep the deep biosphere goes. Many archaea appear to be the most adapted to life in extreme heat due to the natural chemical stability of their biomolecules, but also in the assembly of these molecules. Currently, the highest temperatures recorded for a hyperthermophile is around

120˚C as recorded in culture experiments by Kashefi & Lovley (2003). These authors found that for a cultured strain of Archaea from a hydrothermal vent site growth occurred up to 121°C. However, a more recent study found a slightly higher threshold of 122°C (Takai et al., 2008), which was produced by hyperthermophilic methanogens under high pressure (40 MPa) cultivation.

The presence of 1G-GDGTs in cores 5 and 6 at ~145˚C suggests that the boundary for the upper thermal limit of life may once again be shifted. This is because IPLs are not stable outside of the cellular membrane and the head groups hydrolyze within days to weeks in normal marine environments (White et al., 1979; Harvey et al., 1986). There are thoughts that IPLs may be stable for longer durations outside of a membrane, however, the harsh conditions of Cathedral Hill would likely promote degradation. The 1G-GDGT-0 is the only structure observed in this interval, and in low concentrations, which is consistent with intact polar GDGTs tending to have higher abundances of acyclic GDGT-0 core structures (Liu et al., 2011). However, pressure is a factor that may potentially play a role in the preservation of these lipids. There is evidence that Archaea experiencing elevated pressure may slightly increase the window for life, allowing them to persist into the observed temperatures as outlined in culture experiments by Kashefi & Lovley (2003) and Takai et al. (2008). The seafloor environmental pressures at Cathedral Hill are 20 Mpa (from a gradient of 1 Mpa /100m), which is likely a conservative estimate. It is expected that with the upward flow of vent waters the shallow subsurface could results in higher pressures as the venting fluids are not able to bubble. Pressure was not directly measured for Cathedral Hill, but other Guaymas Basin sites of similar water depths have reported values reaching 35 Mpa

(Canganella et al., 1997). Such elevated pressures enhance the thermo-tolerance of various hyperthermophiles (Holden and Baross 1995; Marteinsson et al., 1997).

Other metrics such as the RI as described in section 4.2., suggest that the Archaea are indeed adapting to the increase in temperature by increasing lipid packing. This line of evidence refutes the idea that there is mechanical smearing in the sample collection or some other analytical error that might allow for the signature to appear in a depth that extends past the known habitable zone. There is the potential to have inaccuracies in the thermal probe data, however, even with error in that measurement there is still a high probability that the observed lipids are above the 121˚C or 122°C limit recorded by Kashefi & Lovley (2003) and Takai et al. (2008) respectively. One factor that is not constrained is the flow of hydrothermal fluid. There is a possibility that there are cyclic events that occur, which temporarily decrease the temperature for durations that allow for those organisms to establish themselves at those core depths. They can then subsequently be exposed to the observed elevated temperatures that would pasteurize even the most resilient of hyperthermophiles. This is a major consideration especially at the scale at which this study was conducted. The slightest variations within the fluid flow and or temperature of those fluids may drastically affect the upper 21 cm of sediment. Additionally, stratigraphic trends show systematic decreases with depth suggesting that the lipids observed are in fact a true signal, indicating that cyclic events likely have not impacted the study area since the microbial community has established itself.

5. Conclusions

The Cathedral Hill push core transect is heavily controlled by the *in situ* temperatures that reach upwards of ~155˚C within the first 21 cmbsf in the most extreme case of Core 5. This extreme temperature drastically limits the diversity of life, however signatures of the living archaeal community in the form of 1G-GDGTs have been found near the bottom of the interval that represent 15-18cmbsf. This interval experiences temperatures up to 145˚C, which is currently outside the known realm of habitability.

This study further suggests either a form of lipid recycling or assimilation as the sources appear consistent with initial influx of sediment at the surface, but this signature decreases with depth to where archaeal communities are thought to thrive. This claim is strongly supported by the ring index trends that point to thriving archaeal communities in the subsurface that are adapting to environmental stress. Ultimately this study highlights the thermal stability of archaeal lipids and their potential extension to the boundary of life. This has implications for the depth that the deep biosphere can extend and the range of conditions in which life could evolve on Earth or on other planets and moons.

References

Bechtel, A., Smittenberg, R.H., Bernasconi, S.M. and Schubert, C.J., 2010. Distribution of branched and isoprenoid tetraether lipids in an oligotrophic and a eutrophic Swiss lake: insights into sources and GDGT-based proxies. Organic Geochemistry, 41(8), 822-832.

Biddle, J.F., Lipp, J.S., Lever, M.A., Lloyd, K.G., Sørensen, K.B., Anderson, R., Fredricks, H.F., Elvert, M., Kelly, T.J., Schrag, D.P. and Sogin, M.L., 2006.

Heterotrophic Archaea dominate sedimentary subsurface ecosystems off Peru. Proceedings of the National Academy of Sciences, 103(10), 3846-3851.
Boyd, E.S., Pearson, A., Pi, Y., Li, W.J., Zhang, Y.G., He, L., Zhang, C.L. and Geesey, G.G., 2011. Temperature and pH controls on glycerol dibiphytanyl glycerol tetraether lipid composition in the hyperthermophilic crenarchaeon Acidilobus sulfurireducens. Extremophiles, 15(1), 59-65.
Calvert, S.E., 1966. Origin of diatom-rich, varved sediments from the Gulf of California. The Journal of Geology, 74(5, Part 1), 546-565.
Campbell, A.C., Bowers, T.S., Measures, C.I., Falkner, K.K., Khadem, M. and Edmond, J.M., 1988. A time series of vent fluid compositions from 21° N, East Pacific Rise (1979, 1981, 1985), and the Guaymas Basin, Gulf of California (1982, 1985). Journal of Geophysical Research: Solid Earth, 93(B5), 4537-4549.
Canganella, F., Jones, W.J., Gambacorta, A. and Antranikian, G., 1998. *Thermococcus guaymasensis* sp. nov. and *Thermococcus aggregans* sp. nov., two novel thermophilic archaea isolated from the Guaymas Basin hydrothermal vent site. International Journal of Systematic and Evolutionary Microbiology, 48(4), 1181-1185.
Chang, E.L., 1994. Unusual thermal stability of liposomes made from bipolar tetraether lipids. Biochemical and biophysical research communications, 202(2), 673-679.
Chen, K., Ríos, J.J., Pérez-Gálvez, A., & Roca, M., 2015. Development of an accurate and high-throughput methodology for structural comprehension of chlorophylls derivatives.(I) Phytylated derivatives. Journal of Chromatography A, 1406, 99-108.
Damsté, J.S.S., Hopmans, E.C., Pancost, R.D., Schouten, S., & Geenevasen, J.A., 2000. Newly discovered non-isoprenoid glycerol dialkyl glycerol tetraether lipids in sediments. Chemical Communications, (17), 1683-1684.
Damsté, J.S.S., Schouten, S., Hopmans, E.C., Van Duin, A.C. and Geenevasen, J.A., 2002. Crenarchaeol the characteristic core glycerol dibiphytanyl glycerol tetraether membrane lipid of cosmopolitan pelagic crenarchaeota. Journal of lipid research, 43(10), 1641-1651.
Damsté, J.S.S., Ossebaar, J., Abbas, B., Schouten, S. and Verschuren, D., 2009. Fluxes and distribution of tetraether lipids in an equatorial African lake: constraints on the application of the TEX86 palaeothermometer and BIT index in lacustrine settings. Geochimica et Cosmochimica Acta, 73(14), 4232-4249.
Daniel, I., Oger, P. and Winter, R., 2006. Origins of life and biochemistry under high-pressure conditions. Chemical Society Reviews, 35(10), 858-875.
De Jonge, C., Hopmans, E.C., Stadnitskaia, A., Rijpstra, W.I.C., Hofland, R., Tegelaar, E. and Damsté, J.S.S., 2013. Identification of novel penta-and hexamethylated branched glycerol dialkyl glycerol tetraethers in peat using HPLC–MS2, GC–MS and GC–SMB-MS. Organic Geochemistry, 54, 78-82.
De Rosa, M. and Gambacorta, A., 1988. The lipids of archaebacteria. Progress in lipid research, 27(3), 153-175.
Elling, F.J., Könneke, M., Lipp, J.S., Becker, K.W., Gagen, E.J., & Hinrichs, K.U., 2014. Effects of growth phase on the membrane lipid composition of the thaumarchaeon Nitrosopumilus maritimus and their implications for archaeal

lipid distributions in the marine environment. Geochimica et Cosmochimica Acta, 141, 579-597.
Gambacorta, A., Gliozzi, A. and De Rosa, M., 1995. Archaeal lipids and their biotechnological applications. World Journal of Microbiology and Biotechnology, 11(1), 115-131.
Gieskes, J.M., Simoneit, B.R., Brown, T., Shaw, T.J., Wang, Y.C. and Magenheim, A., 1988. Hydrothermal fluids and petroleum in surface sediments of Guaymas Basin, Gulf of California: a case study. The Canadian Mineralogist, 26(3), 589-602.
Gliozzi, A., Paoli, G., De Rosa, M. and Gambacorta, A., 1983. Effect of isoprenoid cyclization on the transition temperature of lipids in thermophilic archaebacteria. Biochimica et Biophysica Acta (BBA)-Biomembranes, 735(2), 234-242.
Gliozzi, A., Relini, A. and Chong, P.L.G., 2002. Structure and permeability properties of biomimetic membranes of bolaform archaeal tetraether lipids. Journal of Membrane Science, 206(1-2), 131-147.
Haberstroh, P.R. and Karl, D.M., 1989. Dissolved free amino acids in hydrothermal vent habitats of the Guaymas Basin. Geochimica et Cosmochimica Acta, 53(11), 2937-2945.
Harvey, H.R., Fallon, R.D. and Patton, J.S., 1986. The effect of organic matter and oxygen on the degradation of bacterial membrane lipids in marine sediments. Geochimica et Cosmochimica Acta, 50(5), pp.795-804.
He, Y., Li, M., Perumal, V., Feng, X., Fang, J., Xie, J., Sievert, S.M. and Wang, F., 2016. Genomic and enzymatic evidence for acetogenesis among multiple lineages of the archaeal phylum Bathyarchaeota widespread in marine sediments. Nature Microbiology, 1(6), 16035.
Holden, J.F. and Baross, J.A., 1995. Enhanced thermotolerance by hydrostatic pressure in the deep-sea hyperthermophile Pyrococcus strain ES4. FEMS microbiology ecology, 18(1), 27-33.
Hopmans, E.C., Weijers, J.W., Schefuß, E., Herfort, L., Damsté, J.S.S., & Schouten, S., 2004. A novel proxy for terrestrial organic matter in sediments based on branched and isoprenoid tetraether lipids. Earth and Planetary Science Letters, 224(1-2), 107-116.
Hopmans, E.C., Schouten, S., Pancost, R.D., van der Meer, M.T. and Sinninghe Damsté, J.S., 2000. Analysis of intact tetraether lipids in archaeal cell material and sediments by high performance liquid chromatography/atmospheric pressure chemical ionization mass spectrometry. Rapid Communications in Mass Spectrometry, 14(7), 585-589.
Kanduč, M., Schlaich, A., de Vries, A.H., Jouhet, J., Maréchal, E., Demé, B., Netz, R.R. and Schneck, E., 2017. Tight cohesion between glycolipid membranes results from balanced water–headgroup interactions. Nature communications, 8, 14899.
Karner, M.B., DeLong, E.F. and Karl, D.M., 2001. Archaeal dominance in the mesopelagic zone of the Pacific Ocean. Nature, 409(6819), 507-510.
Kashefi, K. and Lovley, D.R., 2003. Extending the upper temperature limit for life. Science, 301(5635), 934-934.

Killops, S.D., Killops, V.J. and Killops, S.D., 1993. An introduction to organic geochemistry (Vol. 1). Essex: Longman Scientific & Technical.

Kleinschmidt, M.G. and McMahon, V.A., 1970. Effect of growth temperature on the lipid composition of *Cyanidium caldarium*: II. Glycolipid and phospholipid components. Plant Physiology, 46(2), 290-293.

Koga, Y. and Morii, H., 2007. Biosynthesis of ether-type polar lipids in archaea and evolutionary considerations. Microbiology and Molecular Biology Reviews, 71(1), 97-120.

Lewalter, K., & Müller, V., 2006. Bioenergetics of archaea: ancient energy conserving mechanisms developed in the early history of life. Biochimica et Biophysica Acta (BBA)-Bioenergetics, 1757(5-6), 437-445.

Lipp, J.S., & Hinrichs, K. U., 2009. Structural diversity and fate of intact polar lipids in marine sediments. Geochimica et Cosmochimica Acta, 73(22), 6816-6833.

Lipp, J.S., Morono, Y., Inagaki, F. and Hinrichs, K.U., 2008. Significant contribution of Archaea to extant biomass in marine subsurface sediments. Nature, 454(7207), p.991-994.

Liu, X.L., Birgel, D., Elling, F.J., Sutton, P.A., Lipp, J.S., Zhu, R., Zhang, C., Könneke, M., Peckmann, J., Rowland, S.J. and Summons, R.E., 2016. From ether to acid: a plausible degradation pathway of glycerol dialkyl glycerol tetraethers. Geochimica et Cosmochimica Acta, 183, 138-152.

Liu, X., Lipp, J.S. and Hinrichs, K.U., 2011. Distribution of intact and core GDGTs in marine sediments. Organic Geochemistry, 42(4), 368-375.

Liu, X. L., Lipp, J. S., Simpson, J. H., Lin, Y. S., Summons, R. E., & Hinrichs, K. U. 2012 a. Mono-and dihydroxyl glycerol dibiphytanyl glycerol tetraethers in marine sediments: Identification of both core and intact polar lipid forms. Geochimica et Cosmochimica Acta, 89, 102-115.

Liu, X.L., Lipp, J.S., Schröder, J.M., Summons, R.E. and Hinrichs, K.U., 2012 b. Isoprenoid glycerol dialkanol diethers: a series of novel archaeal lipids in marine sediments. Organic Geochemistry, 43, 50-55.

Liu, X. L., Summons, R. E., & Hinrichs, K. U., 2012 c. Extending the known range of glycerol ether lipids in the environment: structural assignments based on tandem mass spectral fragmentation patterns. Rapid Communications in Mass Spectrometry, 26(19), 2295-2302.

McClymont, E.L., Ganeshram, R.S., Pichevin, L.E., Talbot, H.M., van Dongen, B.E., Thunell, R.C., Haywood, A.M., Singarayer, J.S. and Valdes, P.J., 2012. Sea-surface temperature records of Termination 1 in the Gulf of California: Challenges for seasonal and interannual analogues of tropical Pacific climate change. Paleoceanography, 27(2).

McKay, L.J., MacGregor, B.J., Biddle, J.F., Albert, D.B., Mendlovitz, H.P., Hoer, D.R., Lipp, J.S., Lloyd, K.G. and Teske, A.P., 2012. Spatial heterogeneity and underlying geochemistry of phylogenetically diverse orange and white Beggiatoa mats in Guaymas Basin hydrothermal sediments. Deep Sea Research Part I: Oceanographic Research Papers, 67, pp.21-31.

Meador, T. B., Zhu, C., Elling, F. J., Könneke, M., & Hinrichs, K. U., 2014. Identification of isoprenoid glycosidic glycerol dibiphytanol diethers and indications for their biosynthetic origin. Organic geochemistry, 69, 70-75.

Meyer, S., Wegener, G., Lloyd, K.G., Teske, A., Boetius, A. and Ramette, A., 2013. Microbial habitat connectivity across spatial scales and hydrothermal temperature gradients at Guaymas Basin. Frontiers in Microbiology, 4, Article 207, 1-11.

Milenković, S. M., Zvezdanović, J. B., Anđelković, T. D., & Marković, D. Z., 2012. The identification of chlorophyll and its derivatives in the pigment mixtures: HPLC chromatography, visible and mass spectroscopy studies. Advanced Technologies, 1, 16-24.

Murga, M.L.F., Bernik, D., de Valdez, G.F. and Disalvo, A.E., 1999. Permeability and stability properties of membranes formed by lipids extracted from *Lactobacillus acidophilus* grown at different temperatures. Archives of Biochemistry and Biophysics, 364(1), pp.115-121.

Pearson, A., Huang, Z., Ingalls, A.E., Romanek, C.S., Wiegel, J., Freeman, K.H., Smittenberg, R.H. and Zhang, C.L., 2004. Nonmarine crenarchaeol in Nevada hot springs. Applied and Environmental Microbiology, 70(9), 5229-5237.

Sakuraba, H., Goda, S. and Ohshima, T., 2004. Unique sugar metabolism and novel enzymes of hyperthermophilic archaea. The Chemical Record, 3(5), 281-287.

Schattenhofer, M., Fuchs, B.M., Amann, R., Zubkov, M.V., Tarran, G.A. and Pernthaler, J., 2009. Latitudinal distribution of prokaryotic picoplankton populations in the Atlantic Ocean. Environmental Microbiology, 11(8), 2078-2093.

Schelbert, S., Aubry, S., Burla, B., Agne, B., Kessler, F., Krupinska, K., & Hörtensteiner, S. 2009. Pheophytin pheophorbide hydrolase (pheophytinase) is involved in chlorophyll breakdown during leaf senescence in *Arabidopsis*. The Plant Cell, 21(3), 767-785.

Schouten, S., Hopmans, E.C., Pancost, R.D. and Damsté, J.S.S., 2000. Widespread occurrence of structurally diverse tetraether membrane lipids: evidence for the ubiquitous presence of low-temperature relatives of hyperthermophiles. Proceedings of the National Academy of Sciences, 97(26), 14421-14426.

Schouten, S., Hopmans, E.C. and Damste, J.S.S., 2004. The effect of maturity and depositional redox conditions on archaeal tetraether lipid palaeothermometry. Organic Geochemistry, 35(5), 567-571.

Schouten, S., Wakeham, S.G., Hopmans, E.C. and Damsté, J.S.S., 2003. Biogeochemical evidence that thermophilic archaea mediate the anaerobic oxidation of methane. Appl. Environ. Microbiol., 69(3), 1680-1686.

Schubotz, F., Wakeham, S.G., Lipp, J.S., Fredricks, H.F., & Hinrichs, K.U., 2009. Detection of microbial biomass by intact polar membrane lipid analysis in the water column and surface sediments of the Black Sea. Environmental Microbiology, 11(10), 2720-2734.

Siebers, B. and Schönheit, P., 2005. Unusual pathways and enzymes of central carbohydrate metabolism in Archaea. Current opinion in microbiology, 8(6), 695-705.

Sollich, M., Yoshinaga, M. Y., Häusler, S., Price, R.E., Hinrichs, K.U., & Bühring, S.I. 2017. Heat stress dictates microbial lipid composition along a thermal gradient in marine sediments. Frontiers in Microbiology, 8, Article 1550, 1-19.

Steele, D.J., Tarran, G.A., Widdicombe, C.E., Woodward, E.M.S., Kimmance, S.A., Franklin, D.J., & Airs, R.L. 2015. Abundance of a chlorophyll a precursor and

the oxidation product hydroxychlorophyll a during seasonal phytoplankton community progression in the Western English Channel. Progress in Oceanography, 137, 434-445.

Sturt, H.F., Summons, R.E., Smith, K., Elvert, M., & Hinrichs, K.U., 2004. Intact polar membrane lipids in prokaryotes and sediments deciphered by high-performance liquid chromatography/electrospray ionization multistage mass spectrometry—new biomarkers for biogeochemistry and microbial ecology. Rapid Communications in Mass Spectrometry, 18(6), 617-628.

Vieille, C. & Zeikus, G.J., 2001. Hyperthermophilic enzymes: sources, uses, and molecular mechanisms for thermostability. Microbiology and Molecular Biology Reviews, 65(1), 1-43.

Von Damm, K. V., Edmond, J.T., Measures, C.I., & Grant, B. 1985. Chemistry of submarine hydrothermal solutions at Guaymas Basin, Gulf of California. Geochimica et Cosmochimica Acta, 49(11), 2221-2237.

Weijers, J.W., Schouten, S., Hopmans, E.C., Geenevasen, J.A., David, O.R., Coleman, J.M., Pancost, R.D. and Sinninghe Damsté, J.S., 2006. Membrane lipids of mesophilic anaerobic bacteria thriving in peats have typical archaeal traits. Environmental Microbiology, 8(4), 648-657.

White, D.C., Bobbie, R. J., King, J. D., Nickels, J., & Amoe, P., 1979. Lipid analysis of sediments for microbial biomass and community structure. In Methodology for biomass determinations and microbial activities in sediments. ASTM International, 87-103.

White, D.C., Ringelberg, D.B., Hedrick, D.B. and Nivens, D.E., 1994, January. Rapid identification of microbes and environmental matrices - characterization of signature lipids. In mass spectrometry for the characterization of microorganisms. American Chemical society 541, 8-17

Woese, C.R., Kandler, O., & Wheelis, M.L., 1990. Towards a natural system of organisms: proposal for the domains Archaea, Bacteria, and Eucarya. Proceedings of the National Academy of Sciences, 87(12), 4576-4579.

Wuchter, C., Schouten, S., Wakeham, S.G. and Sinninghe Damsté, J.S., 2005. Temporal and spatial variation in tetraether membrane lipids of marine Crenarchaeota in particulate organic matter: Implications for TEX86 paleothermometry. Paleoceanography, 20(3).

Yoshinaga, M.Y., Kellermann, M.Y., Rossel, P.E., Schubotz, F., Lipp, J.S. and Hinrichs, K.U., 2011. Systematic fragmentation patterns of archaeal intact polar lipids by high-performance liquid chromatography/electrospray ionization ion-trap mass spectrometry. Rapid Communications in Mass Spectrometry, 25(23), 3563-3574.

Yurkova, I., Kisel, M., Arnhold, J., & Shadyro, O., 2005. Iron-mediated free-radical formation of signaling lipids in a model system. Chemistry and Physics of Lipids, 137(1-2), 29-37.

Zhang, Y. G., Zhang, C.L., Liu, X.L., Li, L., Hinrichs, K.U., & Noakes, J.E., 2011. Methane Index: a tetraether archaeal lipid biomarker indicator for detecting the instability of marine gas hydrates. Earth and Planetary Science Letters, 307(3-4), 525-534.

Zhu, C., Lipp, J.S., Wörmer, L., Becker, K.W., Schröder, J., & Hinrichs, K.U., 2013. Comprehensive glycerol ether lipid fingerprints through a novel reversed phase liquid chromatography–mass spectrometry protocol. Organic Geochemistry, 65, 53-62.

Chapter 3: Hydrothermal influences on tetraether lipid environmental proxies

Jeremy N. Bentley [a,*] †, Carl A. Peters [a] †, Sievert, Stefan [b], Jeffery Seawald [b], G. Todd Ventura [a]

[a] *Department of Geology, Saint Mary's University, Halifax, Nova Scotia B3H 3C3, Canada.*

[b] *Woods Hole Oceanographic Institution, Woods Hole, USA*

* *Corresponding author: Jeremy.Bentley@smu.ca*
† *Indicates that these authors contributed equally*

Number of pages: 40 + 3 supplementary pages
Number of Figures: 8
Number of Tables: 2
For submission to: Earth and Planetary Science Letters

Abstract

The diversity of tetraether lipids found in soils and sediments is increasingly used to assess environmental change. For instance, the TetraEther indeX of 86 carbon atoms (TEX_{86}) paleoclimate proxy, based on archaeal glycerol dialkyl glycerol tetraether (GDGT) lipids is frequently used to reconstruct sea-surface temperatures (SST). However, in recent years, TEX_{86} temperature reconstructions have not always been representative of sea-surface conditions and its integrity as a paleo-proxy has been questioned. Here we show, with a series of push cores collected at the Cathedral Hill hydrothermal vent system in Guaymas Basin, Gulf of California that the TEX_{86} proxy is strongly influenced by *in situ* hydrothermal temperatures ($R^2 = 0.83$) indicating the proxy can be heavily attenuated by subsurface rather than upper water-column factors. In this regard, we have also found that branched isoprenoid tetraether (BIT), cyclization of branched tetraethers (CBT), and degree of cyclization (DC) indices are also affected by the high-temperature vent settings, demonstrating that GDGT proxies have to be treated with caution when sourced from marine sediments that are undergoing secondary alteration by hydrothermalism. We have therefore modified the TEX_{86} with the inclusion of hydroxlated GDGTs that are less stable at higher temperatures. The HydrOxy Tetraether index with 86 carbon atoms (HOT_{86}) is calibrated for hydrothermal vent systems and appears to track *in situ* temperatures ($R^2 = 0.89$) better than the TEX_{86}. This novel proxy may provide the ability to monitor sediment pore water profiles within hydrothermal environments without the use of thermal probes. It may also provide additional information to evaluate the integrity of sea-surface temperatures and other parameters calculated with GDGTs long after the sediments have been removed from their site of collection. As an extension of these outcomes, we suggest that reconstructed

SST profiles derived from sediments initially buried deep enough to be exposed to >60°C (HOT_{86} >= 0.7; TEX_{86} >= 0.56) may need to be corrected for *in situ* geothermal offsets caused by GDGT overprinting.

Highlights

1- GDGT and brGDGT proxies are influenced by geothermal temperatures when exposed to temperatures above ~ 60-70°C.
2- We suggest these proxies are influenced by *in situ* production of GDGTs.
3- We suggest that the newly developed HOT_{86} describes geothermal temperatures.
4- With this proxy, negative effects on GDGT and brGDGT proxies can be quality controlled and corrected.

1. Introduction

Intact polar lipids (IPLs) and core lipids (CLs), which lack a polar head group attachment to the glycerol of the lipid, have become common molecular markers for tracking the presence of living and dead archaea and bacteria within the geosphere (e.g., Lipp et al., 2008, Schouten et al., 2013). For example, archaeal CLs in the form of GDGTs and, in some cases, bacterial CLs comprised of branched GDGTs (brGDGTs) are widespread and easily detectable in the water columns of lakes, rivers, swamps, bogs as well as in soils and sediments of terrestrial and aquatic landscapes (Schouten et al., 2013). The structural diversity and chemical stability of GDGTs has resulted in the development of several geochemical lipid proxies (Schouten et al., 2002; Hopmans et al., 2004). The most commonly used GDGT-based proxy is the TetraEther indeX with 86 carbon atoms (TEX_{86}) introduced by Schouten et al. (2002). The TEX_{86} proxy is now frequently used to reconstruct sea-surface temperatures (SST), aiding in paleo-oceanography studies in many different regions around the world (i.e. Huguet et al., 2006; Kim et al., 2008; McClymont et al., 2012). This proxy measures variations in the number of cyclopentyl rings within the hydrocarbon skeleton of the CLs (excluding caldarchaeol and crenarchaeol) with the assumption that cyclization is an organismal response to changing temperature conditions in the external environment. However, for this proxy to be a viable SST indicator, the archaea producing the GDGTs extracted from ocean bottom sediments must be almost exclusively sourced from marine planktonic Euryarchaeota, such as Thaumarchaeota, that inhabit the pelagic zone (Tierney 2014). These lipids are similarly required to be efficiently transported to the sediment surface after cell death to

become consecutively buried and preserved to allow for a chemostratigraphic record of changing SSTs (Wuchter et al., 2005).

Over the last 10 years, this proxy has encountered numerous issues. These include SSTs reconstructed from archaea harvested within deeper portions of the water column (Lipp & Hinrichs 2009). For example, artificially hydrolyzed headgroups of marine archaeal IPLs harvested from a sediment trap indicate the production of GDGTs by microbial communities living within ocean bottom sediments. These may impact TEX_{86} values because offsets were demonstrated between sedimentary communities and fossil remains from planktonic communities (Lipp & Hinrichs, 2009). Similarly, Elling et al. (2015) demonstrated that TEX_{86} values can represent a mixed GDGT signal from both active microbial production in shallow sediments and fossil lipids sourced from the water column, ultimately suggesting that the sedimentary community compositions may exert controls on the TEX_{86} signal. Besseling et al. (2019) extended these concerns, suggesting TEX_{86} reflects subsurface temperatures rather than SSTs, as the input of GDGTs in marine settings are not exclusive to Thaumarchaeota, because a majority of marine group I (MGI) archaea also reside in subsurface waters. Collectively, these observations indicate that sub-pelagic zone microbial fauna may overprint the GDGT signals used to calculate the TEX_{86} proxy.

It is likely that the particles settling in the water column contain GDGTs. However, SSTs are subject to a seasonal bias from the increased production of GDGTs in the summer and the lack of production in the winter (Shintani et al. 2011). Additionally, many studies have neglected the impact of *in situ* production of GDGTs and of the

potential for post depositional transformations or degradation of upper water column inputs (Schouten et al., 2013).

The transport and transformation of GDGTs have also been investigated. Specifically, both stomachs and intestines of decapods were studied by Huguet et al. (2007). These authors highlighted a resilience of this class of molecules as TEX_{86} values did not show significant differences between the stomach and intestines of decapods. This also implies that there is minimal modification to the GDGT compositions as they pass through the gut of an organism and are deposited as fecal pellets. This transport mechanism can occur in the water-column and with other benthic organisms that may rework seafloor sediments.

The effects of thermal maturity has long been thought to influence proxy-based paleo-reconstructions. Schouten et al. (2004) conducted a hydrous pyrolysis experiment, which showed that at extreme temperatures (ca. >160°C), the TEX_{86} is negatively influenced producing lower values than their reference material. The outcome of their study was due to the preferential destruction of GDGT 2-5+5'. These temperatures are more extreme than those of our study area, however preferential destruction may still occur. Combining all the criticism of the TEX_{86} proxy, there seems to be a fundamental issue on the appropriate constraints for its use.

Other tetraether lipid proxies, such as the Branched Tetraether Index (BIT), which is used as an indication of terrestrial input have also received criticism. Xing et al. (2016) demonstrated the BIT index, does not always indicate soil organic matter in marine sediments as their study area should have had considerable amounts of brGDGTs, but did not. More recent studies using brGDGTs likewise appear to indicate water-

column rather than terrestrial sources for these molecules (Sinninghe Damsté et al., 2009; Tierney et al., 2012). The Methylation of Branched Tetraethers (MBT) and the Cyclization of Branched Tetraethers (CBT) proxies, which are often used to identify soil temperature and pH, are subject to seasonal bias because they seem to reflect soil temperatures rather than air temperatures (Schouten et al., 2013). Thus, reconstructing mean annual air temperatures (MAAT) with these proxies may not actually be reflective of true air temperatures. It also appears that these proxies also lack constraints on their use.

We examined near-surface ocean floor sediments from the Cathedral Hill hydrothermal vent complex located in the Guaymas Basin, Gulf of California (Figure 3.1) to determine if sea surface signals are impacted by the subsurface production of GDGTs in highly productive sites such as a hydrothermal vent. This type of site allows for an investigation of the potential maximum of a subsurface overprint. The Guaymas Basin experiences high sedimentation rates between 0.4-2 cm/yr (Curray et al., 1979; Gieskes et al., 1988), which should, in principle, enable a high-resolution archaeal lipid-based climate record. Seafloor spreading over the last 4 million years has resulted in the formation of a series of smaller sub-basins (Calvert, 1966; Moore, 1973). Deeply buried sediments within these sub-basins are intersected by magmatic sills. In the case of the Southern Trough, these sills promote the discharge of hydrothermal fluids that reach the ocean floor (Lonsdale and Becker, 1985). Many of the hydrothermal vents are covered by *Beggiatoa* spp. microbial mats. These mats have been extensively studied (McKay et al.,

2012; Meyers et al., 2013; Teske et al., 2016).

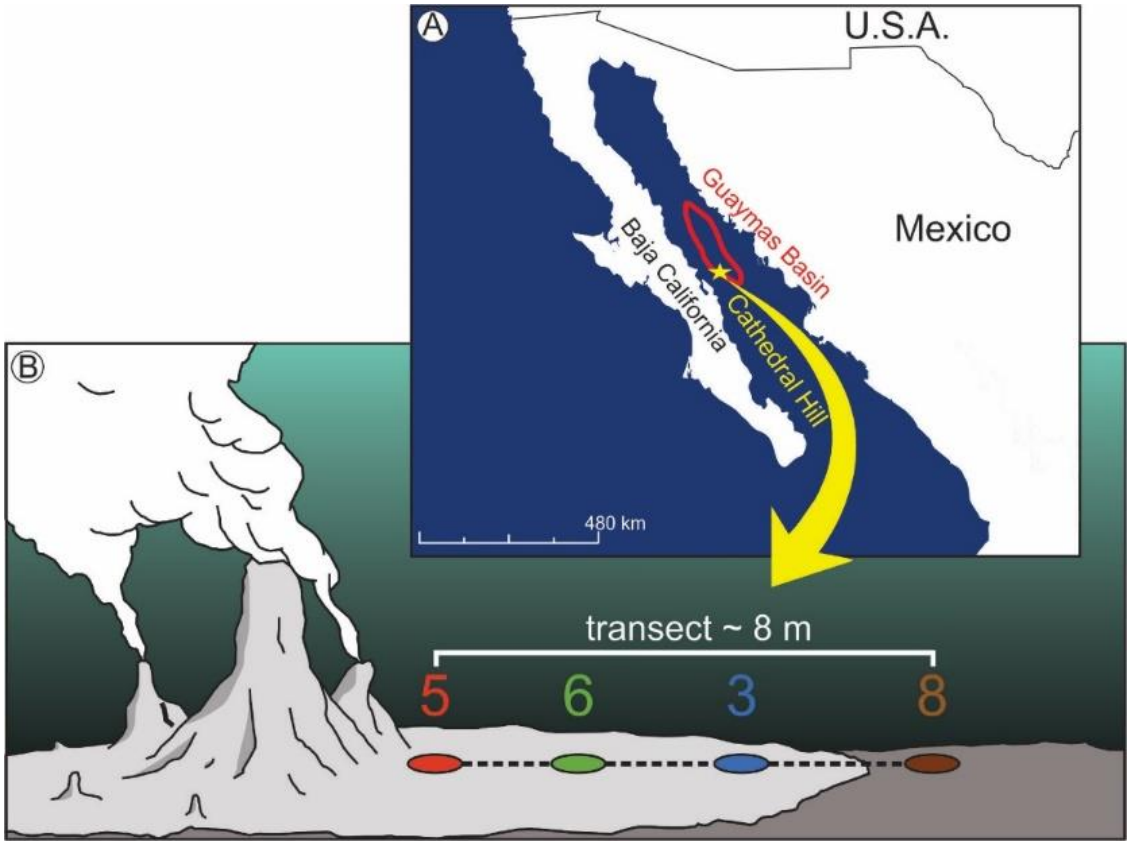

Figure 3.1- A) Location map of Guaymas Basin (red). Cathedral Hill in the Southern Trough is denoted as a yellow star. B) Schematic of the push core transect.

In this study, we evaluate the distribution of GDGTs and their corresponding proxy signals within the push core transect that were collected at the Cathedral Hill hydrothermal vent system, providing an opportunity to evaluate the response of the TEX_{86} and other proxies with exposure to increasing vent temperatures. Such a setting would not typically be ideal for paleo-environmental reconstructions. However, this unique setting allows for the ability to test the stability of the TEX_{86} proxy and to determine if overprinting and thermal decay of the proxy-based lipids occurs from the flourishing subsurface communities and extreme thermal gradients. Additionally, we have investigated a modified TEX_{86} thermometer termed HOT_{86} that includes a larger suite of

iGDGTs, particularly incorporating hydroxylated GDGTs (OH-GDGTs). We suggest it can be used to determine a wide gradient of sediment porewater temperatures (~20-160°). We further identify biological irregularities that influence the obtained TEX_{86} and HOT_{86} values. Lastly, we present confidence intervals for the use of tetraether lipid proxies and a correction factor for SST reconstructions using TEX_{86} values to back out the original signal in areas where *in situ* biota may be overprinting the upper water column thermal signature.

2. Material and methods

2.1. Study location and sampling

A four push core transect sampled with ~2m spacing was collected at the Cathedral Hill hydrothermal vent system in Guaymas Basin, Gulf of California (Figure 3.1). These push cores were collected by DSV-2 Alvin, a manned submersible from the Woods Hole Oceanographic Institution (WHOI) on Dive 4462 (10/22/08). The push cores were labeled Cores 5, 6, 3, and 8. Cores 5, 6, and 3 trend outboard from the vent complex, but are still within an area covered by white-, orange, and yellow filamentous *Beggioatoa* spp. microbial mat. Core 8 was collected furthest away from the vent and exterior to the mat. The sediments in Core 8 were exposed to more ambient pore water temperatures. Accompanying these push cores are *in situ* pore water temperature measurements obtained with a thermal probe that was inserted into the sediments directly adjacent to each push core. Once the samples were collected they were subsampled into 2-3 cm-thick intervals (Table 4) and immediately stored at -40°C (onboard the ship) and -80°C (within the

laboratory) temperatures. The subsamples were then freeze-dried, homogenized, and kept at −80°C until extraction.

Table 4. Details of the sample set

	Depth (cmbsf)	Location	Temperature (°C)
GB4462-5	**0-2**	Near vent	19
GB4462-5	**2-4**	Near vent	67
GB4462-5	**4-6**	Near vent	85
GB4462-5	**6-8**	Near vent	105
GB4462-5	**8-10**	Near vent	117
GB4462-5	**10-12**	Near vent	125
GB4462-5	**12-15**	Near vent	135
GB4462-5	**15-18**	Near vent	145
GB4462-5	**18-21**	Near vent	153
GB4462-6	**0-2**	Mid microbial mat	11
GB4462-6	**2-4**	Mid microbial mat	22
GB4462-6	**4-6**	Mid microbial mat	20
GB4462-6	**6-8**	Mid microbial mat	47
GB4462-6	**8-10**	Mid microbial mat	60
GB4462-6	**10-12**	Mid microbial mat	73
GB4462-6	**12-15**	Mid microbial mat	87
GB4462-6	**15-18**	Mid microbial mat	105
GB4462-6	**18-21**	Mid microbial mat	125
GB4462-3	**0-2**	Fringe of microbial mat	3.2
GB4462-3	**2-4**	Fringe of microbial mat	8
GB4462-3	**4-6**	Fringe of microbial mat	15
GB4462-3	**6-8**	Fringe of microbial mat	26
GB4462-3	**8-10**	Fringe of microbial mat	34
GB4462-3	**10-12**	Fringe of microbial mat	43
GB4462-3	**12-15**	Fringe of microbial mat	54
GB4462-3	**15-18**	Fringe of microbial mat	66
GB4462-3	**18-21**	Fringe of microbial mat	80
GB4462-8	**0-2**	Ambient sediment	0
GB4462-8	**2-4**	Ambient sediment	8
GB4462-8	**4-6**	Ambient sediment	16
GB4462-8	**6-8**	Ambient sediment	18
GB4462-8	**8-10**	Ambient sediment	21
GB4462-8	**10-12**	Ambient sediment	23
GB4462-8	**12-15**	Ambient sediment	25

2.2. Sample extraction

The samples were spiked with a recovery standard (1-alkyl-2-acetoyl-*sn*-glycero-3-phosphocholine (PAF); Avanti Polar Lipids, Inc.) and extracted using a modified Bligh and Dyer protocol after Sturt et al. (2004). The extraction involved six steps using 3 different solvent mixtures. For the first four steps solvent mixtures of methanol/dichloromethane/buffer [2:1:0.8; v/v] were used. The first two steps used a phosphate buffer (5.5g/L Na_2HPO_4; Avantor Performance Materials, LLC.) adjusted to pH of 7.4 with HCl; Anachemia Co.), while the third and fourth steps employed a trichloroacetic acid buffer (50 g/L $C_2HCl_3O_2$; Avantor Performance Materials, LLC. (pH of 2). The final two steps used a solvent mixture of methanol/dichloromethane [5:1; v/v]. Each extraction step consisted of a 6 ml of solvent mixture, which was sonicated for 5 minutes and centrifuged for 5 minutes at 1250 rpm. After each extraction step, the solvent was decanted and combined in a separation funnel. Once all of the steps were combined, the extract was purified with milliQ water, heated at ca. 60°C, and evaporated to dryness under a gentle steam of dry nitrogen. The resulting total lipid extract (TLE) was then spiked with 1, 2-diheneicosanoyl-*sn*-glycero-3-phosphocholine (C_{21}-PC; Avanti Polar Lipids, Inc.) and subsequently stored at -20°C before it was injected for mass spectral analysis.

2.3. High performance liquid chromatography – mass spectrometry (HPLC-MS)

A reverse phase electrospray ionization method with a scan range from 100-3000 *m/z* was chosen for its ability to simultaneously resolve archaeal IPLs and CLs. An

aliquot of each sample representing 1% of the TLE was analyzed using an Agilent Technologies 1260 Infinity II HPLC coupled to an Agilent Technologies 6530 quadruple time-of-flight mass spectrometer (qToF-MS). Separation was achieved following the method described by Zhu et al. (2013) using an Agilent Technologies ZORBAX RRHD Eclipse Plus C_{18} (2.1 mm × 150 mm × 1.8 μm) reverse phase column, fitted with a guard column and maintained at 45°C. The flow rate was set to 0.25 mL/min. and the gradients were: mobile phase A (methanol/formic acid/ammonium hydroxide [100:0.04:0.10] v/v) held at 100% for 10 min., followed by a linear gradient to 24% mixing with mobile phase B (propan-2-ol/formic acid/ammonium hydroxide [100:0.04:0.10] v/v) extending for 5 min., a linear gradient to 65% B for 75 min., followed by 70% B for 15 min., that finished by re-equilibrating with 100% A for 15 min. The injection solvent was methanol.

Analyte identification was achieved by mass spectral analysis via spectra with accurate mass resolution and similarities of fragmentation patterns as presented in the literature (e.g. Knappy et al., 2009; Liu et al., 2010; Yoshinaga et al., 2011) using Agilent Technology's MassHunter software. Quantification was achieved by summing the integration of peak areas of adducts $[M+H]^+$, $[M+NH_4]^+$, and $[M+Na]^+$ for the respective GDGTs of interest. Once the integrated peak areas were determined for each GDGT, concentration values were obtained relative to the internal C_{21}-PC standard and reported in μg/g dry sediment weight.

Response factors were determined by a series of injections of a standard solution containing: 1,2-diacyl-3-O-(α-D-galactosyl1-6)-β-D-galactosyl-*sn*-glycerol (DGDG), 1,2-diacyl-3-O-β-D-galactosyl-*sn*-glycerol (MGDG), 1-alkyl-2-acetoyl-*sn*-glycero-3-phosphocholine (PAF), 1,2-di-O-phytanyl-*sn*-glycerol (Archaeol), 1',3'-bis[1,2-

dimyristoyl-*sn*-glycero-3-phospho]-glycerol (14:0 Cardiolipin), 1,2-diheneicosanoyl-*sn*-glycero-3-phosphocholine (C_{21}-PC) from Avanti Polar Lipids, Inc., USA, and 2,2′-di-O-decyl-3,3′-di-O-(1′′,ω′′-eicosanyl)-1,1′-di-(rac-glycerol) (C_{46}-GTGT) from Pandion Laboratories, LLC in amounts ranging from 100 pg to 30 ng. Concentrations of the standard mix were then calculated from peak areas of molecular ions in mass chromatograms. Response factors were calculated relative to the C_{21}-PC, and the appropriate correction factor was applied to the particular lipid class of interest.

A series of samples were re-run to identify or confirm deviations in the data set. The variations between the concentrations of GDGTs in the re-run and the initial runs yielded a maximum difference of ~ ± 4 μg/g per GDGT compound, providing confidence in the initial results and confirming the presence of two outlies in the data set. These outliers are Core 8 at 8-10 cm, with abnormally low concentrations of all compounds that is likely ion suppression in the analysis from a sample heavily impregnated with oil, and Core 3 at 15-18 cm, which contains relatively high lipid concentrations that are yet to be explained.

2.4. Tetraether environmental proxies

The following section will outline the various tetraether proxies that have been investigated. The numbers in the equations represent the specific GDGTs structures (Figure 3.2) whereas brGDGTs are referred to in Roman numerals (Supplementary Fig. S1-1). The TEX_{86} paleoclimate proxy (Schouten et al., 2002) (Eq. 1):

(1) $TEX_{86} = \frac{2+3+5'}{1+2+3+5'}$

is widely used to reconstruct SSTs. TEX_{86} values tend to range from 0.2-0.9 in both marine and lake sediment (Damsté et al., 2009; Powers et al., 2010; Schouten et al. 2013). However, TEX_{86} reconstructions in lakes can be problematic in settings lacking Crenarchaeota as the production of these archaea is water-depth dependent (Powers et al. 2010; Zink et al., 2010).

The ring index (RI) (Eq. 2):

(2) $RI = \frac{\mathbf{0}\,x\,(GDGT-\mathbf{0}) + \mathbf{1}\,x\,(GDGT-\mathbf{1}) + \mathbf{2}\,x\,(GDGT-\mathbf{2}) + \mathbf{3}\,x\,(GDGT-\mathbf{3}) + \mathbf{4}\,x\,(GDGT-\mathbf{4}) + \mathbf{5}\,x\,(GDGT-\mathbf{5}) + \mathbf{5}\,x\,(GDGT-\mathbf{5'})}{sum\ of\ all\ GDGTs}$

is a weighted average of the number of rings within a sample (calculated after Pearson et al., 2004; Eq 2). This ratio records the increasing number of rings within the archaeal core lipid pool, which can be used to infer the adaptive strategy that regulates the flow in and out of a cellular membrane by decreasing fluidity but increasing rigidity. Rigidification of the cellular membrane serves as an adaptive strategy within environments that have elevated temperatures or increased acidity (Gliozzi et al., 1983; Macalady et al., 2004; Boyd et al., 2013).

The Methane index (MI) as described by Zhang et al. (2011) (Eq. 3):

(3) $MI = \frac{\mathbf{1+2+3}}{\mathbf{1+2+3+5+5'}}$

describes areas of normal marine conditions and active anaerobic oxidation of methane (AOM). MI values between 0-0.3 are characteristic of normal marine conditions. Values greater than 0.5-1 are observed for hydrate impacted areas or within environments where high levels of AOM occur.

Various proxies are based on distributions of brGDGTs. The Cyclization ratio of Branched Tetraether (CBT) index (Eq. 4):

(4) $$\text{CBT} = -log\frac{Ib+IIb}{Ia+IIa}$$

calculated after Weijers et al. (2007) is often used to evaluate soil pH where values range from 0 - 2.2.

The Methyl Branched Tetraether (MBT) index calculated after Weijers et al. (2007) (Eq. 5):

(5) $$\text{MBT} = \frac{Ia+Ib+Ic}{Ia+IIa+IIIc+Ib+IIb+IIIb+Ic+IIc+IIIc}$$

represents the degree of methylations that occurs at the C-5 and C-5' positions with values that range from 0.15-1.

The Degree of Cyclization (DC; after Sinninghe Damsté et al., 2009) (Eq. 6):

(6) $$DC = \frac{Ib+IIb}{Ia+IIa+Ib+IIb}$$

measures the amount of cyclopentane moieties within brGDGTs and has values that range from 0-0.4.

The branched isoprenoid tetraether (BIT) index (Hopmans et al., 2004; Eq. 7):

(7) $$BIT = \frac{I+II+III}{I+II+III+(GDGT-5)}$$

describes input of terrestrial soil organic matter. The brGDGTs are predominantly produced in terrestrial settings and thus represent depositional of terrestrial organic matter. BIT values range from 0-1.

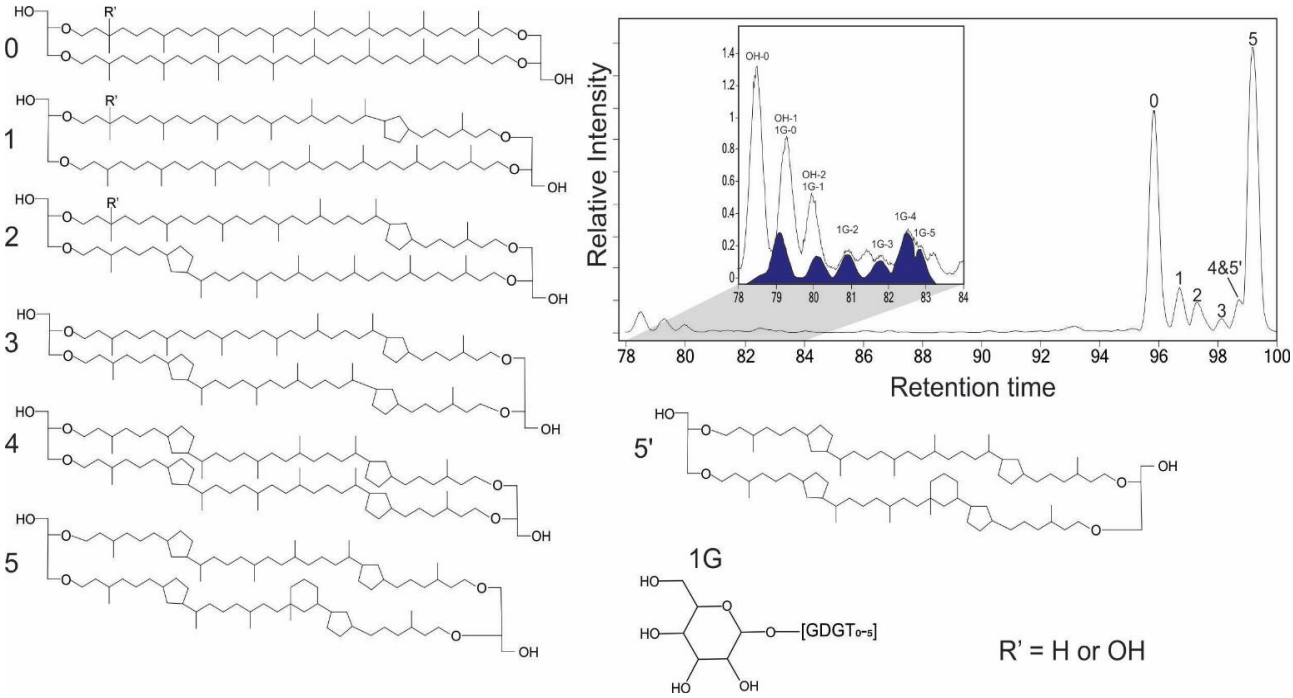

Figure 3.2 - Chemical structures of GDGTs and their elution patterns on a reconstructed BPC from 500-3000 m/z (note that 1G-GDGTs in blue were obtained from an EIC and overlayed on the BPC to denote their elution positions).

3. Results and discussion

3.1. Core lipid concentrations

Assessing GDGT concentrations, independent of ratio based comparisons, spatially (both across the transect and with depth) is vital to understand how these molecules are changing and how this may inevitably be influencing tetraether-based proxies. Core 8 of the transect offers the closest approximation to an ambient ocean bottom sediment and can therefore be considered equivalent to a water-column sediment trap. Summed concentrations of all GDGTs in Core 8 are consistent at ~ 400 μg/g sediment from top to bottom of the core (Table 5), which indicates a relatively constant

input of organic matter. The other three transect cores (5, 6, and 3) have higher summed concentrations of GDGTs. For these surface sediments, yields of ~ 500 μg/g are likely resulting from the rapid redox changes and the presence of metabolically-important substrates and metabolites within the vent fluids that enables the growth of *Beggiatoa* colonies, whose filaments penetrate ~ 4 - 8 cm into the underlying sediment. The three cores experience dramatic increases in down core temperatures. The temperature increases closely parallel decreasing GDGT concentrations with depth. At the bottom of Core 5 and 6 (18-21 cmbsf) GDGTs record roughly 90-94% reductions in yields with concentrations of ~ 40 μg/g at 153°C and ~ 30 μg/g at 125°C, respectively. The depletion is less extreme with a ~ 60% loss in Core 3 (18-21 cmbsf), where GDGT concentrations are ~200 μg/g at 80°C.

OH-GDGTs follow similar trends, but these lipids are in much lower concentrations than that of the GDGTs. For instance, in Core 8 the summed OH-GDGTs are ~20 μg/g all the way down core. Similar elevated concentrations are observed at the surface of Cores 5, 6, and 3 with OH-GDGT concentrations of ~ 28 μg/g sediment and similar to GDGTs a decrease in concentration is observed with depth. The bottom of Core 5 and 6 (18-21 cmbsf) have OH-GDGT concentrations that are near detection limits at ~ 0.25 μg/g at 153°C and ~ 0.35 μg/g at 125°C, respectively. OH-GDGT concentrations are ~ 9.3 μg/g at 80°C at the bottom of Core 3 (18-21 cmbsf).

The brGDGTs in Core 8 have a consistent range of concentrations (~ 5.5 μg/g). For cores 6 and 3 concentrations are ~ 7 μg/g at the surface. Core 5 has a lower concentration of ~ 5 μg/g observed within the surface sediment. Subsurface depletion trends in Cores 5 and 6 are similar with the bottom of each core (18-21 cmbsf) having a

brGDGT concentration of ~ 0.86 µg/g at 153°C, and ~ 1 µg/g at 125°C, respectively. The brGDGT concentration at the bottom of Core 3 (18-21 cmbsf) has a concentration of 4 µg/g at 80°C.

There are two notable outliers in the sample set as previously discussed in section 2.5, one being in Core 8 and one being in Core 3. The outlier in Core 8 (8-10cm) is likely an analytical artifact attributed to matrix effects from *in situ* petroleum. This would likely cause ion suppression in HPLC runs. The outlier in Core 3 (15-18 cm) is less explainable, providing concentrations for cGDGT and brGDGTs that are approximately double the intervals above and below it. Absolute concentration values can be found in Table 5 below, however individual structure concentrations can be found in the supplementary data (Appendix A-3). In some cases, the bottom of Core 8 (12-15 cm) has the potential to be an outlier as the sample extracted only contained 0.32 g of material compare to ~3 grams, which was the target weight for extraction.

Unlike GDGTs and OH-GDGTs, monoglycosidic-GDGTs (1G-GDGTs) concentrations follow slightly different trends. In Core 8, the concentrations of 1G-GDGTs are rather consistent and average concentration are ~ 8 µg/g with slightly elevated concentrations of 11 µg/g sediment at the surface and slightly depleted concentrations of 6 µg/g sediment near the bottom of the core. The same enrichment occurs at the surface of Cores 5, 6, and 3, where concentrations are ~ 15 µg/g. However, the subsurface concentrations display deviations. In Core 5, 1G-GDGTs extend to 15-18 cmbsf having a concentration of 0.11 µg/g at 145°C. In Core 6, the signature for 1G-GDGTs extends to 12-15 cmbsf having a concentration of 1 µg/g at 87°C. In Core 3, the

signature of 1G-GDGT persists all the way down core (18-21 cmbsf) having a concentration of 5.22 µg/g at 80°C.

Table 5 - Concentrations of lipids of interest in µg/g sediment.

Sample Id and Temp (°C)	cGDGT	OH-GDGT	1G-GDGT	brGDGTs
GB4462-5-0-2cm-19°C	506.01	25.76	14.86	5.19
GB4462-5-2-4cm-67°C	459.21	24.07	13.37	5.75
GB4462-5-4-6cm-85°C	204.18	10.38	6.00	2.37
GB4462-5-6-8cm-105°C	153.66	6.69	4.31	1.98
GB4462-5-8-10cm-117°C	60.10	2.41	3.19	1.07
GB4462-5-10-12cm-125°C	49.73	1.63	1.66	1.52
GB4462-5-12-15cm-135°C	84.29	1.39	1.39	3.29
GB4462-5-15-18cm-145°C	44.91	0.43	0.11	1.12
GB4462-5-18-21cm-153°C	39.84	0.26	0.00	0.86
GB4462-6-0-2cm-11°C	595.98	28.84	16.20	7.05
GB4462-6-2-4cm-22°C	267.74	14.81	6.69	4.00
GB4462-6-4-6cm-20°C	88.12	4.67	2.27	1.68
GB4462-6-6-8cm-47°C	71.46	3.08	3.33	2.80
GB4462-6-8-10cm-60°C	49.63	1.81	1.98	1.29
GB4462-6-10-12cm-73°C	53.18	2.07	1.97	1.51
GB4462-6-12-15cm-87°C	45.19	1.37	1.00	1.12
GB4462-6-15-18cm-105°C	22.95	0.12	0.00	0.66
GB4462-6-18-21cm-125°C	31.82	0.35	0.00	1.00

GB4462-3-0-2cm-3.2°C	513.50	30.60	14.17	7.73
GB4462-3-2-4cm-8°C	309.79	15.89	7.56	4.07
GB4462-3-4-6cm-15°C	284.17	14.77	6.38	3.82
GB4462-3-6-8cm-26°C	276.48	15.24	6.79	4.18
GB4462-3-8-10cm-34°C	252.32	13.69	5.18	5.19
GB4462-3-10-12cm-43°C	229.71	13.21	5.33	5.20
GB4462-3-12-15cm-54°C	180.75	10.08	6.53	5.11
GB4462-3-15-18cm-66°C	254.38	12.38	6.45	10.99
GB4462-3-18-21cm-80°C	186.72	9.31	5.22	4.88
GB4462-8-0-2cm-0°C	486.08	27.77	11.12	6.36
GB4462-8-2-4cm-8°C	419.45	21.35	8.83	5.43
GB4462-8-4-6cm-16°C	482.69	26.81	11.03	6.64
GB4462-8-6-8cm-18°C	361.13	18.60	8.82	4.68
GB4462-8-8-10cm-21°C	154.65	9.66	2.42	2.22
GB4462-8-10-12cm-23°C	462.82	23.28	6.47	6.77
GB4462-8-12-15cm-25°C	517.35	22.57	6.05	6.27

3.2. Core lipid based proxies and the impact of temperatures

The TEX_{86} values for Core 8 span a narrow range of values (0.52 to 0.54). These values extend down the entirety of the 15 cm length of the core, which translates to

~ 7.5 to 37.5 yrs with sedimentation rates estimated to be maximum of 2 cm/yr or minimum of 0.4 cm/yr (Curray et al., 1979; Gieskes et al., 1988). The TEX_{86} values equate to reconstructed SST of ~ 19°C following the calibration model of Kim et al. (2010) (Supplementary Table A 3-7), which is between the recorded modern winter and summer sea surface conditions reported for the Gulf of California (McClymont et al., 2012). These results strongly suggest the GDGTs in the ambient sediments are largely sourced by settling of particles from the upper water column.

The TEX_{86} values as recorded in the other transect core sediments have a considerably larger range of values from 0.52 and 0.63 that systematically increase with sediment pore water temperatures that range from 2 to 153°C (R^2= 0.83; Fig. 3.3A, where an R^2 value greater than 0.6 is considered significant). In this regard, Cores 5, 6, and 3 that are most closely associated with the hydrothermal system record progressively high TEX_{86} values with sediment depth. This is most noticeable in Core 5 where the highest TEX_{86} values are obtained for the bottom core sediments (0.55-0.63; Fig 3.3A). These results suggest the source of the archaeal CLs progressively becomes more dominated by a subsurface microbial community that is itself responding to the hotter geothermal temperatures of the venting hydrothermal fluids. As such, the results indicate that in some settings the TEX_{86} SST-proxy is recording *in situ* geothermal temperatures. This concept has been discussed in several studies (Lipp & Hinrichs, 2009; Elling et al., 2015; Besseling et al., 2019). However, to our knowledge it has not yet been systematically demonstrated.

These results show a direct impact on the TEX_{86} values by hydrothermalism. Higher TEX_{86} values obtained in the hotter intervals at Cathedral Hill are supported by

earlier observations by studies such as Huguet et al. (2007), Kim et al. (2012) and others who reported that the TEX_{86} values may be representative of subsurface temperatures rather than sea-surface temperatures. Alternatively, various GDGT core lipids could be thermally unstable and preferentially removed from the lipid pool when exposed to the sharp geothermal gradient of Cathedral Hill. However, hydrous pyrolysis experiments conducted by Schouten et al. (2004) indicate that only at extreme temperatures greater than 160°C does the TEX_{86} values become negatively influenced due to the preferential destruction of GDGT 2-5+5'. The preferential destruction does not appear to be occurring nor do temperatures reach this threshold.

To better interpret the TEX_{86} trends and to ensure that reconstructed temperatures were not influenced by other forcing factors such as, the RI and MI (Figure 3.3, B, D) were plotted against recorded *in situ* pore water temperatures. As seen in Chapter 2, both Cores 5 and 6 have RI values that are highly correlated with temperature (R^2 = 0.87 and 0.75, respectively). However, a single trend line (R^2 = 0.16) to evaluate the whole system indicates that temperature is not the primary driving force for the RI across the transect of the core. Furthermore, these results are consistent with a significant proportion of measured GDGTs being sourced from the shallow sediments. The relationship between the RI and temperature may be coupled with optimal growth temperature, as demonstrated in Wuchter et al. (2004) and Elling et al. (2015). In this regard, the lipid cyclization pattern could reflect stratigraphically discrete thermophile to extremophile communities that are selectively adapted to more extreme temperature conditions. RI values in core sediments with elevated temperatures show the best correlations and appear to reach a maximum RI value at ~ 120°C in Core 5 and ~ 80°C in

Core 6. These values may potentially be the optimal growth for the dominant Archaea present. The cyclization pattern may also be a microbial response whereby Archaea selectively modify their lipid structures through the incorporation of new ring cycles in order to decrease membrane fluidity within the thermally stressed environment (Gliozzi et al., 1983; De Rosa and Gambacorta, 1988; Uda et al., 2001; Schouten et al., 2002).

The MI describes areas that experience high levels of AOM (Zhang et al., 2012). The data suggests that there is no correlation between MI and temperature for the Cathedral Hill system (R^2= 0.09). The Cathedral Hill sediment samples have moderate to low MI values (0.25 - 0.38). This suggests that the MI likely has little influence on the TEX_{86} values obtained in the push core transect as *in situ* production of GDGTs from methanotrophic archaea should be minimal. Conversely, in areas where higher MI values are obtained, SST reconstructions may be influenced by the *in situ* production of GDGTs as previously described by Zhang et al. (2011).

The incorporation of OH-GDGTs into a paleoclimate proxy has previously been suggested as an alternative to the TEX_{86} SST proxy (Huguet et al., 2013) even though the physiological function of OH-GDGTs is relatively unknown (Huguet et al., 2017). Following on this, we have similarly modified the TEX_{86} to include both OH-GDGTs and GDGT-4, since these molecules are thought to potentially be produced under different environmental stress (Liu et al., 2012) and have different thermochemical stabilities (Sollich et al., 2017). In this regard, we introduce the HydrOxy Tetraether index with 86 carbon atoms (HOT_{86}):

(8) $$HOT_{86} = \frac{2+3+4+5'+(1-OH)+(2-OH)}{1+2+4+5'+(0-OH)+(1-OH)}$$

with this modification a slightly stronger linear correlation is observed between the HOT_{86} values and measured temperatures ($R^2 = 0.89$; p = 2.2e-16) (Fig. 3.3C), suggesting the new index is sensitive to a large range of hydrothermal vent fluid temperatures with a higher goodness of fit. Additionally, %GDGT was calculated (Table A3-7), which were found to be under the outline 67% which is thought to be an indicator of non-water column sources if greater than this assigned value (Sinninghe Damste et al., 2012).

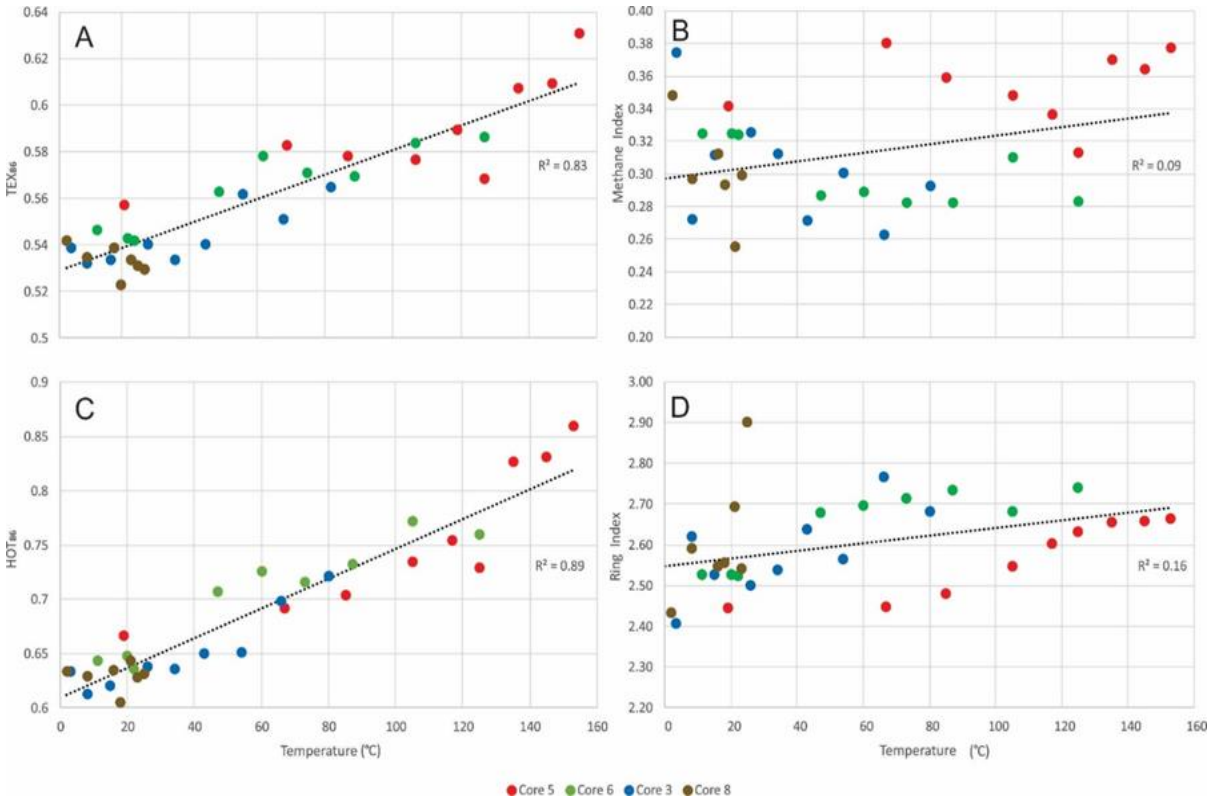

Figure 3.3 - Indices vs. temperature, A) TEX_{86} vs. temperature, B) Methane index vs. temperature, C) HOT_{86} vs. temperature, D) Ring index vs. temperature. Trend lines for this data are present as single trend lines for the whole data set to demonstrate the overall control or lack of control over the system. Equations of these lines are; A (y = 0.0005x + 0.53), B (y = 0.0003x + 0.30), C (y = 0.0014x + 0.61), and D (y = 0.0009x + 2.55).

To evaluate the potential impact of reconstructing past environments in settings that are deemed unreliable due to hydrothermallism, we have calculated SST

values using the global core top calibration model of Kim et al. (2008) with SST = -0.178 + 56.2 * TEX_{86} and compared our predicted temperature values with the measured pore water vent temperatures (Figure 3.4). A systematic increase in reconstructed SST with increased *in situ* temperature is observed (R^2 = 0.83; Figure 3.4). All the cores in the push core transect are arguably expected to receive the same input from the upper water column and their respective reconstructed SSTs should be comparable to Core 8. However, it is clear that the cores that are thermally influenced produce SST values that are much higher than the ambient cores (Figure 3.4) suggesting an overprinting of the original SST signal. Thus, we suggest that within hydrothermal environments, samples with HOT_{86} values >0.7 and likewise TEX_{86} values >0.56 may likely record geothermal temperatures (Fig. 3.3 A & C). In an attempt to make this new proxy usable to evaluate SSTs in areas where GDGT pools may be influenced by *in situ* production or *in situ* destruction of GDGTs (i.e. sediment cores deeper than ~2500 m, pockmarks, mud volcanoes) we have established a correction factor that can be applied to SSTs calculated with the original TEX_{86}. The correction factor (CF; Eq 10) is calibrated for hydrothermal vent systems and is described as follows:

(9) $SST_{real} = SST_{TEX86} + CF$

(10) $CF = TEX_{86}/LOG(HOT_{86})+2.65$

However, this correction factor still needs to be applied to other study areas to test its validity, but appears promising.

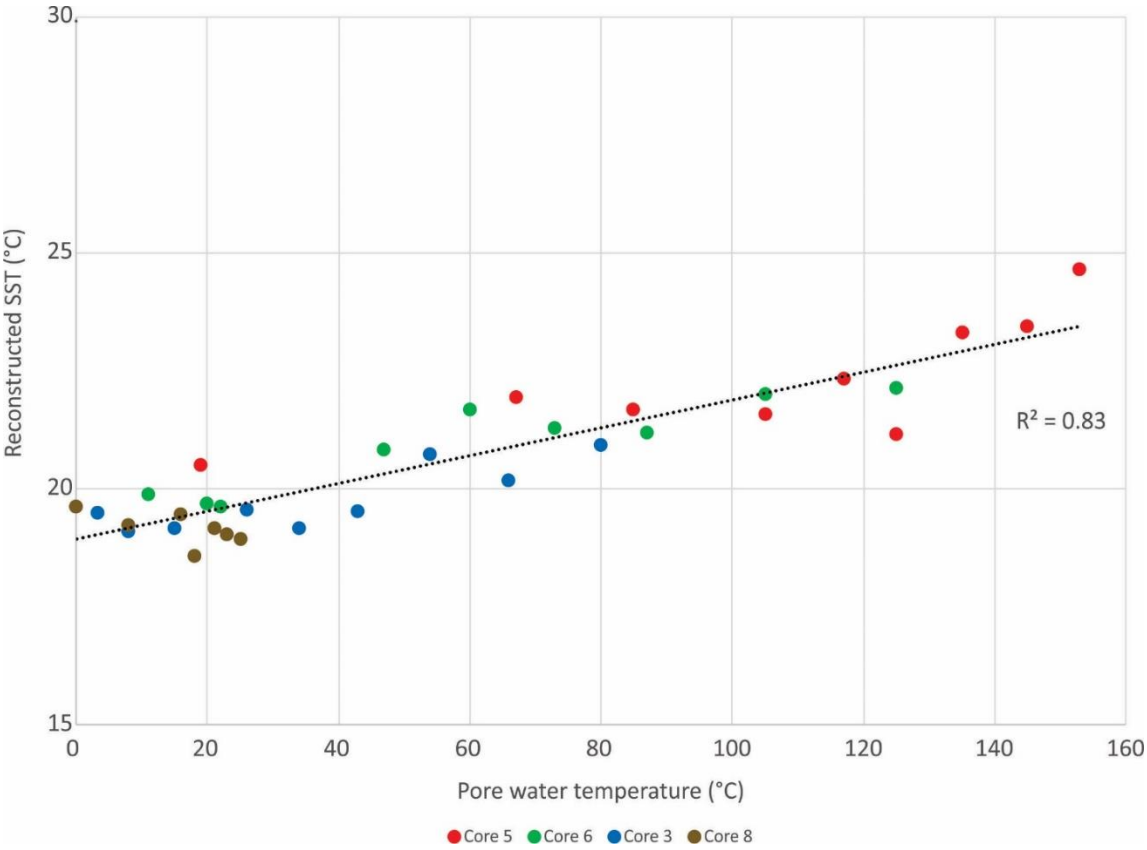

Figure 3.4- Reconstructed SST from TEX_{86} values vs pore water temperatures, showing that the cores that experience higher pore water temperatures, reconstruct higher sea surface temperatures (y = 0.0005x + 0.53).

3.3. Signal sourcing

As an attempt to validate the dominant signature (detrital or *in situ*) in the TEX_{86} and HOT_{86}, we compare the values obtained from core GDGTs and 1G-GDGT (Figure 3.5). The 1G-GDGTs are produced by marine benthic archaea, which are still alive (e.g., Schouten et al., 2013), representing a living signal that can be used to calculate the tetraether indices. Where the core GDGT is likely to represent the signal from the dead. Furthermore, we observed three clusters of points (A_1, B_1, C_1; Figure 3.5 A), suggesting there is a mixed signal for sourcing of archaeal GDGTs from living and

dead pools of archaea. This is consistent with observations of Shah et al. (2008), who suggested that *in situ* production of core GDGTs from microbial communities contribute to the general GDGT pool producing a of mixed origins. In this plot an assumption was made that clusters that fall on the 1:1 line likely indicates the living biota is contributing to the "dead pool" of GDGTs, thereby masking the proxy's intended sea-surface temperature value. Overall, three clusters were observed which appear to be representing the ambient sea floor (Core 8) and the surface of Core 3 as well as Core 6 (A_1), an active archaeal communities (B_1), and sediment that are likely heavily influenced by the *in situ* biota (C1) as the signal is likely driven by the living biota overprinting the original GDGT signal, ultimately producing high TEX_{86} values. The process of how this occurs is currently unknown but we speculate that recycling may account for this phenomena. There is a possibility that archaea are recycling lipid in the environment and modifying them only to subsequently reintroduce them back into the environment.

Cluster C_1 is one of the more interesting clusters, which we suggest has new implications for the reliability of the TEX_{86}. The samples in these intervals would experience similar thermal gradients as samples in locations, which may include, but are not limited to hydrothermal vents, near mid-ocean spreading ridges, submarine volcanoes, pockmarks, accretionary melanges, or samples at depth that experience geothermal gradients resulting in temperatures higher than 60°C. A similar comparison with HOT_{86} values of CLs and IPLs was done and this plot generates similar clusters (A_2, B_2, C_2; Figure 3.5 B). The clustering shifts to the left, which we believe is evidence that this new proxy tracks the living extremophile benthic communities closer than TEX_{86}. Consequently, the clusters may represent the broad classification of the subsurface

communities present, potentially distinguishing mesophilic and hyperthermophilic archaea. We believe that A_2 represents a similar classification of ambient or surficial sediments just like A_1 of the TEX_{86} clusters. Cluster B_2 likely represents mesophilic archaea and cluster C_2 likely represents hyperthermophilic archaea. Archaea such as *Methanopyrus kandleri* may be a potential candidate for a hyperthemophilic source as outlined in Teske et al. (2014), a study conducted in the Guaymas Basin. These hyperthermophic archaea may produce the signal of cluster C_2 in our study.

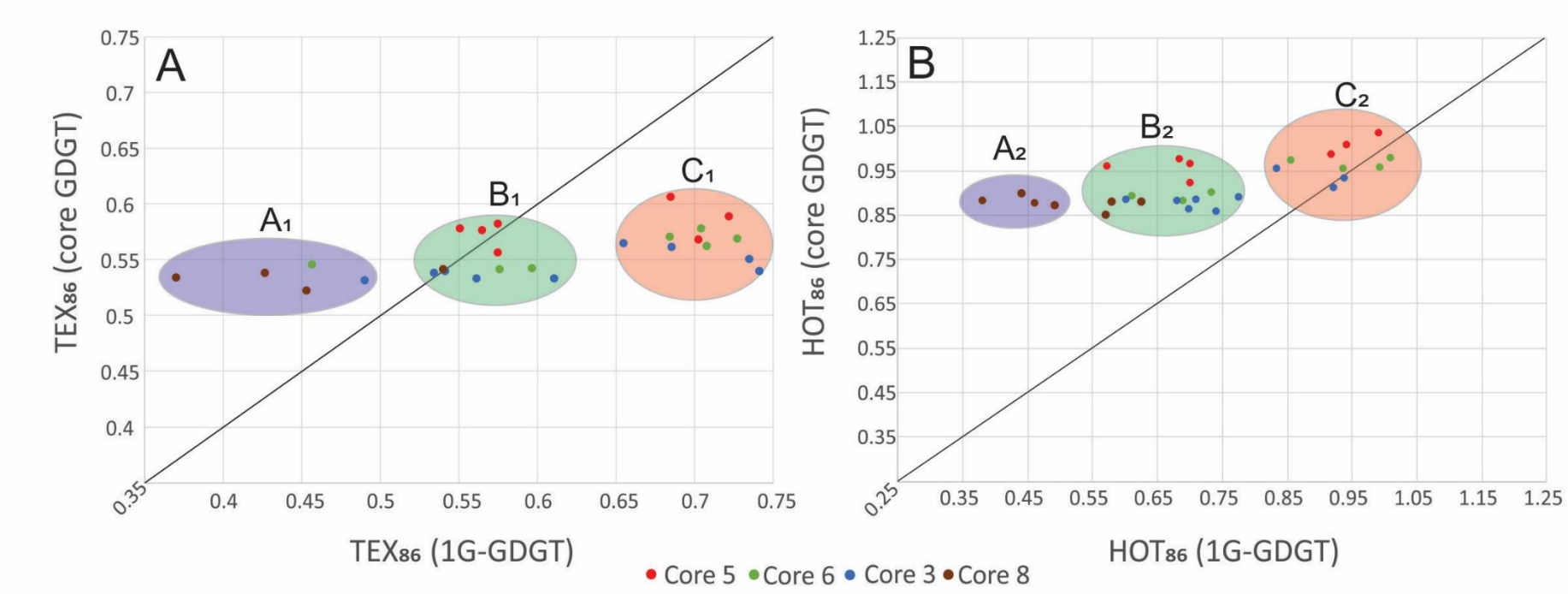

Figure 3.5 - A) TEX_{86} values and B) HOT_{86} proxy values of core GDGTs vs 1G-GDGTs. Clusters A1-C1 and A2-C2 represent different archaeal communities that are contributing to the GDGT lipid pool. The diagonal line indicates equal contribution of both 1G-GDGT and Core GDGT to the GDGT pool. A shift between convention TEX_{86} clusters and HOT_{86} clusters indicating a closer tracking of subsurface communities with the HOT_{86}.

3.4. Thermal impact on brGDGTs

We also investigated the potential impact of brGDGT proxies. In Figure 3.6 the values of the BIT, CBT, DC, and MBT indices are compared. In an attempt to evaluate the influence of other indices with both depths and temperatures we have plotted these indices against the value of depth divided by temperature. The BIT index, for instance, can change with depth as the source input of terrestrial soil organic matter is variable due to seasonal fluctuations and upwelling events (Hopmans et al., 2004), but should not be affected by temperature. However, in Figure 3.6 A, there is a greater variability with BIT values in Core 5, which experienced the most elevated temperatures. The variability of this proxy becomes less drastic outwards from the vent center. When evaluating the integrity of the DC index (Figure 3.6 B), the index is negatively affected by increased temperature, producing lower DC values. The CBT index appears to be influenced similarly to the BIT index, having increased proxy values in the hotter cores, with minimal variation in Core 8. On the other hand, it appears that MBT is less affected by increased temperatures (Figure 3.6 C) as there is no systematic increase in any particular core. Therefore the MBT may be a more reliable proxy that does not require a correction factor at higher geothermal temperatures.

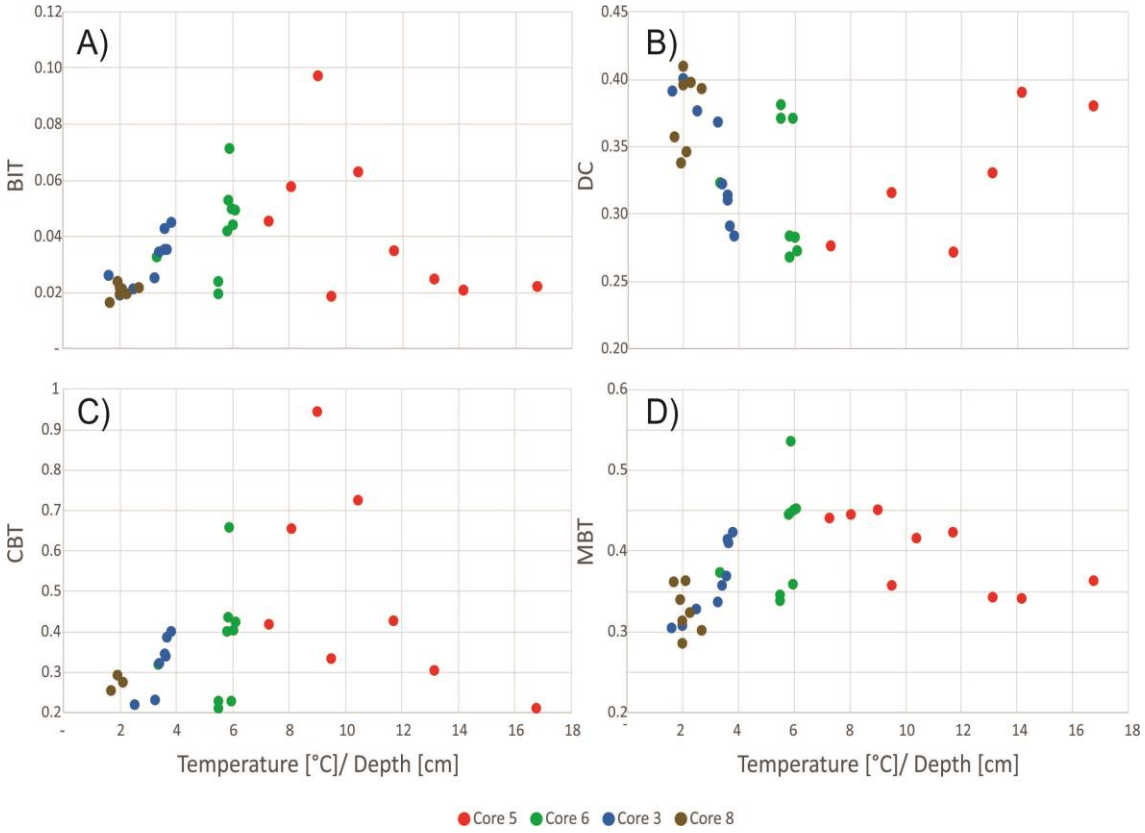

Figure 3.6 - brGDGT proxies vs Temperature (T) / Depth (D). A) BIT vs T/D B) DC vs T/D C) CBT vs T/D and D) MBT vs T/D. These plots show that there tends to be a wider variation of the proxy values with increased thermal gradients (T/D values).

3.5. Potential limitations to the use of tetraether-based proxies

GDGTs have varying thermochemical stabilities (Schouten et al., 2004) and the use of proxies that relate to archaeal-based paleoclimate proxies may be compromised if one or more of the core lipid isomers within the proxy is selectively degraded. This will lead to statistical loading of one structural isomer. We therefore suggest sediments with HOT_{86} values >0.7 are likely influenced by elevated temperatures. A HOT_{86} value of 0.7 (TEX_{86} value of ~ 0.56) approximately translates to 60°C, suggesting that any samples subjected to this temperature may be influenced by the *in situ* production, partial

destruction, and or recycling of GDGTs as proposed by Takano et al. (2010), providing biased SSTs. Figure 3.7 outlines potential depths of concern in systems that experience varying thermal conditions. This schematic shows hypothetically where tetraether lipid proxies may have been affected by geothermal temperatures provided that there is evdience of a strong enough subsurface archaeal community signature to overprint the paleoclimatological signal. The grey intervals represent the area of uncertainty. If a sediment is exposed to geothermal gradients producing temperatures above ~60°C then it may potentially be compromised by biological overprinting and or destruction of certain GDGT structures. This figure shows two different continental margins with varying geothermal gradients. In continental margins, geothermal gradients of ~ 60°C are achieved at ~ 900 - 2750 m depending on the geothermal gradient present (~23.1°C/km, Long et al., 2008; and ~70°C/km, Vanneste et al., 2005). The thermal gradient around mud volcanoes are often elevated, an example of a geothermal gradients present at this type of site location is ~60°C by around 250 m (Feseker et al., 2008). Pockmarks are another feature that can have elevated temperatures. For instance, a pockmark cluster on the continental margin of Nigeria as described by Wei et al. (2015), suggests that around 240-250 m, samples would be thermally influenced for paleo-reconstruction using tetraether lipids. The last thermal gradient that may influence samples is near spreading ridges as outlined in Wilson et al. (2019) which indicates that in some cases samples deeper than approximately 125 m are exposed to temperatures that may cause these proxies to be thermally influenced.

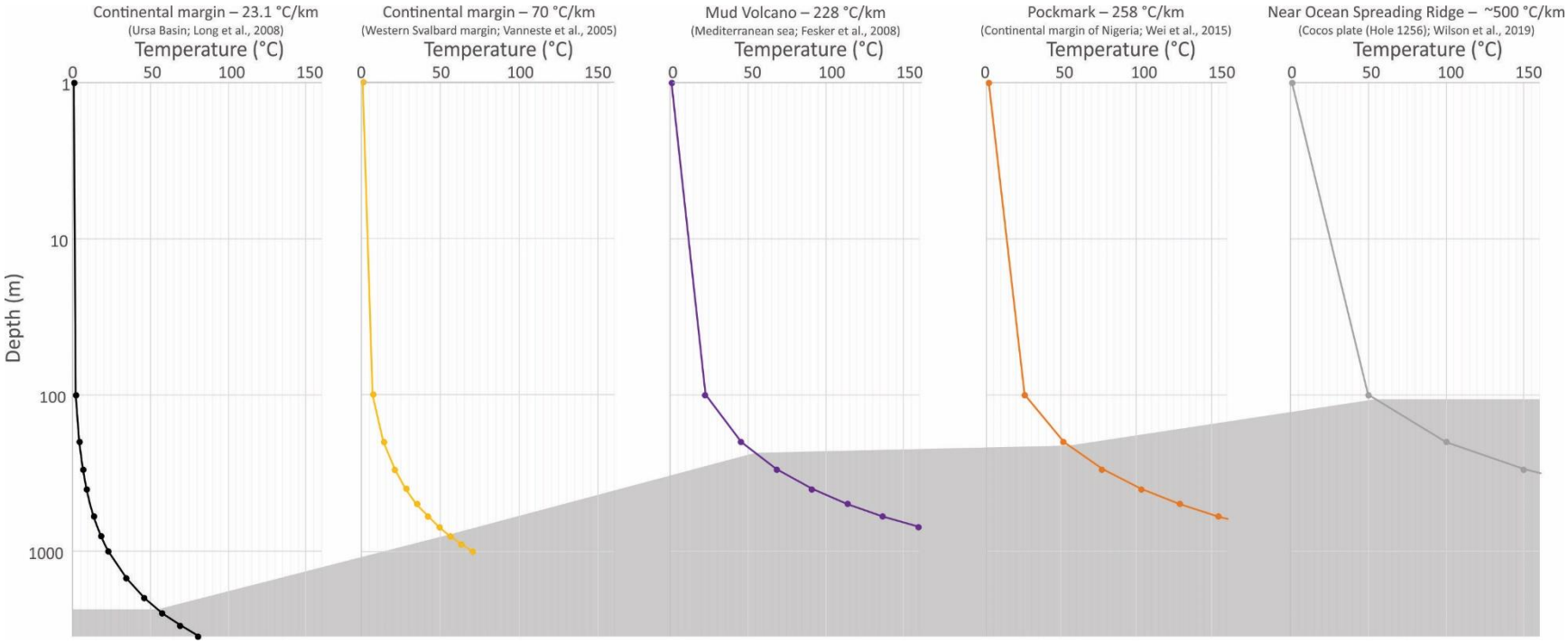

Figure 3.7 - Thermal gradients for varying marine settings. The greyed out area represents depths that may yield compromised proxy values due to overprinting and or destruction of specific molecules when they exceed temperatures of approximately 60°C.

4. Conclusions

In this study, we demonstrate that all of the commonly used GDGT proxies (isoprenoidal and branched) excluding the MBT are highly impacted by *in situ* pore water temperature at the Cathedral Hill hydrothermal vent site at Guaymas Basin. The mechanism for this is likely degradation, but also the contribution of the living subsurface archaeal community. This suggests that vent fluid temperatures may be capable of being estimated in GDGT hosted sediments independent of direct physical temperature sampling techniques. We therefore modified the TEX_{86} to include hydroxylated GDGTs as a novel proxy, namely the HOT_{86} which appears to track the geothermal temperatures. Ultimately, this study suggests that the TEX_{86} is more sensitive than previously thought at sample sites that may be affected by perturbed temperatures such as hydrothermal vents or by deeper samples that experience increased geothermal temperatures. These types of sites may provide a signal from the subsurface and not from the sea surface, as previously thought. This implies the reconstructed SSTs in settings where geothermal gradients are elevated by heat sources may ultimately provide compromised results. This process leads to the higher number of rings that may be produced in a hyperthermophilic Archaea. However, this phenomenon needs to be further investigated to fully understand the loss of the SST signature and the overprinting of the *in situ* temperature. We have also identified a potential correction factor using the newly developed HOT_{86} proxy which may be able to back out the original SST value. We also speculate that the HOT_{86} may be useful for reconstructing hydrothermal temperatures, but this will need to be further tested to understand its potential applications.

References

Boyd, E., Hamilton, T., Wang, J., He, L. and Zhang, C., 2013. The role of tetraether lipid composition in the adaptation of thermophilic Archaea to acidity. Frontiers in Microbiology, 4, Article 62, 1-15.

Calvert, S.E., 1966. Origin of diatom-rich, varved sediments from the Gulf of California. The Journal of Geology, 74(5, Part 1), 546-565.

Curray, J.R., Moore, D. G., Lawver, L.A., Emmel, F.J., Raitt, R.W., Henry, M., & Kieckhefer, R. 1979. Tectonics of the Andaman Sea and Burma: convergent margins

Damsté, J.S.S., 2016. Spatial heterogeneity of sources of branched tetraethers in shelf systems: The geochemistry of tetraethers in the Berau River delta (Kalimantan, Indonesia). Geochimica et Cosmochimica Acta, 186, 13-31

Damsté, J.S.S., Ossebaar, J., Abbas, B., Schouten, S. and Verschuren, D., 2009. Fluxes and distribution of tetraether lipids in an equatorial African lake: constraints on the application of the TEX86 palaeothermometer and BIT index in lacustrine settings. Geochimica et Cosmochimica Acta, 73(14), 4232-4249.

Damsté, J.S.S., Ossebaar, J., Schouten, S. and Verschuren, D., 2012. Distribution of tetraether lipids in the 25-ka sedimentary record of Lake Challa: extracting reliable TEX86 and MBT/CBT palaeotemperatures from an equatorial African lake. Quaternary Science Reviews, 50, pp.43-54.

De Rosa, M. and Gambacorta, A., 1988. The lipids of archaebacteria. Progress in lipid research, 27(3), 153-175.

Dos Santos, R.A.L., Prange, M., Castañeda, I.S., Schefuß, E., Mulitza, S., Schulz, M., Niedermeyer, E.M., Damste, J.S.S. and Schouten, S., 2010. Glacial–interglacial variability in Atlantic meridional overturning circulation and thermocline adjustments in the tropical North Atlantic. Earth and Planetary Science Letters, 300(3-4), 407-414.

Elling, F.J., Könneke, M., Mußmann, M., Greve, A. and Hinrichs, K.U., 2015. Influence of temperature, pH, and salinity on membrane lipid composition and TEX86 of marine planktonic thaumarchaeal isolates. Geochimica et Cosmochimica Acta, 171, 238-255.

Feseker, T., Dählmann, A., Foucher, J.P., & Harmegnies, F. 2009. In-situ sediment temperature measurements and geochemical porewater data suggest highly dynamic fluid flow at Isis mud volcano, eastern Mediterranean Sea. Marine Geology, 261(1-4), 128-137.

Gieskes, J.M., Simoneit, B.R., Brown, T., Shaw, T.J., Wang, Y.C. and Magenheim, A., 1988. Hydrothermal fluids and petroleum in surface sediments of Guaymas Basin, Gulf of California: a case study. *The Canadian Mineralogist*, *26*(3), 589.

Gliozzi, A., Paoli, G., De Rosa, M. and Gambacorta, A., 1983. Effect of isoprenoid cyclization on the transition temperature of lipids in thermophilic archaebacteria. Biochimica et Biophysica Acta (BBA)-Biomembranes, 735(2), 234-242.

Hopmans, E.C., Weijers, J.W., Schefuß, E., Herfort, L., Damsté, J.S.S. and Schouten, S., 2004. A novel proxy for terrestrial organic matter in sediments based on branched and isoprenoid tetraether lipids. Earth and Planetary Science Letters, 224(1-2), 107-116.

Huguet, C., Cartes, J.E., Sinninghe Damsté, J.S. and Schouten, S., 2006. Marine crenarchaeotal membrane lipids in decapods: Implications for the TEX86 paleothermometer. Geochemistry, Geophysics, Geosystems, 7(11).

Huguet, C., Fietz, S., Rosell-Melé, A., Daura, X. and Costenaro, L., 2017. Molecular dynamics simulation study of the effect of glycerol dialkyl glycerol tetraether hydroxylation on membrane thermostability. Biochimica et Biophysica Acta (BBA)-Biomembranes, 1859(5), 966-974.

Huguet, C., Schimmelmann, A., Thunell, R., Lourens, L.J., Sinninghe Damsté, J.S. and Schouten, S., 2007. A study of the TEX86 paleothermometer in the water column and sediments of the Santa Barbara Basin, California. Paleoceanography, 22(3).

Jenkyns, H.C., Schouten-Huibers, L., Schouten, S. and Sinninghe Damsté, J.S., 2012. Warm Middle Jurassic–Early Cretaceous high-latitude sea-surface temperatures from the Southern Ocean. Climate of the Past, 8(1), 215-226.

Kashefi, K. and Lovley, D.R., 2003. Extending the upper temperature limit for life. Science, 301(5635), 934-934.

Kim, J.H., Schouten, S., Hopmans, E.C., Donner, B. and Damsté, J.S.S., 2008. Global sediment core-top calibration of the TEX86 paleothermometer in the ocean. *Geochimica et Cosmochimica Acta*, *72*(4), 1154-1173.

Kim, J.H., Van der Meer, J., Schouten, S., Helmke, P., Willmott, V., Sangiorgi, F., Koç, N., Hopmans, E.C. and Damsté, J.S.S., 2010. New indices and calibrations derived from the distribution of crenarchaeal isoprenoid tetraether lipids: Implications for past sea surface temperature reconstructions. Geochimica et Cosmochimica Acta, 74(16), 4639-4654.

Kim, J.H., Crosta, X., Willmott, V., Renssen, H., Bonnin, J., Helmke, P., Schouten, S. and Sinninghe Damsté, J.S., 2012. Holocene subsurface temperature variability in the eastern Antarctic continental margin. Geophysical Research Letters, 39(6).

Knappy, C.S., Chong, J.P. and Keely, B.J., 2009. Rapid discrimination of archaeal tetraether lipid cores by liquid chromatography-tandem mass spectrometry. Journal of the American Society for Mass Spectrometry, 20(1), 51-59.

Liu, X.L., Leider, A., Gillespie, A., Gröger, J., Versteegh, G.J. and Hinrichs, K.U., 2010. Identification of polar lipid precursors of the ubiquitous branched GDGT orphan lipids in a peat bog in Northern Germany. Organic Geochemistry, 41(7), 653-660.

Liu, X.L., Lipp, J.S., Simpson, J.H., Lin, Y.S., Summons, R.E. and Hinrichs, K.U., 2012. Mono-and dihydroxyl glycerol dibiphytanyl glycerol tetraethers in marine sediments: Identification of both core and intact polar lipid forms. Geochimica et Cosmochimica Acta, 89, 102-115.

Lipp, J.S. and Hinrichs, K.U., 2009. Structural diversity and fate of intact polar lipids in marine sediments. Geochimica et Cosmochimica Acta, 73(22), 6816-6833.

Lipp, J.S., Morono, Y., Inagaki, F. and Hinrichs, K.U., 2008. Significant contribution of Archaea to extant biomass in marine subsurface sediments. Nature, 454(7207), 991.

Long, H., Flemings, P. B., Dugan, B., Germaine, J. T., & Ferrell, D. 2008. Data report: penetrometer measurements of in situ temperature and pressure, IODP Expedition 308. In Proc. IODP| Volume Vol. 308.

Lonsdale, P. and Becker, K., 1985. Hydrothermal plumes, hot springs, and conductive heat flow in the Southern Trough of Guaymas Basin. *Earth and Planetary Science Letters*, *73*(2-4), 211-225.

Macalady, J.L., Vestling, M.M., Baumler, D., Boekelheide, N., Kaspar, C.W. and Banfield, J.F., 2004. Tetraether-linked membrane monolayers in Ferroplasma spp: a key to survival in acid. Extremophiles, 8(5), 411-419.

McClymont, E.L., Ganeshram, R.S., Pichevin, L.E., Talbot, H.M., van Dongen, B.E., Thunell, R.C., Haywood, A.M., Singarayer, J.S. and Valdes, P.J., 2012. Sea-surface temperature records of Termination 1 in the Gulf of California: Challenges for seasonal and interannual analogues of tropical Pacific climate change. Paleoceanography, 27(2).

McKay, L.J., MacGregor, B.J., Biddle, J.F., Albert, D.B., Mendlovitz, H.P., Hoer, D.R., Lipp, J.S., Lloyd, K.G. and Teske, A.P., 2012. Spatial heterogeneity and underlying geochemistry of phylogenetically diverse orange and white Beggiatoa mats in Guaymas Basin hydrothermal sediments. Deep Sea Research Part I: Oceanographic Research Papers, 67, 21-31.

Meyer, S., Wegener, G., Lloyd, K.G., Teske, A., Boetius, A. and Ramette, A., 2013. Microbial habitat connectivity across spatial scales and hydrothermal temperature gradients at Guaymas Basin. Frontiers in microbiology, 4, 207.

Moore, D. G. 1973. Plate-edge deformation and crustal growth, Gulf of California structural province. Geological Society of America Bulletin, 84(6), 1883-1906.

Pearson, A., Huang, Z., Ingalls, A.E., Romanek, C.S., Wiegel, J., Freeman, K.H., Smittenberg, R.H. and Zhang, C.L., 2004. Nonmarine crenarchaeol in Nevada hot springs. Appl. Environ. Microbiol., 70(9), 5229-5237.

Powers, L., Werne, J.P., Vanderwoude, A.J., Damsté, J.S.S., Hopmans, E.C. and Schouten, S., 2010. Applicability and calibration of the TEX86 paleothermometer in lakes. Organic Geochemistry, 41(4), 404-413.

Schouten, S., Hopmans, E.C. and Damste, J.S.S., 2004. The effect of maturity and depositional redox conditions on archaeal tetraether lipid palaeothermometry. Organic Geochemistry, 35(5), 567-571.

Schouten, S., Hopmans, E.C., Schefuß, E. and Damste, J.S.S., 2002. Distributional variations in marine crenarchaeotal membrane lipids: a new tool for reconstructing ancient sea water temperatures?. *Earth and Planetary Science Letters*, *204*(1-2), 265-274.

Shah, S.R., Mollenhauer, G., Ohkouchi, N., Eglinton, T.I. and Pearson, A., 2008. Origins of archaeal tetraether lipids in sediments: Insights from radiocarbon analysis. *Geochimica et Cosmochimica Acta*, *72*(18), 4577-4594.

Shintani, T., Yamamoto, M. and Chen, M.T., 2011. Paleoenvironmental changes in the northern South China Sea over the past 28,000 years: a study of TEX86-derived sea surface temperatures and terrestrial biomarkers. Journal of Asian Earth Sciences, 40(6), 1221-1229.

Sturt, H.F., Summons, R.E., Smith, K., Elvert, M. and Hinrichs, K.U., 2004. Intact polar membrane lipids in prokaryotes and sediments deciphered by high-performance liquid chromatography/electrospray ionization multistage mass spectrometry—new biomarkers for biogeochemistry and microbial ecology. *Rapid Communications in Mass Spectrometry*, *18*(6), 617-628.

Teske, A., Callaghan, A.V. and LaRowe, D.E., 2014. Biosphere frontiers of subsurface life in the sedimented hydrothermal system of Guaymas Basin. Frontiers in microbiology, 5, 362.

Teske, A., de Beer, D., McKay, L.J., Tivey, M.K., Biddle, J.F., Hoer, D., Lloyd, K.G., Lever, M.A., Røy, H., Albert, D.B. and Mendlovitz, H.P., 2016. The Guaymas Basin hiking guide to hydrothermal mounds, chimneys, and microbial mats: Complex seafloor expressions of subsurface hydrothermal circulation. Frontiers in Microbiology, 7, 75.

Tierney, J.E., Schouten, S., Pitcher, A., Hopmans, E.C. and Damsté, J.S.S., 2012. Core and intact polar glycerol dialkyl glycerol tetraethers (GDGTs) in Sand Pond, Warwick, Rhode Island (USA): Insights into the origin of lacustrine GDGTs. Geochimica et Cosmochimica Acta, 77, 561-581.

Tierney, J.E., 2014. Biomarker-based inferences of past climate: the TEX86 paleotemperature proxy.

Uda, I., Sugai, A., Itoh, Y.H. and Itoh, T., 2001. Variation in molecular species of polar lipids from Thermoplasma acidophilum depends on growth temperature. Lipids, 36(1), 103-105.

Vanneste, M., Guidard, S., & Mienert, J. 2005. Bottom-simulating reflections and geothermal gradients across the western Svalbard margin. Terra Nova, 17(6), 510-516.

Wei, J., Pape, T., Sultan, N., Colliat, J.L., Himmler, T., Ruffine, L., de Prunelé, A., Dennielou, B., Garziglia, S., Marsset, T. and Peters, C.A., 2015. Gas hydrate distributions in sediments of pockmarks from the Nigerian margin–Results and interpretation from shallow drilling. Marine and Petroleum Geology, 59, pp.359-370.Weijers, J.W., Schouten, S., van den Donker, J.C., Hopmans, E.C. and Damsté, J.S.S., 2007. Environmental controls on bacterial tetraether membrane lipid distribution in soils. Geochimica et Cosmochimica Acta, 71(3), 703-713.

Weijers, J.W., Schouten, S., van den Donker, J.C., Hopmans, E.C. and Damsté, J.S.S., 2007. Environmental controls on bacterial tetraether membrane lipid distribution in soils. Geochimica et Cosmochimica Acta, 71(3), 703-713.

Wilson, D.S., Teagle, D.A., Alt, J.C., Banerjee, N.R., Umino, S., Miyashita, S., Acton, G.D., Anma, R., Barr, S.R., Belghoul, A. and Carlut, J., 2006. Drilling to gabbro in intact ocean crust. science, 312(5776), 1016-1020.

Wuchter, C., Schouten, S., Coolen, M.J. and Sinninghe Damsté, J.S., 2004. Temperature-dependent variation in the distribution of tetraether membrane lipids of marine Crenarchaeota: Implications for TEX86 paleothermometry. *Paleoceanography*, *19*(4).

Wuchter, C., Schouten, S., Wakeham, S.G. and Sinninghe Damsté, J.S., 2005. Temporal and spatial variation in tetraether membrane lipids of marine Crenarchaeota in particulate organic matter: Implications for TEX86 paleothermometry. *Paleoceanography*, *20*(3).

Yoshinaga, M.Y., Kellermann, M.Y., Rossel, P.E., Schubotz, F., Lipp, J.S. and Hinrichs, K.U., 2011. Systematic fragmentation patterns of archaeal intact polar lipids by high-performance liquid chromatography/electrospray ionization ion-trap mass spectrometry. Rapid Communications in Mass Spectrometry, 25(23), 3563-3574.

Zhang, Y.G., Pagani, M. and Wang, Z., 2016. Ring Index: A new strategy to evaluate the integrity of TEX86 paleothermometry. Paleoceanography, 31(2), 220-232.

Zhang, Y.G., Zhang, C.L., Liu, X.L., Li, L., Hinrichs, K.U. and Noakes, J.E., 2011. Methane Index: A tetraether archaeal lipid biomarker indicator for detecting the

instability of marine gas hydrates. Earth and Planetary Science Letters, 307(3-4), 525-534.
Zhu, C., Lipp, J.S., Wörmer, L., Becker, K.W., Schröder, J. and Hinrichs, K.U., 2013. Comprehensive glycerol ether lipid fingerprints through a novel reversed phase liquid chromatography–mass spectrometry protocol. *Organic Geochemistry*, *65*, 53-62.

Supplementary figures and tables for Chapter 3

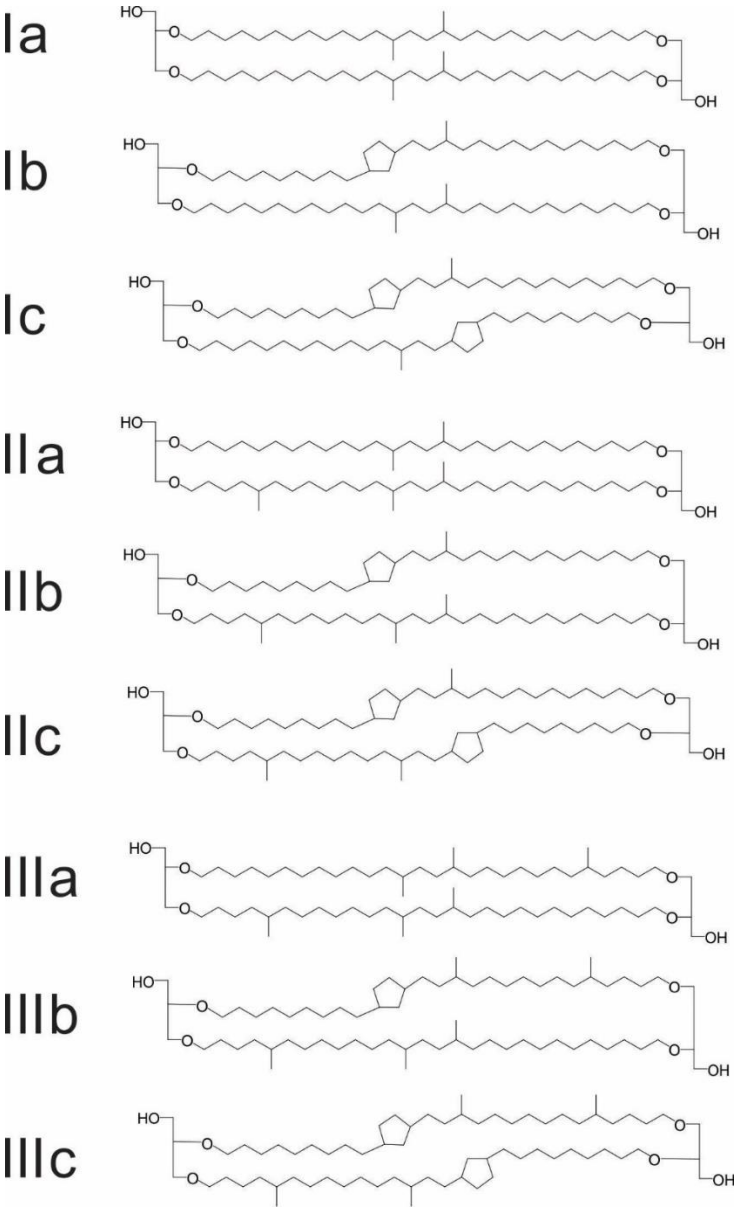

Figure S1- 1 – Chemical structures of brGDGTs

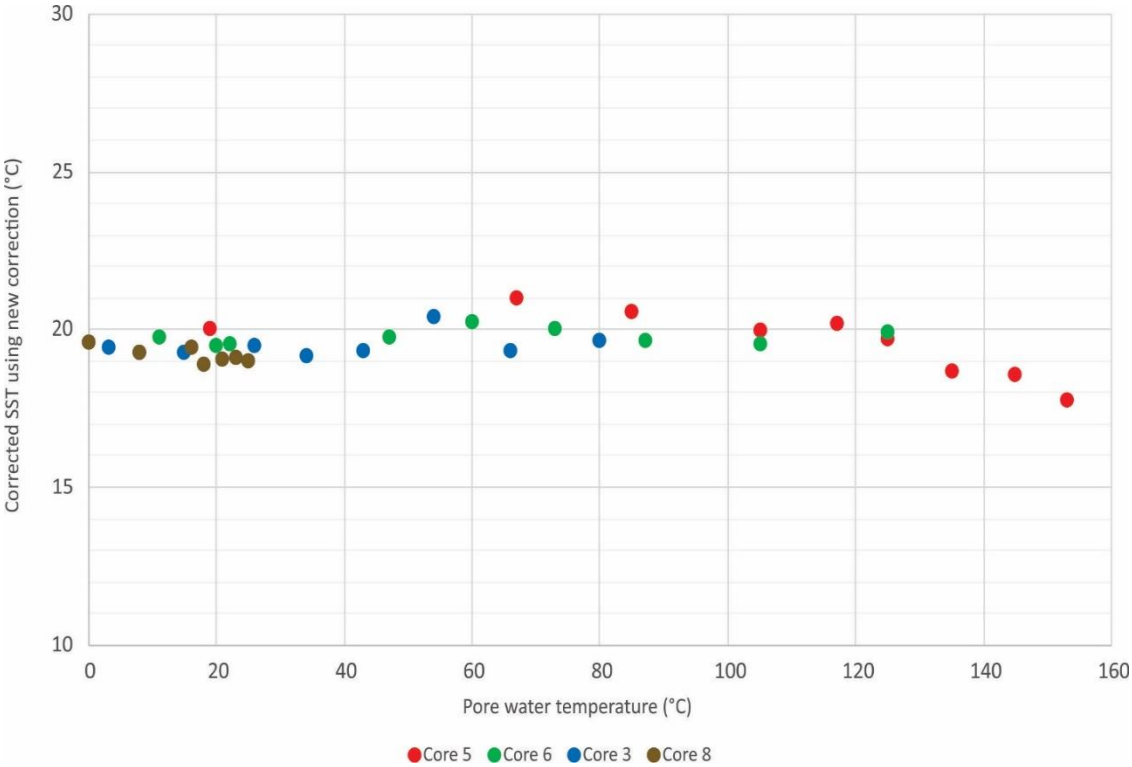

Figure S1- 2 – Corrected SSTs using new correction factor

Core	Depth interval (cmbsf)	Temperature	SST (Kim et al., 2010)	Corrected SST
GB4462-5	**0-2**	19	20.52	20.01
GB4462-5	**2-4**	67	21.97	20.99
GB4462-5	**4-6**	85	21.71	20.57
GB4462-5	**6-8**	105	21.61	19.97
GB4462-5	**8-10**	117	22.34	20.19
GB4462-5	**10-12**	125	21.17	19.69
GB4462-5	**12-15**	135	23.33	18.67
GB4462-5	**15-18**	145	23.46	18.54
GB4462-5	**18-21**	153	24.67	17.75
GB4462-6	**0-2**	11	19.92	19.72
GB4462-6	**2-4**	22	19.65	19.55
GB4462-6	**4-6**	20	19.71	19.49
GB4462-6	**6-8**	47	20.85	19.76
GB4462-6	**8-10**	60	21.71	20.21
GB4462-6	**10-12**	73	21.30	20.02
GB4462-6	**12-15**	87	21.21	19.66
GB4462-6	**15-18**	105	22.03	19.51
GB4462-6	**18-21**	125	22.17	19.92
GB4462-3	**0-2**	3.2	19.50	19.44
GB4462-3	**2-4**	8	19.11	19.27
GB4462-3	**4-6**	15	19.20	19.28
GB4462-3	**6-8**	26	19.57	19.45
GB4462-3	**8-10**	34	19.20	19.14
GB4462-3	**10-12**	43	19.57	19.33
GB4462-3	**12-15**	54	20.77	20.42
GB4462-3	**15-18**	66	20.19	19.31
GB4462-3	**18-21**	80	20.96	19.63
GB4462-8	**0-2**	0	19.65	19.57
GB4462-8	**2-4**	8	19.26	19.25
GB4462-8	**4-6**	16	19.48	19.41
GB4462-8	**6-8**	18	18.60	18.86
GB4462-8	**8-10**	21	19.19	19.06
GB4462-8	**10-12**	23	19.06	19.08
GB4462-8	**12-15**	25	18.98	18.98

Table S1- 1 - Sample set SST values and corrected SST values produced from the correction factor in this study.

Chapter 4: Key conclusions and future work

4.1. Key conclusions

This section is used to address the questions proposed in the objectives section (Chapter 1 section 1.1.2).

1) Subsurface microbial communities were detected at Cathedral Hill using lipidomic techniques. The results from the survey indicates that the lipids from the subsurface communities have a limited diversity of IPLs and CLs that make up their cellular membranes. However, these lipids indicate that these organisms are adapting to their harsh environments as seen in the ring index.

2) The thermochemical stability of detectable polar lipids indicate a preference for higher numbers of rings within core GDGTs. The highest relative abundances of GDGT-3, 4 and 5' are found in Core 5, with the most extreme thermal gradient. Additionally, 1G-GDGTs, which are markers for living cells, are found in intervals that experience up to ~145°C, potentially pushing the boundaries for life.

3) Lipid-based paleoclimate proxies become progressively compromised with elevated subsurface sediment pore water temperatures as the adapting archaea overprint the original GDGT signal that is often used for reconstructions, and possibly selective thermal degradation. This led to the development of the HOT_{86} proxy, a modification of the TEX_{86} proxy, which appears to track this adaptation and thermal effect. However, the potential use of this new proxy to reconstruct hydrothermal temperatures or recalculate SSTs from compromised SSTs using our correction factor are still to be determined.

4.2. Future work

The Guaymas Basin sediment samples were analysed using a reverse phase-HPLC-ESI-MS method. By using only a single LC-MS method the full range of potential detectible lipid signatures was limited. Re-running the samples with a HILIC (hydrophilic interaction liquid chromatography) method as outlined in Wörmer et al. (2017) to identify bacterial lipids can help improve the range of lipid markers that represents the microbiome at Cathedral Hill. This technique will also allow for a more accurate thermo-tolerability comparison between the bacterial and archaeal domains of life. The upper limit for both Bacteria and Archaea have been tentatively set to 110°C (Jorgensen et al., 1992) and 122°C (Takai et al., 2008), respectively, however there is always a potential for a new discovery which may push this boundary further. Additionally, analyzing the samples with a normal phase HPLC method is required to determine if core glycerol monoalkyl glycerol tetrathers (GMGTs) are present (Wormer et al., 2017), which are thought to be a further adaptation to increase stability within a lipid. The identification of GMGTs may be useful in further understanding the adaptation mechanisms at Cathedral Hill.

This hydrothermal setting provides the possibility that the thermal degradation of IPLs to intermediate products of GDGTs, hydrocarbons, and ultimately oxidation to CO_2 is possible at deeper sediment depths at Cathedral Hill. Tracking the diagenetic to metagenetic fate of membrane lipids is worthy of a follow-up study. The resulting IPL, CL and hydrocarbon oxidation products likely contribute to the production of hydrocarbons. The precise set of reactions that break down organic material to generate hydrocarbons is largely unknown and thus makes an interesting topic for a future study.

In addition to this, if the intermediate products are not found then there is a potential to define assimilation or recycling pathways within Archaea. Currently this idea has been considered but to the best of our knowledge it has not been demonstrated in any natural samples.

Appendix

A-1 Pre-experiment oil influence study

A preliminary data set produced by another masters student investigating the aliphatic fraction obtained from the same sample set indicated the potential for hydrocarbon staining within a few of the intervals. This potential for hydrocarbon staining within the samples raised concerns with LC analysis specifically with the electrospray ionization (ESI) source. The presence of oil within a sample can cause ion suppression which relates to the presence of non-volatile species which can cause co-precipitation of analyte in the droplet which ultimately prevents ionization. It can also prevent the droplets from evaporating properly within the nebulizer preventing efficient ionization. To identify the potential effects of ion suppression within an environmental sample, a series of oil spiked samples were prepared to identify the effects that may occur.

This microstudy was conducted by taking our Bay of Fundy reference material which is a bulk estuary mud sample that was collected and homogenized, extracted and compound classes were identified within the samples prior to this microstudy. This reference material was then spiked with either 100, 1,000 or 10,000 ppm oil. The oil used to spike these samples was a light oil from Hebron I-18. A duplicate of each amount was analysed (Table A1-1) to ensure the values obtained were accurate.

Sample ID	ppm oil added	Oil added (mg)	µg/g sediment of TLE	Relative standard deviation
OSS-1	10,000	35	7265.25	0.42%
OSS-2	10,000	35	7222.70	-
OSS-3	1,000	3.495	2412.74	4.39%
OSS-4	1,000	3.495	2567.42	-
OSS-5	100	.355	1903.41	0.67%
OSS-6	100	.355	1921.57	-
Standard	-	-	~ 1500	-

Table A1- 2 - Experiment parameters and yield

The result of this microstudy indicates that if a sample does contain oil staining there is a potential for ion suppression within a sample and thus the values of those samples may be vastly under represented when integrated. As seen in figure A1-1, GDGTs are visible within the highlighted area of "a" where it is almost non existent in "b". In addition to this BPCs were generated for this sample set from 100-500 m/z and 500-3000 m/z. The 100-500 m/z range represents the hypothetical hydrocarbon range, this shows that the increase in oil spike results in unresolved complex mixtures (UCMs). This is clear in the 10,000 ppm sample. Furthermore, the BPCs for the 500-3000 m/z range represents the hypothetical lipid range as they tend to be larger organic molecules. The increased amounts of oil added to the sample results in a decrease in lipid resolution which may once again under evaluate the actual abundance present.

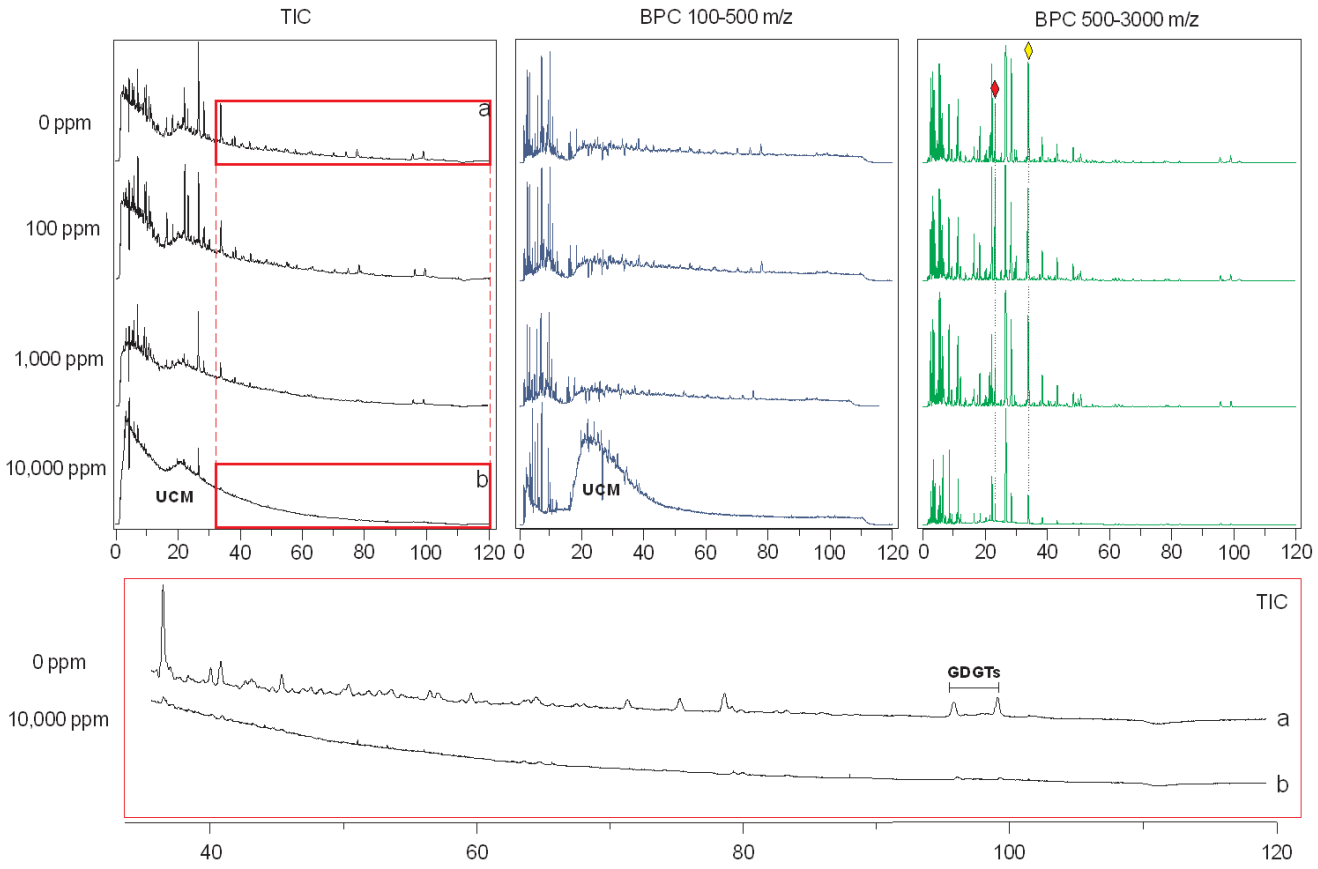

Figure A1- 3 - Chromatograms showing ion suppression with increasing amounts of oil

A-2 Core descriptions

GB 4462 - Push Core 5

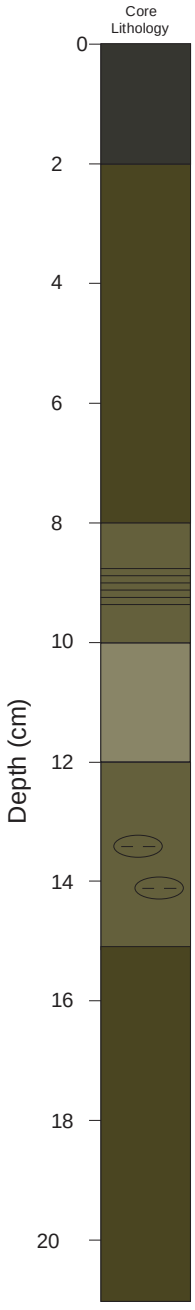

Very unconsolidated, sediment has an H2S smell, very dark black liquified mud with white filament

Brownish dark green siliceous mud some black mud (no black mud between 4-6 cm)

Greenish brown mud with silica silt

Greenish grey brown mud

Greenish brown consolidated mud with yellow green clay shards

Very consolidated clay brownish green

GB 4462 - Push Core 6

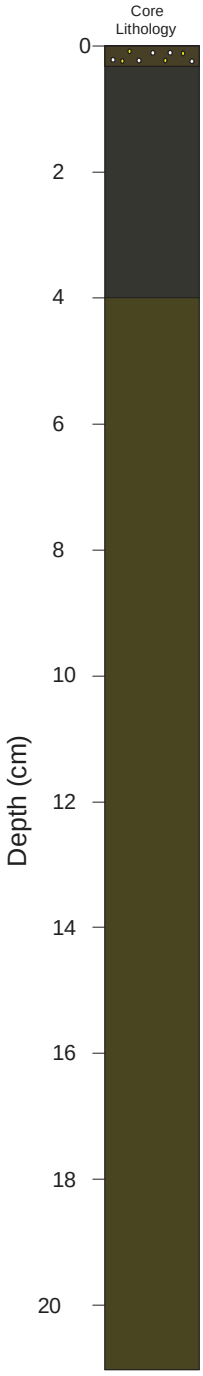

Greenish brown liquified mud with yellow and white granules with black flecks ~ 0.25cm thick top layer below its all black (top layer maybe oxidized

oil slick, top black siliceous mud some fragments of microbial siliceous mat

more consolidated mud very strong H2S smell

GB 4462 - Push Core 3

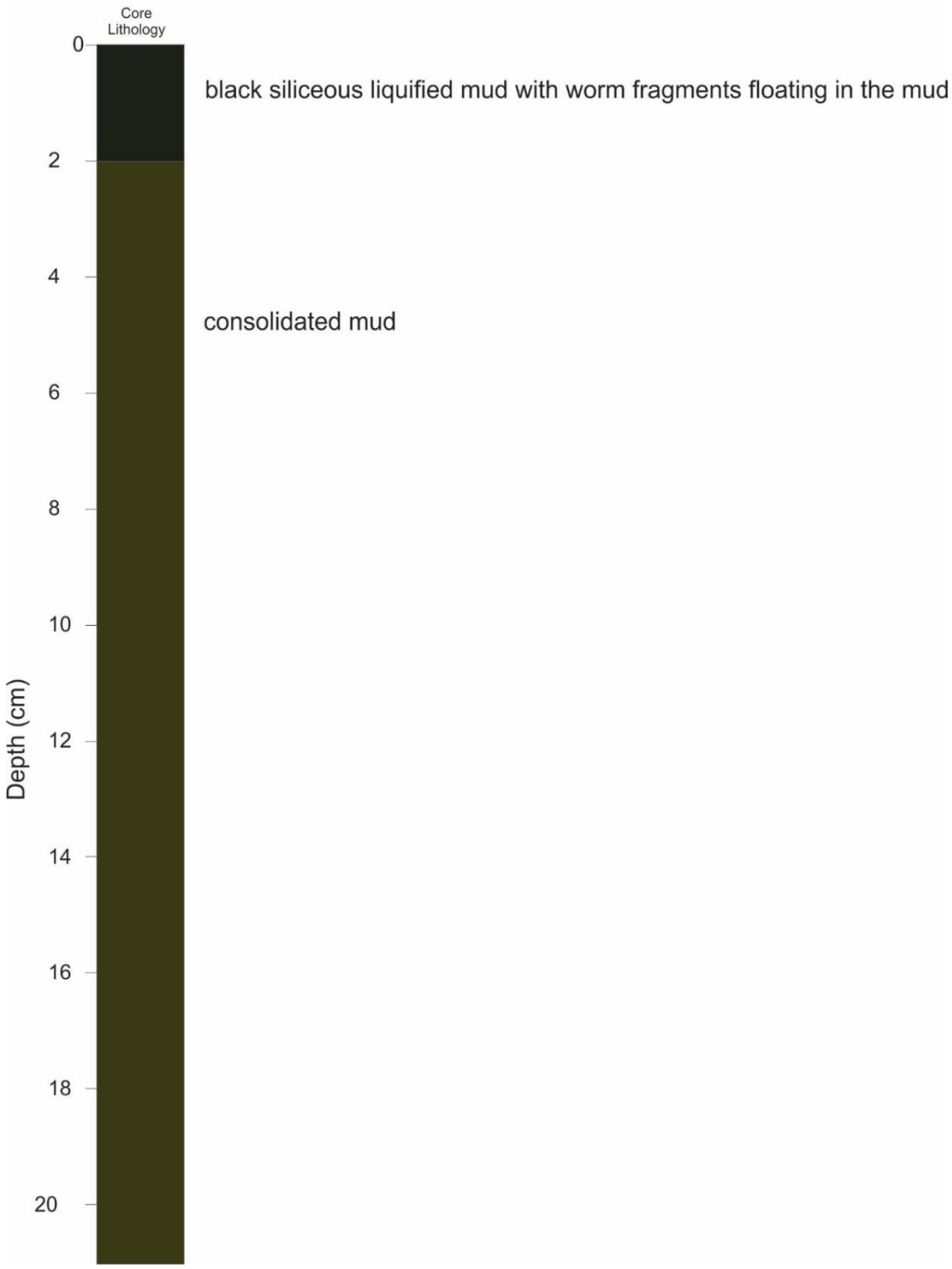

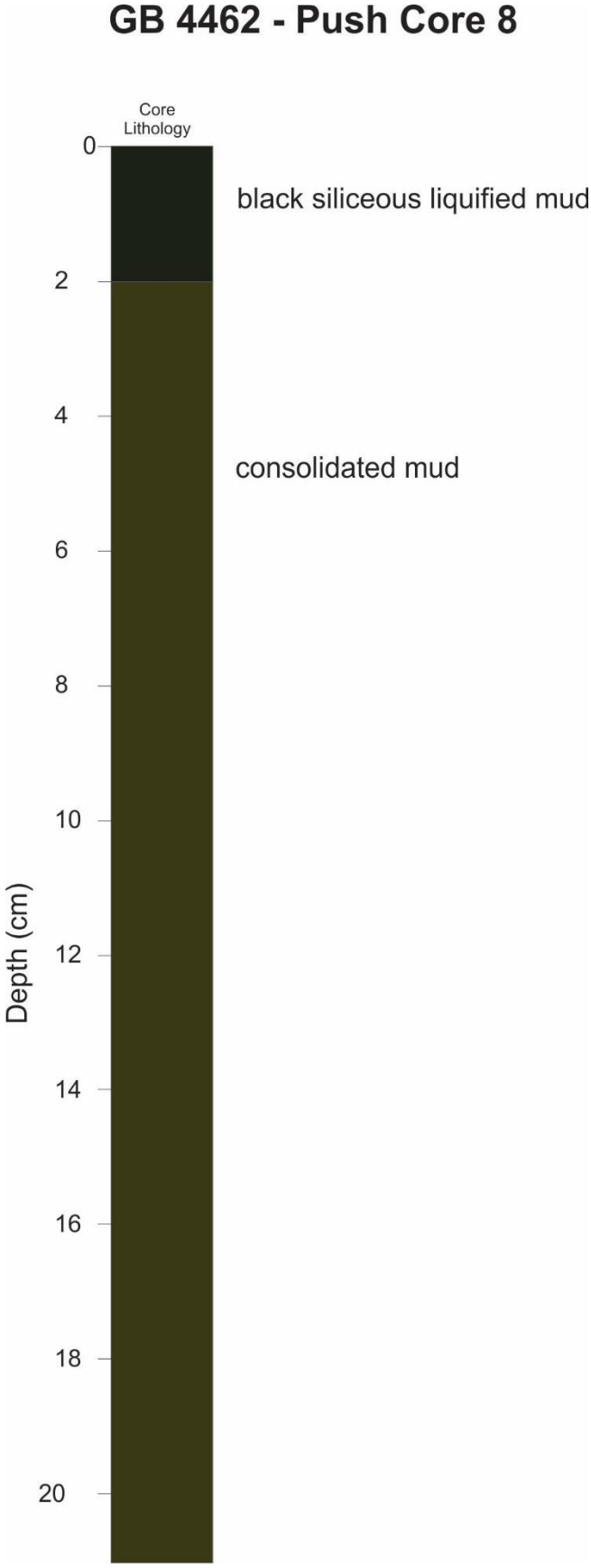

Note the description for Core 8 reads "same as others" and was left open for some interpretation, thus is closely mirrors Core 3 in the depiction.

A-3 Supplementary data

This appendix is for the individual concentration data of lipids that are observed having varying number of cyclizations occurring in their structure. These compounds have been identified and discussed in Chapter two.

Table A3-1 – Core GDGTs

Table A3-2 – 1G-GDGTs

Table A3-3 – 2G-GDGTs

Table A3-4 – BrGDGTs

Table A3-5 – GDDs

Table A3-6 – Unknown lipids

Table A3-7 – GDGT proxy values

Table A3-1 – Individual concentrations of GDGT compounds, values are reported in µg/g sediment with response factors included.

	GDGT-0	GDGT-1	GDGT-2	GDGT-3	GDGT-4	GDGT-5	GDGT-5'	OH-GDGT-0	OH-GDGT-1	OH-GDGT-2
Core 5										
0-2 cm	184.78	49.03	41.76	12.61	15.50	192.17	7.26	13.09	8.17	4.51
2-4 cm	160.85	48.87	44.80	15.74	13.24	170.49	7.73	12.39	7.76	3.91
4-6 cm	71.50	20.14	17.86	6.58	7.49	76.55	3.15	5.21	3.38	1.79
6-8 cm	50.75	13.97	11.99	4.67	9.77	55.07	2.35	3.39	2.22	1.08
8-10 cm	19.71	5.35	4.67	2.12	3.22	23.04	0.89	1.17	0.80	0.44
10-12 cm	16.41	4.36	3.47	1.51	2.52	19.72	0.76	0.81	0.54	0.27
12-15 cm	24.28	7.01	6.64	3.21	8.83	27.71	0.98	0.69	0.50	0.20
15-18 cm	13.23	3.81	3.51	1.84	4.17	15.43	0.59	0.21	0.15	0.07
18-21 cm	11.70	3.45	3.36	1.98	3.42	13.94	0.55	0.13	0.08	0.05
Core 6										
0-2 cm	208.96	58.31	47.78	12.21	17.23	236.25	10.22	15.08	8.70	5.06
2-4 cm	94.13	26.69	21.65	5.22	6.65	107.31	4.66	7.31	4.87	2.64
4-6 cm	30.87	8.79	6.80	1.93	2.64	34.70	1.69	2.33	1.55	0.79
6-8 cm	23.54	5.84	4.70	1.71	3.41	29.43	1.11	1.55	1.02	0.51
8-10 cm	16.19	4.05	3.36	1.30	2.29	20.55	0.90	0.87	0.64	0.30
10-12 cm	17.24	4.33	3.60	1.24	2.36	22.37	0.92	0.95	0.74	0.38
12-15 cm	14.43	3.68	2.96	1.18	2.13	19.13	0.72	0.63	0.46	0.29
15-18 cm	7.30	1.88	1.63	0.70	1.38	9.08	0.30	0.05	0.05	0.02
18-21 cm	10.18	2.46	2.14	0.91	1.55	13.49	0.45	0.17	0.12	0.06

	GDGT-0	GDGT-1	GDGT-2	GDGT-3	GDGT-4	GDGT-5	GDGT-5'	OH-GDGT-0	OH-GDGT-1	OH-GDGT-2
Core 3										
0-2 cm	182.40	58.57	47.30	11.97	14.16	187.75	9.15	15.44	9.76	5.40
2-4 cm	109.85	27.00	20.89	4.72	5.64	135.69	5.07	8.21	5.09	2.60
4-6 cm	101.52	28.02	22.08	4.88	5.58	116.33	5.06	7.22	4.88	2.67
6-8 cm	98.79	27.50	22.38	5.40	6.55	110.21	4.50	7.35	4.93	2.96
8-10 cm	89.25	24.74	18.96	4.89	6.15	102.63	4.44	6.67	4.24	2.78
10-12 cm	80.39	19.37	15.09	3.92	5.92	99.31	3.72	6.31	4.30	2.60
12-15 cm	66.03	17.19	13.99	4.31	0.43	78.97	3.71	4.42	3.44	2.22
15-18 cm	154.30	38.95	30.34	9.35	19.59	212.44	8.11	10.31	8.14	5.07
18-21 cm	60.66	15.83	12.84	4.37	8.79	76.47	3.34	4.01	3.24	2.07
Core 8										
0-2 cm	176.52	51.76	41.96	10.04	10.74	185.22	9.14	13.58	8.71	5.47
2-4 cm	146.40	39.72	31.19	7.04	8.73	177.32	7.36	10.25	6.83	4.28
4-6 cm	169.92	47.40	37.07	9.00	11.11	196.83	9.24	13.04	8.47	5.30
6-8 cm	129.68	33.76	26.00	5.60	7.08	152.16	5.39	9.54	6.07	2.99
8-10 cm	53.35	12.39	9.41	2.73	3.93	69.63	2.02	3.17	2.05	1.06
10-12 cm	166.36	42.70	32.74	8.68	11.97	190.17	6.91	12.04	7.61	3.63
12-15 cm	168.78	34.67	25.85	6.69	8.90	263.79	6.47	11.01	7.33	4.23

Table A3-2 – Individual concentrations of 1G-GDGT compounds, values are reported in µg/g sediment with response factors included.

	1G-GDGT-0	1G-GDGT-1	1G-GDGT-2	1G-GDGT-3	1G-GDGT-4	1G-GDGT-5	1G-GDGT-5'	1G-OH-GDGT-0	1G-OH-GDGT-1	1G-OH-GDGT-2
Core 5										
0-2 cm	4.94	1.27	0.99	0.64	0.81	6.12	0.09	0.87	0.35	0.18
2-4 cm	5.00	0.93	0.95	0.18	0.53	5.66	0.12	1.26	0.37	0.22
4-6 cm	2.12	0.58	0.40	0.21	0.40	2.19	0.09	0.42	0.26	0.14
6-8 cm	1.32	0.50	0.38	0.11	0.31	1.53	0.15	0.46	0.34	0.17
8-10 cm	0.75	0.39	0.49	0.41	0.73	0.30	0.11	0.32	0.29	0.17
10-12 cm	0.45	0.23	0.27	0.21	0.37	0.08	0.06	0.12	0.11	0.05
12-15 cm	0.40	0.23	0.21	0.24	0.22	0.05	0.04	0.03	0.02	0.01
15-18 cm	0.00	0.00	0.00	0.00	0.00	0.00	0.00	0.00	0.00	0.00
18-21 cm	0.00	0.00	0.00	0.00	0.00	0.00	0.00	0.00	0.00	0.00
Core 6										
0-2 cm	5.94	1.51	0.97	0.19	0.86	6.63	0.11	0.78	0.50	0.25
2-4 cm	2.32	0.43	0.35	0.12	0.29	3.06	0.12	0.39	0.27	0.12
4-6 cm	0.77	0.21	0.18	0.09	0.11	0.88	0.04	0.22	0.18	0.09
6-8 cm	0.65	0.36	0.39	0.37	0.99	0.45	0.11	0.38	0.34	0.21
8-10 cm	0.36	0.26	0.34	0.23	0.57	0.17	0.05	0.29	0.24	0.06
10-12 cm	0.40	0.29	0.37	0.20	0.47	0.19	0.06	0.02	0.22	0.10
12-15 cm	0.28	0.11	0.17	0.07	0.18	0.14	0.05	0.01	0.09	0.05
15-18 cm	0.00	0.00	0.00	0.00	0.00	0.00	0.00	0.00	0.00	0.00
18-21 cm	0.00	0.00	0.00	0.00	0.00	0.00	0.00	0.00	0.00	0.00

	1G-GDGT-0	1G-GDGT-1	1G-GDGT-2	1G-GDGT-3	1G-GDGT-4	1G-GDGT-5	1G-GDGT-5'	1G-OH-GDGT-0	1G-OH-GDGT-1	1G-OH-GDGT-2
Core 3										
0-2 cm	4.95	1.09	1.15	0.00	0.62	6.26	0.10	0.67	0.39	0.15
2-4 cm	2.91	0.55	0.30	0.14	0.59	2.98	0.08	0.37	0.26	0.22
4-6 cm	2.36	0.38	0.31	0.10	0.20	2.96	0.07	0.30	0.20	0.13
6-8 cm	2.56	0.49	0.34	0.14	0.22	2.95	0.09	0.37	0.27	0.15
8-10 cm	1.74	0.45	0.54	0.00	0.31	1.98	0.17	0.42	0.36	0.22
10-12 cm	2.11	0.43	0.81	0.31	0.00	1.55	0.12	0.84	0.51	0.35
12-15 cm	1.59	0.79	0.84	0.58	0.86	1.56	0.31	0.59	0.77	0.48
15-18 cm	3.46	1.25	1.73	1.12	1.28	2.78	0.61	1.21	1.57	0.86
18-21 cm	1.54	0.72	0.85	0.31	0.58	0.99	0.22	0.44	0.55	0.30
Core 8										
0-2 cm	4.34	0.75	0.61	0.27	0.00	5.16	0.00	0.48	0.32	0.14
2-4 cm	3.73	0.70	0.41	0.00	0.00	3.98	0.00	0.40	0.25	0.20
4-6 cm	4.25	0.72	0.53	0.00	0.00	5.54	0.00	0.47	0.41	0.29
6-8 cm	3.81	0.64	0.53	0.00	0.00	3.84	0.00	0.40	0.31	0.23
8-10 cm	1.26	0.22	0.00	0.00	0.00	0.93	0.00	0.18	0.15	0.09
10-12 cm	3.73	0.66	0.00	0.00	0.00	2.08	0.00	0.55	0.37	0.23
12-15 cm	2.98	0.00	0.00	0.00	0.00	3.07	0.00	0.47	0.16	0.13

Table A3-3 – Individual concentrations of 2G-GDGT compounds, values are reported in µg/g sediment with response factors included.

	2G-GDGT-0	2G-GDGT-1	2G-GDGT-2	2G-OH-GDGT-0	2G-OH-GDGT-1	2G-OH-GDGT-2
Core 5						
0-2 cm	0.65	0.78	1.04	1.85	1.67	0.76
2-4 cm	0.51	0.50	0.73	1.34	1.08	0.54
4-6 cm	0.00	0.00	0.00	0.44	0.43	0.23
6-8 cm	0.00	0.00	0.00	0.28	0.25	0.14
8-10 cm	0.00	0.00	0.00	0.03	0.03	0.01
10-12 cm	0.00	0.00	0.00	0.00	0.00	0.00
12-15 cm	0.00	0.00	0.00	0.00	0.00	0.00
15-18 cm	0.00	0.00	0.00	0.00	0.00	0.00
18-21 cm	0.00	0.00	0.00	0.00	0.00	0.00
	0.65	0.78	1.04	1.85	1.67	0.76
Core 6						
0-2 cm	0.77	0.72	0.83	1.54	1.38	0.70
2-4 cm	0.25	0.35	0.43	0.76	0.68	0.33
4-6 cm	0.06	0.10	0.15	0.20	0.18	0.09
6-8 cm	0.00	0.00	0.08	0.09	0.10	0.05
8-10 cm	0.00	0.00	0.00	0.01	0.01	0.00
10-12 cm	0.00	0.00	0.00	0.00	0.00	0.00
12-15 cm	0.00	0.00	0.00	0.00	0.00	0.00
15-18 cm	0.00	0.00	0.00	0.00	0.00	0.00
18-21 cm	0.00	0.00	0.00	0.00	0.00	0.00

	2G-GDGT-0	2G-GDGT-1	2G-GDGT-2	2G-OH-GDGT-0	2G-OH-GDGT-1	2G-OH-GDGT-2
Core 3						
0-2 cm	0.55	0.46	0.71	1.47	1.22	0.58
2-4 cm	0.27	0.32	0.39	0.69	0.60	0.34
4-6 cm	0.16	0.24	0.34	0.51	0.45	0.27
6-8 cm	0.24	0.30	0.40	0.59	0.54	0.29
8-10 cm	0.18	0.22	0.33	0.52	0.47	0.25
10-12 cm	0.17	0.20	0.29	0.50	0.42	0.20
12-15 cm	0.00	0.00	0.00	0.13	0.12	0.04
15-18 cm	0.00	0.00	0.00	0.30	0.32	0.17
18-21 cm	0.00	0.00	0.00	0.07	0.08	0.04
Core 8						
0-2 cm	0.34	0.37	0.43	0.74	0.59	0.35
2-4 cm	0.24	0.27	0.36	0.51	0.49	0.27
4-6 cm	0.28	0.37	0.53	0.77	0.67	0.42
6-8 cm	0.25	0.29	0.30	0.48	0.49	0.28
8-10 cm	0.15	0.00	0.22	0.63	0.57	0.32
10-12 cm	0.47	0.51	1.03	1.43	1.36	0.63
12-15 cm	0.00	0.00	0.00	0.00	0.00	0.00

Table A3-4 – Individual concentrations of brGDGTs compounds, values are reported in µg/g sediment with response factors included.

	brGDGT-1a	brGDGT-1b	brGDGT-1c	brGDGT-2a	brGDGT-2b	brGDGT-2c	brGDGT-3a	brGDGT-3b
Core 5								
0-2 cm	1.26	0.39	0.21	1.06	0.68	0.24	1.35	0.00
2-4 cm	1.24	0.61	0.25	1.10	0.82	0.24	1.51	0.00
4-6 cm	0.46	0.24	0.11	0.40	0.32	0.09	0.75	0.00
6-8 cm	0.44	0.16	0.08	0.40	0.26	0.10	0.55	0.00
8-10 cm	0.32	0.10	0.04	0.23	0.11	0.00	0.28	0.00
10-12 cm	0.53	0.08	0.02	0.40	0.10	0.00	0.39	0.00
12-15 cm	1.32	0.12	0.05	0.93	0.14	0.00	0.74	0.00
15-18 cm	0.39	0.07	0.03	0.27	0.07	0.00	0.28	0.00
18-21 cm	0.26	0.08	0.03	0.18	0.09	0.00	0.21	0.00
Core 6								
0-2 cm	1.49	0.59	0.28	1.27	1.03	0.26	1.91	0.23
2-4 cm	0.78	0.37	0.16	0.75	0.56	0.17	1.08	0.14
4-6 cm	0.41	0.14	0.06	0.31	0.21	0.06	0.44	0.05
6-8 cm	1.24	0.17	0.06	0.47	0.21	0.06	0.54	0.04
8-10 cm	0.41	0.12	0.05	0.23	0.13	0.04	0.31	0.00
10-12 cm	0.47	0.16	0.05	0.30	0.13	0.00	0.39	0.00
12-15 cm	0.32	0.12	0.06	0.25	0.10	0.00	0.27	0.00
15-18 cm	0.21	0.06	0.03	0.15	0.06	0.00	0.15	0.00
18-21 cm	0.23	0.09	0.04	0.19	0.16	0.00	0.29	0.00

	brGDGT-1a	brGDGT-1b	brGDGT-1c	brGDGT-2a	brGDGT-2b	brGDGT-2c	brGDGT-3a	brGDGT-3b
Core 3								
0-2 cm	1.39	0.61	0.28	1.45	1.22	0.32	2.21	0.26
2-4 cm	0.70	0.36	0.15	0.73	0.59	0.18	1.22	0.14
4-6 cm	0.71	0.36	0.15	0.70	0.50	0.16	1.13	0.12
6-8 cm	0.83	0.38	0.16	0.73	0.53	0.16	1.27	0.10
8-10 cm	1.17	0.45	0.19	1.00	0.58	0.18	1.48	0.14
10-12 cm	1.20	0.47	0.20	1.05	0.55	0.19	1.40	0.15
12-15 cm	1.31	0.56	0.21	1.09	0.54	0.16	1.14	0.09
15-18 cm	2.94	1.05	0.43	2.33	1.11	0.38	2.53	0.23
18-21 cm	1.39	0.45	0.20	1.04	0.51	0.06	1.16	0.06
Core 8								
0-2 cm	1.01	0.51	0.23	1.18	1.02	0.26	1.88	0.27
2-4 cm	0.91	0.50	0.25	0.99	0.75	0.22	1.65	0.17
4-6 cm	1.12	0.57	0.27	1.23	0.95	0.30	2.03	0.18
6-8 cm	0.83	0.46	0.19	0.88	0.66	0.22	1.33	0.11
8-10 cm	0.49	0.22	0.08	0.44	0.27	0.09	0.58	0.05
10-12 cm	1.43	0.55	0.27	1.28	0.84	0.26	1.96	0.19
12-15 cm	1.42	0.63	0.23	1.11	0.77	0.27	1.84	0.00

Table A3-5 – Individual concentrations of GDD compounds, values are reported in µg/g sediment with response factors included.

	GDD-0	GDD-1	GDD-2	GDD-3	GDD-4	GDD-5	OH-GDD-0	OH-GDD-1	OH-GDD-2
Core 5									
0-2 cm	6.92	1.60	0.97	0.48	1.21	14.14	1.06	0.87	0.66
2-4 cm	7.94	2.02	1.30	0.78	0.99	17.11	1.30	1.11	0.76
4-6 cm	3.52	0.84	0.45	0.25	0.34	7.22	0.49	0.41	0.28
6-8 cm	2.27	0.53	0.24	0.15	0.30	4.27	0.34	0.32	0.21
8-10 cm	0.75	0.16	0.07	0.03	0.06	1.33	0.08	0.06	0.04
10-12 cm	0.73	0.17	0.06	0.04	0.06	1.28	0.08	0.06	0.04
12-15 cm	1.15	0.28	0.12	0.06	0.16	1.98	0.00	0.00	0.00
15-18 cm	0.73	0.18	0.08	0.03	0.07	1.27	0.00	0.00	0.00
18-21 cm	0.66	0.15	0.09	0.05	0.12	1.34	0.00	0.00	0.00
Core 6									
0-2 cm	8.55	2.07	1.07	0.62	1.12	18.65	1.47	1.28	0.85
2-4 cm	4.72	1.13	0.51	0.29	0.44	10.08	0.79	0.66	0.51
4-6 cm	1.64	0.40	0.18	0.08	0.13	3.26	0.30	0.23	0.17
6-8 cm	1.08	0.25	0.10	0.03	0.08	1.92	0.15	0.12	0.10
8-10 cm	0.58	0.13	0.05	0.02	0.05	1.07	0.08	0.07	0.04
10-12 cm	0.71	0.17	0.07	0.02	0.06	1.26	0.09	0.07	0.05
12-15 cm	0.51	0.12	0.05	0.02	0.05	0.91	0.06	0.04	0.04
15-18 cm	0.31	0.08	0.03	0.01	0.03	0.47	0.00	0.00	0.00
18-21 cm	0.42	0.10	0.04	0.00	0.03	0.65	0.00	0.00	0.00

	GDD-0	GDD-1	GDD-2	GDD-3	GDD-4	GDD-5	OH-GDD-0	OH-GDD-1	OH-GDD-2
Core 3									
0-2 cm	9.34	2.39	1.21	0.64	1.11	20.73	1.70	1.44	0.93
2-4 cm	3.90	0.89	0.43	0.16	0.34	8.05	0.79	0.69	0.48
4-6 cm	4.19	0.97	0.45	0.23	0.36	9.44	0.80	0.66	0.39
6-8 cm	4.89	1.16	0.58	0.29	0.39	10.59	0.76	0.55	0.45
8-10 cm	4.84	1.11	0.52	0.26	0.40	10.35	0.88	0.73	0.50
10-12 cm	4.14	0.91	0.41	0.13	0.33	7.95	0.76	0.65	0.43
12-15 cm	2.65	0.60	0.28	0.15	0.22	5.16	0.41	0.37	0.21
15-18 cm	6.30	1.48	0.67	0.26	0.52	12.14	0.86	0.84	0.54
18-21 cm	2.37	0.55	0.23	0.11	0.21	4.60	0.32	0.30	0.18
Core 8									
0-2 cm	7.66	1.96	0.97	0.43	0.79	18.10	1.39	1.04	0.94
2-4 cm	5.94	1.49	0.67	0.35	0.51	14.61	1.06	0.85	0.66
4-6 cm	7.42	1.86	0.87	0.45	0.70	17.53	1.45	1.14	0.81
6-8 cm	5.24	1.24	0.59	0.22	0.55	11.77	1.00	0.68	0.55
8-10 cm	2.11	0.50	0.24	0.15	0.27	4.69	0.34	0.29	0.17
10-12 cm	7.38	1.72	0.83	0.48	1.10	16.54	1.46	1.17	0.80
12-15 cm	7.09	1.64	0.60	0.26	1.01	18.22	1.50	1.38	0.78

Table A3-6 – Individual concentrations of unknown lipids, values are reported in µg/g sediment with response factors included.

	U-Cer-1	U-Cer-2	U-DAG-1	U-DAG-2
Core 5				
0-2 cm	5.77	11.00	1.82	5.77
2-4 cm	4.84	11.41	1.58	4.84
4-6 cm	0.29	3.79	0.43	0.29
6-8 cm	0.00	1.77	0.07	0.00
8-10 cm	0.00	0.25	0.02	0.00
10-12 cm	0.00	0.03	0.00	0.00
12-15 cm	0.00	0.00	0.00	0.00
15-18 cm	0.00	0.00	0.00	0.00
18-21 cm	0.00	0.00	0.00	0.00
Core 6				
0-2 cm	6.34	11.12	3.07	6.34
2-4 cm	2.47	5.22	1.01	2.47
4-6 cm	0.07	1.27	0.12	0.07
6-8 cm	0.02	0.56	0.01	0.02
8-10 cm	0.00	0.12	0.01	0.00
10-12 cm	0.00	0.05	0.00	0.00
12-15 cm	0.00	0.02	0.00	0.00
15-18 cm	0.00	0.00	0.00	0.00
18-21 cm	0.00	0.00	0.00	0.00
Core 3				
0-2 cm	7.18	11.52	4.25	7.18
2-4 cm	3.74	6.07	2.05	3.74
4-6 cm	3.05	5.27	1.59	3.05
6-8 cm	2.66	5.04	1.18	2.66
8-10 cm	1.86	4.52	0.81	1.86
10-12 cm	0.77	3.99	0.72	0.77
12-15 cm	0.00	1.61	0.14	0.00
15-18 cm	0.00	1.23	0.08	0.00
18-21 cm	0.00	0.83	0.04	0.00
Core 8				
0-2 cm	5.82	9.39	4.01	5.82
2-4 cm	4.61	8.08	3.01	4.61
4-6 cm	5.09	8.90	3.27	5.09
6-8 cm	3.57	6.40	2.10	3.57
8-10 cm	1.36	2.68	0.57	1.36
10-12 cm	5.26	9.62	2.22	5.26
12-15 cm	5.40	9.96	3.68	5.40

Table A3-7 – GDGT proxy values

Core 5	RI	MI	TEX_{86}	SST(°C)	HOT_{86}	BIT	MBT	DC	CBT	%GDGT
0-2 cm	2.44	0.34	0.56	21.21	0.67	0.02	0.36	0.32	0.34	49.02
2-4 cm	2.45	0.38	0.58	22.56	0.69	0.02	0.36	0.38	0.21	48.54
4-6 cm	2.48	0.36	0.58	22.32	0.7	0.02	0.34	0.39	0.19	48.29
6-8 cm	2.55	0.35	0.58	22.23	0.73	0.02	0.34	0.33	0.31	47.96
8-10 cm	2.60	0.34	0.59	22.90	0.75	0.03	0.42	0.27	0.43	46.10
10-12 cm	2.63	0.31	0.57	21.82	0.73	0.06	0.42	0.16	0.73	45.42
12-15 cm	2.65	0.37	0.61	23.77	0.83	0.1	0.45	0.1	0.95	46.70
15-18 cm	2.66	0.36	0.61	23.88	0.83	0.06	0.45	0.18	0.66	46.17
18-21 cm	2.66	0.38	0.63	24.92	0.86	0.05	0.44	0.28	0.42	45.62
Core 6										
0-2 cm	2.52	0.32	0.55	20.64	0.64	0.02	0.35	0.37	0.23	46.94
2-4 cm	2.52	0.32	0.54	20.38	0.64	0.02	0.34	0.38	0.21	46.73
4-6 cm	2.52	0.33	0.54	20.44	0.65	0.03	0.37	0.32	0.32	47.08
6-8 cm	2.68	0.29	0.56	21.52	0.71	0.07	0.54	0.18	0.66	44.44
8-10 cm	2.69	0.29	0.58	22.33	0.73	0.04	0.45	0.28	0.40	44.06
10-12 cm	2.71	0.28	0.57	21.95	0.72	0.05	0.45	0.27	0.43	43.52
12-15 cm	2.73	0.28	0.57	21.86	0.73	0.04	0.45	0.28	0.40	42.99
15-18 cm	2.68	0.31	0.58	22.61	0.77	0.05	0.45	0.27	0.44	44.55
18-21 cm	2.74	0.28	0.59	22.74	0.76	0.05	0.36	0.37	0.23	43.00
Core 3										
0-2 cm	2.41	0.37	0.54	20.23	0.63	0.03	0.31	0.39	0.19	49.28
2-4 cm	2.62	0.27	0.53	19.85	0.61	0.02	0.31	0.40	0.18	44.74
4-6 cm	2.53	0.31	0.53	19.93	0.62	0.02	0.33	0.38	0.22	46.60
6-8 cm	2.50	0.33	0.54	20.30	0.64	0.03	0.34	0.37	0.23	47.27
8-10 cm	2.54	0.31	0.53	19.93	0.64	0.03	0.36	0.32	0.32	46.52
10-12 cm	2.64	0.27	0.54	20.29	0.65	0.04	0.37	0.31	0.35	44.74
12-15 cm	2.56	0.30	0.56	21.45	0.65	0.04	0.41	0.31	0.34	45.54
15-18 cm	2.77	0.26	0.55	20.90	0.70	0.04	0.41	0.29	0.39	42.07
18-21 cm	2.68	0.29	0.56	21.63	0.72	0.04	0.42	0.28	0.40	44.24
Core 8										
0-2 cm	2.43	0.35	0.54	20.38	0.63	0.02	0.29	0.41	0.16	48.80
2-4 cm	2.59	0.30	0.53	19.99	0.63	0.02	0.31	0.40	0.18	45.23
4-6 cm	2.55	0.31	0.54	20.21	0.63	0.02	0.30	0.39	0.19	46.33
6-8 cm	2.55	0.29	0.52	19.33	0.60	0.02	0.32	0.40	0.18	46.01
8-10 cm	2.69	0.26	0.53	19.92	0.64	0.02	0.36	0.35	0.28	43.38
10-12 cm	2.54	0.30	0.53	19.79	0.63	0.02	0.34	0.34	0.29	46.66
12-15 cm	2.90	0.20	0.53	19.71	0.63	0.02	0.36	0.36	0.25	39.02